

UNCLASSIFIED

AD NUMBER

ADB009489

LIMITATION CHANGES

TO:

Approved for public release; distribution is unlimited.

FROM:

Distribution authorized to U.S. Gov't. agencies only; Test and Evaluation; MAY 1975. Other requests shall be referred to Air Force Avionics Lab., Wright-Patterson AFB, OH 45433.

AUTHORITY

AFAL ltr 7 May 1979

THIS PAGE IS UNCLASSIFIED

THIS REPORT HAS BEEN DELIMITED
AND CLEARED FOR PUBLIC RELEASE
UNDER DOD DIRECTIVE 5200.20 AND
NO RESTRICTIONS ARE IMPOSED UPON
ITS USE AND DISCLOSURE.

DISTRIBUTION STATEMENT A

APPROVED FOR PUBLIC RELEASE;
DISTRIBUTION UNLIMITED.

✓
AFAL-TR-74-314

OPTICAL COUPLERS

SPECTRONICS, INC.
830 EAST ARAPAHO ROAD
RICHARDSON, TEXAS 75080

DECEMBER 1975



AD B009489
AD No. _____
DDC FILE COPY

INTERIM TECHNICAL REPORT AFAL-TR-74-314

DDC
RECEIVED
MAR 4 1976
A

82
Distribution limited to US Government Agencies only: Test and Evaluation; May 1975. Other requests for this document must be referred to AFAL/AAM, Wright-Patterson AFB, Ohio 45433.

AIR FORCE AVIONICS LABORATORY
AIR FORCE WRIGHT AERONAUTICAL LABORATORIES
Air Force Systems Command
Wright-Patterson Air Force Base, Ohio 45433

NOTICE

When Government drawings, specifications, or other data are used for any purpose other than in connection with a definitely related Government procurement operation, the United States Government thereby incurs no responsibility nor any obligation whatsoever; and the fact that the government may have formulated, furnished, or in any way supplied the said drawings, specifications, or other data, is not to be regarded by implication or otherwise as in any manner licensing the holder or any other person or corporation, or conveying any rights or permission to manufacture, use, or sell any patented invention that may in any way be related thereto.

ACCESSION FOR	
NTIS	White Section <input checked="" type="checkbox"/>
DOC	USC Section <input checked="" type="checkbox"/>
UNCLASSIFIED	<input type="checkbox"/>
JUSTIFICATION	
BY	
DISSEMINATION/SECURITY CODE	
REMARKS/SPECIAL	
B	

Copies of this report should not be returned unless return is required by security considerations, contractual obligations, or notice on a specific document.

UNCLASSIFIED

SECURITY CLASSIFICATION OF THIS PAGE (When Data Entered)

19 REPORT DOCUMENTATION PAGE		READ INSTRUCTIONS BEFORE COMPLETING FORM																					
1. REPORT NUMBER (18) AFAL-TR-74-314	2. GOVT ACCESSION NO.	3. RECIPIENT'S CATALOG NUMBER																					
4. TITLE (and Subtitle) (6) OPTICAL COUPLERS.	5. TYPE OF REPORT & PERIOD COVERED (9) Interim Technical Report. October 1973 - June 1974																						
7. AUTHOR(s) (10) James R. Biard John E. Shaunfield	8. CONTRACT OR GRANT NUMBER(s) (15) F33615-74-C-1001																						
9. PERFORMING ORGANIZATION NAME AND ADDRESS Spectronics, Inc. 830 E. Arapaho Road Richardson, Texas 75080	10. PROGRAM ELEMENT, PROJECT, TASK AREA & WORK UNIT NUMBERS Project 2003 Task 07-04																						
11. CONTROLLING OFFICE NAME AND ADDRESS Air Force Avionics Laboratory AFAL/AAM Air Force System Command Wright-Patterson AFB, Ohio 45433	12. REPORT DATE (11) December 1975																						
14. MONITORING AGENCY NAME & ADDRESS (if different from Controlling Office) (16) AF-2903	13. NUMBER OF PAGES (12) 181p. 166																						
15. SECURITY CLASS. (of this report) (17) 200307 UNCLASSIFIED		15a. DECLASSIFICATION/DOWNGRADING SCHEDULE																					
16. DISTRIBUTION STATEMENT (of this Report) Distribution limited to US Government Agencies only; Test and Evaluation; May 1976. Other requests for this document must be referred to AFAL/AAM Wright-Patterson AFB, Ohio 45433.																							
17. DISTRIBUTION STATEMENT (of the abstract entered in Block 20, if different from Report)																							
18. SUPPLEMENTARY NOTES																							
19. KEY WORDS (Continue on reverse side if necessary and identify by block number)																							
<table border="0"> <tr> <td>optoelectronic</td> <td>LED</td> <td>optical termination</td> <td>T coupler</td> </tr> <tr> <td>electro-optic</td> <td>photodiode</td> <td>packing fraction</td> <td>data rate</td> </tr> <tr> <td>data bus</td> <td>fiber optic bundle</td> <td>radial coupler</td> <td></td> </tr> <tr> <td>data transmission</td> <td>optical interconnect</td> <td>bit error rate</td> <td></td> </tr> <tr> <td>light emitting diode</td> <td>passive coupler</td> <td>photodetector</td> <td></td> </tr> </table>				optoelectronic	LED	optical termination	T coupler	electro-optic	photodiode	packing fraction	data rate	data bus	fiber optic bundle	radial coupler		data transmission	optical interconnect	bit error rate		light emitting diode	passive coupler	photodetector	
optoelectronic	LED	optical termination	T coupler																				
electro-optic	photodiode	packing fraction	data rate																				
data bus	fiber optic bundle	radial coupler																					
data transmission	optical interconnect	bit error rate																					
light emitting diode	passive coupler	photodetector																					
20. ABSTRACT (Continue on reverse side if necessary and identify by block number) (continued on reverse side) This document is an interim report describing the development of optical couplers for use in an eight station EMI/EMP resistant avionic data bus being developed on this program. Airborne avionics systems are moving toward the use of party line multiplex data buses for the transmission of the growing number of digital signals found in modern aircraft. Optoelectronic technology provides a data bus interface system consistent with military requirements that is potentially superior to wire techniques--particularly in the areas of ground loop noise																							

DD FORM 1473 1 JAN 73 EDITION OF 1 NOV 65 IS OBSOLETE

UNCLASSIFIED

SECURITY CLASSIFICATION OF THIS PAGE (When Data Entered)

389 381 ✓ VB

UNCLASSIFIED

SECURITY CLASSIFICATION OF THIS PAGE(When Data Entered)

20. ABSTRACT (continued from Front)

immunity and EMI/EMP sensitivity. Passive optical directional couplers are required in an optoelectronic data bus so that each station can receive optical signals from the bus and transmit optical signals onto the bus. By this means, each station on the bus can communicate with every other station. The report identifies the basic optical loss and attenuation mechanisms that affect the quality of optical couplers and describes the techniques developed to minimize these losses. Since low-loss fiber optic bundle terminations are required at all optical interfaces, this topic is discussed separately. Conventional terminations are described which have losses of 34.8%; compression techniques are described that reduce the loss to 24.4%. The report also describes the design, fabrication and evaluation of two versions of a duplex T coupler and one radial coupler. An improved version of the radial coupler is described and recommended for use in the EMI/EMP resistant data bus.

UNCLASSIFIED

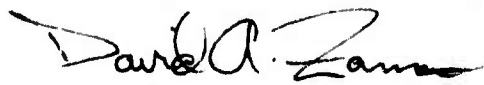
SECURITY CLASSIFICATION OF THIS PAGE(When Data Entered)

FOREWORD

This interim report describes the design, fabrication and evaluation of optical couplers by Spectronics, Incorporated, Richardson, Texas. The work was performed for the System Avionics Division, Air Force Avionics Laboratory, Wright-Patterson AFB, Ohio. The work was done on Contract Number F33615-74-C-1001, Project 2003-07-04. The United States Air Force project engineer was David A. Zann of the Information Management Branch (AFAL/AAM). The program manager was J. R. Biard; the project engineers were G. E. Pittman, J. E. Shaunfield, B. J. Cottongim and R. L. Glass. The report covers research on this contract conducted from 1 October 1973 through 30 June 1974.

The authors wish to acknowledge the contributions to this program made by David A. Zann and Kenneth C. Trumble of the Avionics Laboratory, and G. E. Pittman of Spectronics, Incorporated.

This report was submitted by the authors in November 1974, has been reviewed and is approved for publication.

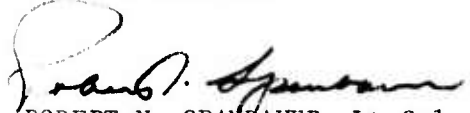


DAVID A. ZANN
Project Engineer



CHARLES C. GAUDER
Acting Chief
Information Management Branch
System Avionics Division

FOR THE DIRECTOR



ROBERT N. SPANBAUER, Lt Col, USAF
Chief, System Avionics Division
AF Avionics Laboratory

ABSTRACT

This document is an interim report describing the development of optical couplers for use in an eight station EMI/EMP resistant avionic data bus being developed on this program. Airborne avionics systems are moving toward the use of party line multiplex data buses for the transmission of the growing number of digital signals found in modern aircraft. Optoelectronic technology provides a data bus interface system consistent with military requirements that is potentially superior to wire techniques--particularly in the areas of ground loop noise immunity and EMI/EMP sensitivity. Passive optical directional couplers are required in an optoelectronic data bus so that each station can receive optical signals from the bus and transmit optical signals onto the bus. By this means, each station on the bus can communicate with every other station. The report identifies the basic optical loss and attenuation mechanisms that affect the quality of optical couplers and describes the techniques developed to minimize these losses. Since low-loss fiber optic bundle terminations are required at all optical interfaces, this topic is discussed separately. Conventional terminations are described which have losses of 34.8%; compression techniques are described that reduce the loss to 24.4%. The report also describes the design, fabrication and evaluation of two versions of a duplex T coupler and one radial coupler. An improved version of the radial coupler is described and recommended for use in the EMI/EMP resistant data bus.

TABLE OF CONTENTS

SECTION	TITLE	PAGE
I	INTRODUCTION AND SUMMARY	1
II	FIBER OPTIC BUNDLE TERMINATIONS	7
	A. DIMENSIONAL MEASUREMENTS	7
	B. CONVENTIONAL TERMINATIONS	18
	C. FIBER BUNDLE INTERFACES	22
	D. ETCHED TERMINATIONS	25
	E. COMPRESSED TERMINATIONS	29
III	PASSIVE COUPLER DEVELOPMENT	47
	A. ANALYSIS	49
	1. T Coupler	53
	2. Radial Coupler	57
	3. T/Radial Comparison	59
	B. SCRAMBLER DESIGN	67
	C. GENERAL CONSIDERATIONS	81
	1. Radiation Resistance/EMI/EMP	81
	2. Thermal	83
	3. Mechanical	86
	4. Index Matching	87
	D. EVALUATION	91
	1. T Coupler	91
	2. Radial Coupler	111
	3. T/Radial Comparison	134
IV	CONCLUSIONS AND RECOMMENDATIONS	141
APPENDIX I	GEOMETRICAL MODEL OF CLAD FIBER	145
	A. GENERAL THEORY	145
	B. OPTICAL LOSSES	150
APPENDIX II	IN-LINE DATA BUS ANALYSIS	153
APPENDIX III	RADIAL DATA BUS ANALYSIS	159
	References	165

LIST OF ILLUSTRATIONS

FIGURE	TITLE	PAGE
1	Passive Couplers	4
2	Number of Fibers That Can Fit Into A Circular Ferrule	8
3	Precision Funnel	10
4	Diameter Relationships	13
5	Core/Cladding Contrast	16
6	End-Push and Side-Push Compression Fixtures	34
7	Compressed Termination Side-Push Fixture	36
8	Y-Push Circular Compression Fixture	38
9	Y-Push Hexagonal Compression Fixture	40
10	Y-Push Compression Fixture Support, Side View	41
11	Y-Push Compression Fixture Support, Top View	42
12	Compressed Termination Y-Push Circular Fixture	44
13	Compressed Termination Y-Push Hexagonal Fixture	46
14	Uniform Duplex Data Bus Loop	48
15	Uniform Duplex T Coupler	49
16	Radial Duplex Data Bus	50
17	Duplex Radial Coupler	52
18	Bipolar and Unipolar Manchester	62
19	Effect of Noise and Drift	64
20	Signals in a Direct Coupled Receiver	65
21	Scrambler Rod	67

LIST OF ILLUSTRATIONS (continued)

FIGURE	TITLE	PAGE
22	Scrambler Rod Operation	70
23	Power Distribution in a Cylindrical Scrambler Rod	74
24	Power Distribution in a Rectangular Scrambler Rod	76
25	Optical Layout of T Coupler	94
26	Slotted Glass Rod Coupler Body	95
27	Coupler Termination Hardware	96
28	Experimental T Coupler	98
29	T Coupler, Top View	99
30	T Coupler Slotted Rod, End View	101
31	Split Rod Coupler Body	106
32	Split Rod T Coupler, Top View	107
33	Split Rod T Coupler, Side View	108
34	T Coupler Split Rod, End View	110
35	Fiber Optic Radial Coupler	112
36	Radial Coupler, Front View	113
37	Radial Coupler, Exposed View	114
38	Side Arm Subassembly	115
39	Measurement of T_*	118
40	Front Surface Reflections at Mirror	121
41	Front Surface Reflection at Scrambler Exit	122
42	Rectangular Radial Coupler	128

LIST OF ILLUSTRATIONS (continued)

FIGURE	TITLE	PAGE
43	Rectangular Ferrule	129
44	Calculation of $T_{\square*}$	130
45	Clad Glass Fiber	146
46	Core/Cladding Boundary	147
47	Skew Ray in a Clad Glass Fiber	150
48	Signal Power Relationships in an In-Line Data Bus	154
49	Signal Power Relationships in a Radial Data Bus	160

LIST OF TABLES

TABLE	TITLE	PAGE
I	Number of Fibers in Standard Diameter Bundles	9
II	Evaluation of Galileo Fiber Optic Bundle	14
III	Passive Coupler Terminations Physical Dimensions	20
IV	Passive Coupler Terminations Optical Transmission	21
V	Front Surface Reflection With Index Matching	25
VI	Fiber Optic Bundles	77
VII	Coupler Designs For 8 Station Data Bus	82
VIII	Slotted Rod T Coupler Performance Comparison	103
IX	Radial Coupler Side Arm Transmission	116
X	Measured T_* For Radial Coupler No. 1	119
XI	Measured T_* For Radial Coupler No. 2	119
XII	Radial Coupler Performance Summary	125
XIII	Data Bus System Comparison	140

LIST OF SYMBOLS

SYMBOL	PAGE	DEFINITION	UNIT
a	18	Fiber optic attenuation	--
a_m	58	Fiber optic attenuation for maximum path length	--
a_o	55	Average fiber optic attenuation between data bus stations	--
C_{opt}	58	Optimum value of C_T	--
C_T	51	T coupler coupling factor	--
C_*	51	Radial coupler coupling factor	--
$C_{\square*}$	131	Rectangular radial coupler coupling factor	--
d	8	Fiber diameter	mil
D	9	Bundle diameter	mil
\varnothing	12	Solid diameter of bundle	mil
D_d	27	Diameter of disc	mil
D_f	10	Funnel or ferrule diameter	mil
D_r	22	Glass rod diameter	mil
D_{RT}	57	Worst case dynamic range for an in-line data bus	--
D_s	70,75	Diameter or diagonal of scrambler	in
D_{R*}	59	Worst Case dynamic range for a radial data bus	--
G	19	Geometrical area coverage of fibers in a termination	--
G_{180}	120	Geometrical area coverage of fibers in a 180mil dia. termination	--
H	39	Distance between flats in the Y-push hexagonal compression fixture	mil

LIST OF SYMBOLS (continued)

SYMBOL	PAGE	DEFINITION	UNIT
L	12	Length, general	in
L_s	67	Length of scrambler rod	in
G_{66}	117	Geometrical area coverage of fibers in a 66mil dia. termination	--
G	129	Geometrical area coverage of fibers in a rectangular ferrule	--
L	58	Total length of data bus	ft
m	3	Overall quality factor of a passive coupler	--
m_C	53	Side arm quality factor of a T coupler	--
m_L	54	LED quality factor	--
m_T	53	Transmission quality factor of a T coupler	--
m_*	57	Quality factor of a radial coupler	--
m_{D*}	132	Quality factor of a rectangular radial coupler	--
n, n_1, n_2	2	Index of Refraction	--
N	8,55	Integer, number of stations, number of fibers	--
NA	68	Numerical aperture	--
NA_s	68	Numerical aperture of scrambler	--
NA_ϕ	69	Numerical aperture of light	--
NR	149	Number of core/cladding reflections per unit length	--
P	18	Packing fraction	--

LIST OF SYMBOLS (continued)

SYMBOL	PAGE	DEFINITION	UNIT
P_a	49	Power at entrance port of a T coupler	μW
P_{i1}	55	LED power at station 1	μW
P_{oN}	55	Detector power at station N	μW
P_t	49	Power at exit port of a T coupler	μW
P_1	121	Optical power, general	μW
R	8	Ratio of bundle diameter to fiber diameter	--
R	24	General front surface reflectivity	--
R_a	17	Ratio of core area to fiber area	--
R_c	16	Core glass front surface reflectivity	--
R_{cl}	16	Cladding glass front surface reflectivity	--
R_m, R_{m1}, R_{m2}	117	Reflectivity of a mirror in a radial coupler	--
R_{pT}	55	Worst case fractional power ratio for an in-line data bus	--
R_{p*}	58	Worst case fractional power ratio for a radial data bus	--
R_s	100	Scrambler rod front surface reflectivity	--
S	48	Symbol for scrambler in passive coupler figures	--
t_s	27	Thickness of material etched off of disc	cm
T_c	20	Transmission of conventional termination	--
T_c	23	Core/air transmissivity ($1-R_c$)	--
T_d	27	Thickness of disc	cm
T_{fk}, T_{fN}	58	Fiber termination transmission at radial coupler interface	--

LIST OF SYMBOLS (continued)

SYMBOL	PAGE	DEFINITION	UNIT
T_s	116	Transmission of the side arms in a radial coupler	--
T_T	51	Transmission of a T coupler	--
T_1, T_2, T_3	18	Transmission of fiber optic bundles	--
T_{46}	21	Value of T_c for a 46mil diameter bundle	--
T_{65}	21	Value of T_c for a 65mil diameter bundle	--
T_{66}	21	Value of T_c for a 66mil diameter bundle	--
T_{180}	21	Value of T_c for a 180mil diameter bundle	--
T_{188}	21	Value of T_c for a 188mil diameter bundle	--
T_*	51	Transmission of a radial coupler	--
$T_{\square*}$	130	Transmission of the rectangular radial coupler	--
W	12	Weight, general	g
x	151	Distance, general	

LIST OF GREEK SYMBOLS

SYMBOL	PAGE	DEFINITION	UNIT
α	58	Loss coefficient of fiber optic bundle	m^{-1}
Δ	22	Displacement between glass rods	mil
ρ	12	Density	g/cm^3
θ_1	68	Angle of ray in medium of index n_1	degree
θ_2	71	Angle of ray in medium of index n_2	degree
θ_3, θ_4	146	Ray angles, general	degree
θ_{1m}	148	Maximum value of θ_1	degree
θ_{2m}	147	Maximum value of θ_2	degree
θ_c	146	Critical angle for total reflection	degree
λ	151	Wavelength of light	nm

SECTION I

INTRODUCTION AND SUMMARY

The primary objective of this program is the design, development and demonstration of an EMI/EMP resistant avionic data bus. The data bus will consist of eight terminals with each terminal providing the basic multiplex terminal unit (MTU) functions. The data bus system will feature plugable optical interfaces with a bit rate of 10M bit/s.

The principal technology-related task in this research and development program concerns the design, fabrication, and evaluation of passive optical directional couplers. The significance of this task is magnified by the lack of previous concentrated effort in this technology area. Signal coupling devices are required in an optoelectronic data bus so that each station can receive signals from the bus and transmit signals onto the bus. By this means, each station on the bus can communicate with every other station. System reliability considerations exclude the use of repeaters in optoelectronic data buses. Thus, low-loss passive optical couplers are a basic requirement for data bus construction. While much of the basic technology for passive coupler fabrication is available, specific efforts to construct practical devices has been limited^{1,2}. By contrast, other aspects of optoelectronic data bus system design have been explored on at least a preliminary basis^{3,4}.

This report describes the passive optical coupler development task performed on this program. The effort may be broken down into two related but relatively independent activities:

- termination of fiber optic bundles, and
- design, fabrication and testing of passive optical couplers.

The construction of low-loss passive couplers depends on success in both of these activities. The terminations are important because the

optoelectronic data bus consists of flexible fiber optic bundles which interconnect the various stations. Thus, at each interface where optical signals are coupled from the passive coupler onto the bus, the light must pass through a fiber optic termination. The optical attenuation (loss) in the termination can be the major portion of the total loss associated with the passive coupler. Fiber optic bundle terminations are also involved in the LED/coupler interface and the photodiode/coupler interface.

The losses in a fiber optic bundle termination are made up of

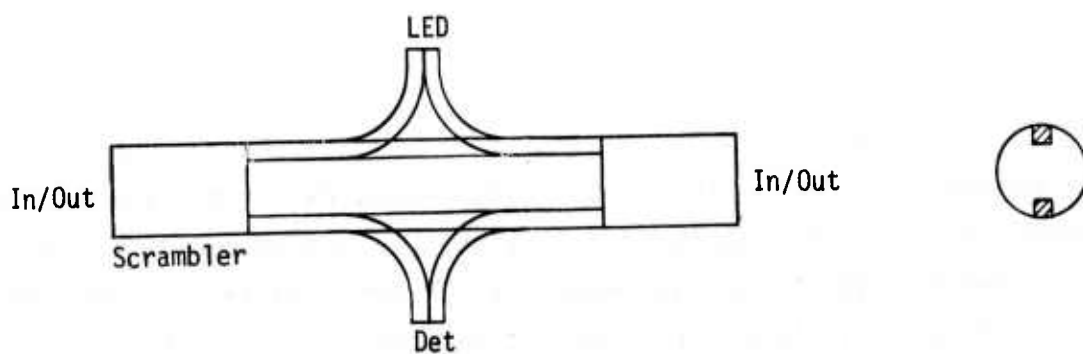
- front surface reflection loss from the core glass, and
- packing fraction loss due to core/fiber area ratio and packing of fibers in the ferrule.

The experimental work on this program has all been done using fiber optic bundles manufactured by Galileo Electro-Optics. However, the techniques developed should be generally applicable to all kinds of fiber optic bundles. The Galileo product has a lead glass core ($n = 1.625$) with a borosilicate glass cladding ($n = 1.48$); the core/fiber diameter ratio is about 19/21. For conventional closely packed terminations in which the fibers are epoxied into a ferrule, the transmission of typical terminations is between 0.60 (-2.22dB) and 0.657 (-1.83dB) for bundle diameters of 46mil and 180mil respectively. The total loss in conventional terminations can be partitioned as follows:

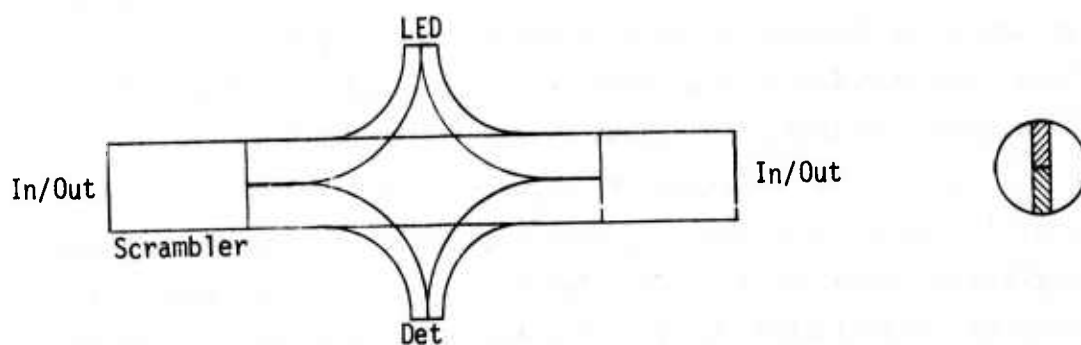
Front surface reflection	-0.26dB
Core/fiber area ratio	-0.87dB
Packing of fibers in ferrule, 180mil	-0.70dB
66mil	-0.75dB
46mil	-1.09dB

Techniques for reducing these losses were evaluated on the program. The front surface reflection loss can be essentially eliminated by using index matching at the optical interfaces. Removal of the cladding glass in the area of the termination by controlled etching could eliminate the core/fiber area ratio loss. Etching experiments have been performed and results are reported; however, a useful process was not achieved. Techniques for compressing the ends of fiber optic bundles to improve the packing density of the fibers in the ferrule have been evaluated. A compressed termination has been achieved in which the fiber packing loss is reduced to 0.08dB. The report also describes two complimentary and useful techniques for measuring the diameter of fiber optic bundles. One of the techniques also gives an accurate value of the average diameter of the individual glass fibers in the bundle.

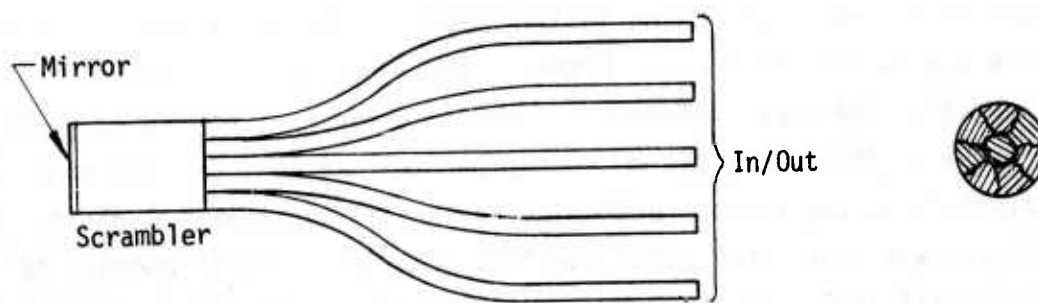
The effort on design, fabrication, and testing of passive optical couplers was concerned with both duplex T couplers and radial couplers as shown in Figure 1. Two types of T couplers were constructed and evaluated; both used solid glass rods for the through transmission path and fiber optic bundles for the LED and photodiode side arms. In one T coupler design, the central rod is slotted to provide space for the side arm fibers. The other T coupler design uses a split rod which allows the side arm fibers to be positioned across a diameter of the central transmission path. The couplers may be compared in terms of an overall quality factor, m , which is a measure of the total losses in the coupler. The split rod T coupler gave the best performance. Without the use of index matching materials, the quality factor in the best coupler is measured to be -1.40dB -- this value can be reduced by the use of index matching materials at the various optical interfaces. An eight-arm radial coupler was fabricated using 66mil diameter fiber optic bundles as the radial arms. The measured quality factor of the best radial coupler is -5.65dB.



a. Slotted Rod T Coupler



b. Split Rod T Coupler



c. Radial Coupler

Figure 1. Passive Couplers

The radial coupler loss will only be experienced one time for any transaction on the data bus. Using T couplers in an in-line data bus, a transaction between the two stations at opposite ends of the bus will experience the T coupler loss $N-1$ times, where N is the number of stations. System calculations for both in-line and radial data buses are presented which include the effects of all losses. For an in-line 8 station 100ft data bus, the loss in the worst case transmission path is -61.82dB. The corresponding worst case loss for a radial data bus is -39.17dB. From this comparison, a radial system is proposed for use in the EMI/EMP resistant data bus. Based on the results of this development effort, an improved radial coupler design is presented that is proposed for use in the data bus. This radial coupler makes use of index matching, rectangular geometry and solid side arms to overcome many of the deficiencies of the couplers constructed during this development effort.

SECTION II

FIBER OPTIC BUNDLE TERMINATIONS

Several types of fiber optic bundle terminations have been investigated on this program. All of the fiber optic bundles used on this program are clad glass fibers manufactured by Galileo Electro-Optics Corporation. Each fiber is composed of a solid lead glass core with $n = 1.625$ and a borosilicate cladding with $n = 1.48$. The diameter of individual glass fibers is nominally 2.5mil. The most basic termination studied is the conventional termination in which the fiber optic bundle is epoxied into a tightly fitting ferrule and then polished on the end to achieve a flat and optically smooth surface. Terminations of this type exhibit loss over and above the normal length dependent attenuation (approximately 0.2dB/ft). The termination loss results from

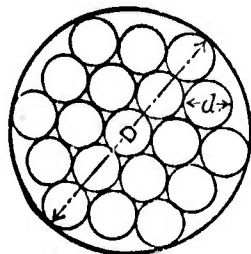
- front surface reflection from the core glass,
- the optically inactive area of the cladding glass, and
- dead space between the individual glass fibers.

Various techniques have been investigated to reduce or eliminate these three sources of optical loss which have lead to more complex terminations and termination procedures. An etched termination has been studied which removes the cladding glass in the vicinity of the termination; a compressed termination uses heat and pressure to reduce the dead space between fibers; and index matching fluids have been used to reduce the front surface reflection at optical interfaces.

A. DIMENSIONAL MEASUREMENTS

One of the most fundamental requirements in working with fiber optic bundles is to be able to measure the important physical

Figure 2. Number of Fibers That Can Fit Into a Circular Ferrule



N = number of fibers

R = ratio $\left(\frac{D}{d}\right)$

D = bundle diameter

d = fiber diameter

Approximate Formulas

$$N = .907(R-.94)^2 + 3.7 \quad R = .94 + \left(\frac{N-3.7}{.907}\right)^{\frac{1}{2}}$$

N	R	N	R	N	R	N	R	N	R
2	2.00	34	6.76	130	12.80	290	18.75	600	26.65
3	2.15	35	6.86	135	13.06	295	18.90	610	26.86
4	2.41	36	7.00	140	13.26	300	19.05	620	27.07
5	2.70	37	7.00	145	13.49	310	19.35	630	27.28
6	3.00	38	7.08	150	13.72	320	19.65	640	27.49
7	3.00	39	7.18	155	13.95	330	19.94	650	27.70
8	3.31	40	7.31	160	14.17	340	20.23	660	27.91
9	3.61	41	7.39	165	14.39	350	20.52	670	28.12
10	3.80	42	7.43	170	14.60	360	20.81	680	28.33
11	3.92	43	7.61	175	14.81	370	21.09	690	28.54
12	4.05	44	7.70	180	15.01	380	21.36	700	28.75
13	4.23	45	7.72	185	15.20	390	21.63	720	29.14
14	4.41	46	7.81	190	15.39	400	21.90	740	29.52
15	4.55	47	7.92	195	15.57	410	22.17	760	29.90
16	4.70	48	8.00	200	15.75	420	22.44	780	30.28
17	4.86	49	8.03	205	15.93	430	22.70	800	30.65
18	5.00	50	8.13	210	16.11	440	22.96	820	31.02
19	5.00	55	8.21	215	16.29	450	23.21	840	31.39
20	5.18	60	8.94	220	16.46	460	23.47	860	31.75
21	5.31	65	9.25	225	16.63	470	23.72	880	32.11
22	5.49	70	9.61	230	16.80	480	23.97	900	32.46
23	5.61	75	9.93	235	16.97	490	24.21	920	32.80
24	5.72	80	10.20	240	17.14	500	24.45	940	33.14
25	5.81	85	10.46	245	17.30	510	24.68	960	33.48
26	5.92	90	10.73	250	17.46	520	24.91	980	33.82
27	6.00	95	11.15	255	17.63	530	25.13	1000	34.15
28	6.13	100	11.34	260	17.79	540	25.35	1100	35.75
29	6.23	105	11.60	265	17.95	550	25.57	1200	37.30
30	6.40	110	11.85	270	18.11	560	25.79	1300	38.80
31	6.44	115	12.10	275	18.27	570	26.01	1400	40.20
32	6.55	120	12.34	280	18.43	580	26.23	1500	41.60
33	6.70	125	12.57	285	18.59	590	26.44	1600	42.95

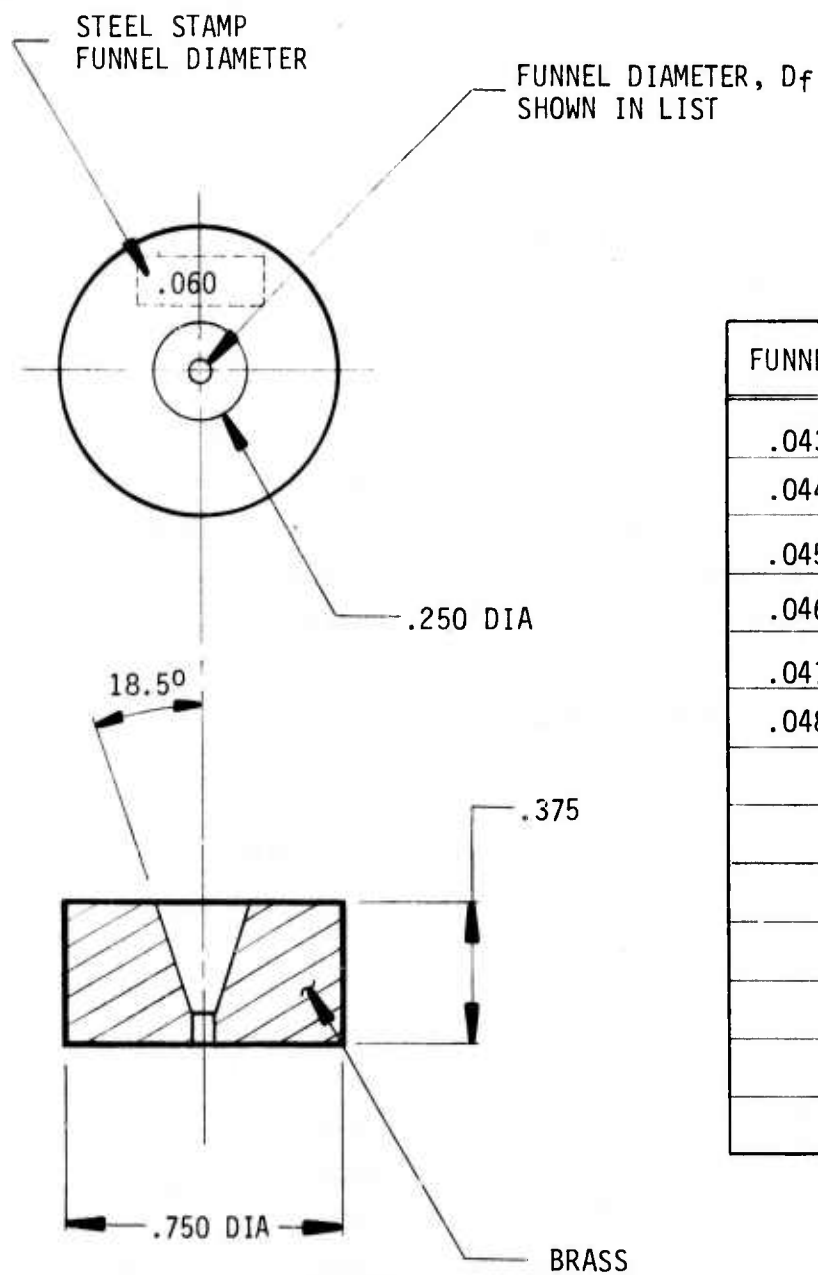
dimensions of the bundle and the individual fibers. The bundle diameter is one of the most important dimensions.

Figure 2 is a mathematical table which indicates how many fibers of outside diameter d can be fitted into a bundle of diameter D . The concept of the diameter of a fiber optic bundle refers to the smallest practical ferrule diameter which will encompass the bundle of fibers. If the diameter of the individual fibers and the number of fibers were accurately known, the bundle diameter could be obtained from Figure 2. The number of fibers is known; however, the diameter of the individual fibers varies within a bundle and from bundle to bundle. Table I shows the number of 2.5mil diameter fibers specified by Galileo for various standard bundle diameters. The fiber count is carefully maintained;

Table I. Number of Fibers in Standard Diameter Bundles-Galileo

Diameter (in)	Number of Fibers
.031	129
.046	285
.062	505
.093	1,131
.125	2,007
.187	4,512
.250	8,018
.312	12,526
1.000	128,232

however, the bundle diameter depends on the diameters of the individual fibers and should be used only as a nominal value.



FUNNEL	DIAMETER	D_f
.043	.060	.173
.044	.062	.175
.045	.063	.176
.046	.064	.177
.047	.065	.178
.048	.066	.180
	.067	.182
	.068	.184
		.185
		.186
		.187
		.189
		.191

Figure 3. Precision Funnel

With a nominal diameter of 2.5mil, the individual fibers are too small to be accurately measured by conventional mechanical techniques. A measurement of this type would be further complicated by the variation in size between the fibers in a given bundle. For these reasons, direct measurement of individual fibers is not recommended as a useful technique for users of fiber optic bundles.

A direct measure of the bundle diameter may be made using a set of precision funnels of the type shown in Figure 3. A set of these funnels has been constructed in 1.0mil diameter increments; the range of sizes is not continuous but is bunched around the standard bundle diameters used on this program. The bundle diameter obtained with a set of precision funnels is somewhat technique dependent. However; this measurement is valuable because it experimentally determines the minimum practical ferrule diameter that can be used with a particular fiber optic bundle.

The measurement technique used with the precision funnels begins by dipping the end of the fiber bundle in deionized water and agitating the bundle until all fibers are wet and standing apart in the water. As the bundle is withdrawn from the water, capillary action pulls the fibers together like the bristles in an artist's paint brush. At this point the bundle is oversize because it holds a considerable amount of excess water; however, the water does serve as a lubricant and helps to order and align the various fibers. As the water evaporates, surface tension pulls the fibers together and the bundle becomes very rigid. It is felt that this rigid condition is associated with a minimum bundle diameter. The removal of excess water from the fiber bundle can be accelerated by inserting the wet bundle into the largest precision funnel and then progressing through the remaining funnels in sequence until the smallest funnel that will accommodate all of the fibers in the bundle has been found. This procedure also helps to order and align the fibers in the bundle. Even with this technique, the packing fraction of the uncompressed fiber optic bundle at the point of measurement is not as high as it should be to match the

numbers in Figure 2. This residual discrepancy is felt to be the result of three factors

- a thin film of water on the individual fibers,
- incomplete ordering of fibers in the funnel, and
- inconsistent ordering to accommodate diameter variations between individual fibers.

Using this technique, four 25 ft lengths of "187mil diameter" fiber optic bundle were measured to have practical bundle diameters of 189mil, 187mil, 177mil and 177mil.

Another technique for measuring the area of fiber optic bundles was developed that provides additional data that compliment the funnel measurements. This technique uses a precision balance to weigh a known length of fiber optic bundle (glass fibers only). With this information and the density of the glass fibers, the total cross sectional area of the fibers can be calculated. The density of the glass fibers can also be measured with good accuracy using the same precision balance. This technique is capable of accuracies of a few tenths of one percent (~.2%). The density of Galileo glass fibers has been measured to be

$$\rho = 3.2778\text{g/cm}^3 \quad (1)$$

Using this figure for density, an equation has been developed for the solid diameter, D , of the fiber optic bundle. This solid diameter defines the smallest circle that the bundle could be compressed into if all space between the fibers were removed.

$$D = 153.96(W/L)^{\frac{1}{2}} \quad (2)$$

where

D is the solid diameter in mils,

W is the weight in grams, and

L is the length in inches.

If the number of glass fibers in the bundle is known, the average fiber diameter, d , can be calculated from

$$d = \frac{D}{N^{\frac{1}{2}}} \quad (3)$$

When both d and N are known, the bundle diameter, D , can be determined from the table and equations shown in Figure 2. Figure 4 shows the relationships among the three diameters d , D and D .

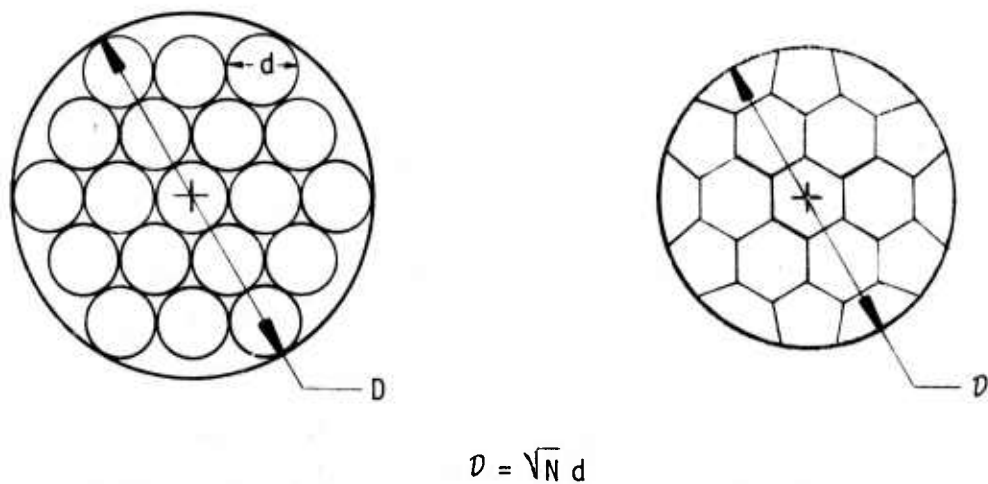


Figure 4. Diameter Relationships

The weighing technique was used to measure various pieces of Galileo fiber optic bundle. The results are shown in Table II along with the diameter measured with the funnel for the large diameter bundles. Comparison of the funnel diameter, D_f , and bundle diameter,

D, show that, on average, D_f is 3.5mils larger than D. Thus, a practical ferrule diameter is about 2% greater than the theoretical bundle diameter measured by the weighing technique.

Table II. Evaluation of Galileo Fiber Optic Bundle

Nominal Diameter (mil)	Funnel Diameter D_f (mil)	\bar{D} (mil)	d (mil)	D (mil)
187	189	174.8	2.602	185.9
187	187	173.1	2.577	184.1
187	177	162.4	2.417	172.7
187	177	162.9	2.425	173.3
46	-	41.58	2.463	45.79

This precise and accurate method for determining the various significant diameters of a fiber optic bundle has been useful in several different areas of passive coupler development.

- For compressed terminations, the technique specifies the diameter of the compression fixture and the scrambler rod.
- For uncompressed terminations, the technique allows accurate prediction of the transmission of the termination.
- The technique can form the basis of more accurate specification and control of fiber optic bundle diameter

The geometrical optical model of a clad glass fiber is presented in Appendix I. The discussion shows how total internal reflection at the core/cladding interface makes it possible to achieve low-loss

transmission in the core of the fiber. The cladding on the fiber is also surrounded by a lower index medium (air, $n=1.0$) over much of its length. This provides total internal reflection at the cladding/air interface and under certain conditions makes it possible to transmit light through the entire cross sectional area of the fiber -- core and cladding. In most cases the cladding touches other fibers and the jacketing material; also, dust and other foreign substances on the surface of the cladding layer act as scattering centers and remove light from the cladding. Thus, the cladding glass has higher attenuation than the core glass and significant transmission in the cladding can normally be achieved only over distances of a few feet. Transmission through the cladding can provide a significant performance improvement in passive couplers where fiber optic bundle lengths of a few inches are normally used.

In the termination region, the fibers are surrounded by an epoxy which normally has an index of refraction between 1.49 and 1.62 which is higher than the index of the cladding glass ($n=1.48$). Because of the presence of this epoxy, there is no total internal reflection at the outer surface of the cladding. Thus, the epoxy used in a conventional termination effectively couples light out of the cladding glass at each end of a fiber optic bundle and optical transmission through the cladding glass is negligible. In certain special cases it is possible to use a low index material like Sylgard ($n=1.43$) in the termination region and achieve useful transmission in the cladding layer. However, in the general case the cladding glass does not transmit light and the cross sectional area of the cladding glass represents a major part of the loss in a conventional termination.

Direct observation of the polished ends of conventional terminations provide a direct measurement of the cladding glass thickness as a fraction of the fiber diameter, d . This important parameter is conveniently expressed as the ratio of core diameter to fiber diameter.

The core cladding interface is visible with front surface illumination in a high power microscope because of the difference in front surface reflection due to the difference in index of refraction. For Galileo fibers the core glass has $n = 1.625$ and the cladding glass has $n = 1.48$. The two front surface reflectivity values are

$$R_c = \left(\frac{1-n}{1+n} \right)^2 = .0567 \quad (\text{core}) \quad (4)$$

$$R_{cl} = .0375 \quad (\text{cladding}) \quad (5)$$

This gives a reflectivity ratio of

$$\frac{\text{core}}{\text{cladding}} = \frac{.0567}{.0375} = 1.521 \quad (6)$$

with the core appearing lighter than the cladding as shown in Figure 5.

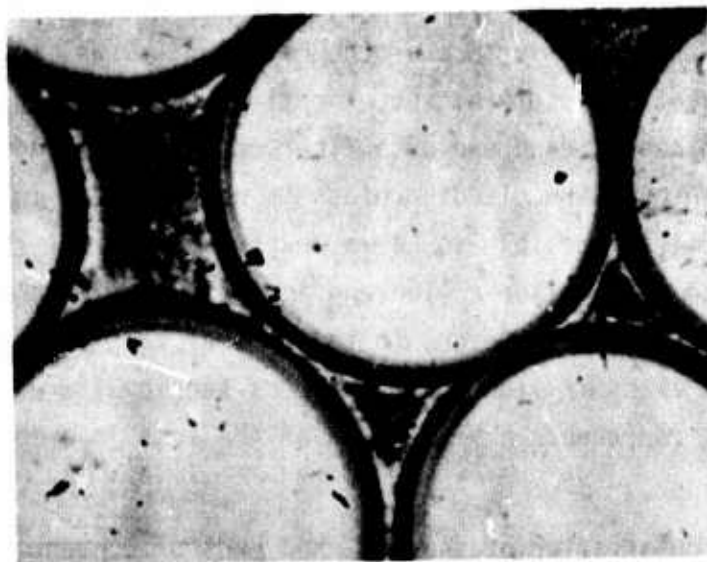


Figure 5. Core/Cladding Contrast

The core/fiber diameter ratio was measured to be 19/21 for several different Galileo fiber optic bundles; the ratio is consistent even for fibers having different diameters. This measured diameter ratio gives a core/fiber area ratio, R_a , of

$$R_a = \left(\frac{19}{21}\right)^2 = 0.8186 \quad (7)$$

For a nominal fiber diameter of 2.5mil and a 19/21 diameter ratio the nominal core diameter is 2.262mil which gives a cladding thickness (radius) of 0.119mil or 3.02 μ m. The area ratio, R_a , could be increased by reducing the thickness of the cladding glass. However, the thickness of the cladding glass is one of the important factors in determining the attenuation of the fiber. Appendix I shows how a thinner cladding layer leads to higher attenuation in the fiber. For uncompressed terminations, Figure 2 shows that a bundle of smaller diameter fibers has a better area coverage than the same bundle diameter made from larger fibers. However, for constant core/cladding diameter ratio, the smaller fibers have less cladding thickness and therefore have higher attenuation. Small fibers also have more core/cladding interface reflections per unit length than large fibers, see Appendix I. This effect also leads to an increase in attenuation due to increased scattering loss for smaller diameter fibers.

The selection of fiber diameter and cladding thickness is normally made by the fiber optic bundle manufacturer. The choices are based on a series of tradeoffs which involve such things as cost, reproducibility, the absorption of the glass being used in the fibers and the performance requirements of the intended market. In general, the fiber diameter and cladding thickness choices that give the highest (best) packing fraction also give the highest (worst) attenuation. The design of the present Galileo fiber optic bundle with a 2.5mil fiber diameter and a 3 μ m cladding thickness seems to offer a good compromise for short distance optoelectronic data transmission with a 0.9 μ m light.

B. CONVENTIONAL TERMINATIONS

Two short fiber optic bundles were made from the 187mil diameter bundle (funnel measurement) for the purpose of evaluating the measured performance of conventional terminations. These two bundles have lengths of 6.25in and 62.5in; the ferrules used have an inside diameter of 188.5mils. The epoxy used in the terminations has $n = 1.52$ which is higher than the index of the cladding glass used in Galileo fibers ($n = 1.48$). The epoxy effectively couples the light out of the cladding, so no light is transmitted through the cladding in either bundle. This has been experimentally verified by microscopic examination of the termination with transmitted white light. The measured transmission of the short fiber bundle is 0.60 and the long fiber bundle is 0.47. Both of the fiber bundles have a good quality end finish. If the loss mechanisms are represented by transmission factors then the total transmission, T_1 , for the 6.25in fiber can be expressed as

$$T_1 = (1-R_c)^2 Pa = 0.60 \quad (8)$$

where R_c is the front surface reflectivity given by Eq (4), $R_c = .0567$.

P is the packing fraction

a is the attenuation of the 6.25in length.

The transmission of the 62.5in fiber, T_2 , is given by

$$T_2 = (1-R_c)^2 Pa^{10} = 0.47 \quad (9)$$

combining Eqs (4), (8) and (9) gives two simultaneous equations in two unknowns

$$Pa = 0.6743 \quad (10)$$

$$Pa^{10} = 0.5282 \quad (11)$$

Solutions of Eqs (10) and (11) give

$$a = .97585 \quad (12)$$

$$P = .69100 \quad (13)$$

From Eq (12) the loss factor of the fiber is 0.2dB/ft which is the expected value for Galileo fiber optic bundles. The packing fraction in Eq (13) is made up of two parts; the geometrical area coverage of the fibers, denoted by G , and the core/fiber area ratio, denoted by R_a . The area coverage of the fibers is given by

$$G = \left(\frac{D}{D_f} \right)^2 \quad (14)$$

where D is the solid diameter shown in Table II and D_f is the internal diameter of the ferrule.

Thus, from Table II

$$G = \left(\frac{173.1}{188.5} \right)^2 = .8433 \quad (15)$$

Combining Eqs (12) and (14) gives

$$R_a = \frac{.6910}{.8433} = .8194 \quad (16)$$

which is in good agreement with the value $R_a = .8186$ obtained from the direct measurement of the core/fiber area ratio discussed earlier in the report.

From Table II, the ferrule diameter used on these fiber optic bundles is larger than the indicated funnel diameter; thus, the measured transmission is slightly lower than if smaller ferrules had been used. There are four specific fiber optic bundle diameters that are of particular interest in the passive optical couplers constructed on this program:

- the 46mil bundle used for the LED and detector ports in the T couplers,
- the 187mil bundle used with the T couplers in a uniform duplex data bus,
- two combined 46mil bundles used as the eight arms in the radial coupler, and
- sixteen combined 46mil bundles used as the main body of the radial coupler.

Table III shows the relevant physical data assumed for these four bundles; all four are based on the 46mil bundle shown in Table II. The D_f values

Table III. Passive Coupler Terminations
Physical Dimensions

Nom. Size (mil)	Fiber Count	D (mil)	d (mil)	D (mil)	D_f (mil)
46	285	41.58	2.463	45.79	46.71
$\sqrt{2} \times 46$	570	58.80	2.463	64.06	65.34
187	4,512	165.44	2.463	175.96	179.48
$\sqrt{16} \times 46$	4,560	166.32	2.463	176.88	180.42

found in Table III are calculated using

$$D_f = 1.02 D \quad (17)$$

The transmission, T_c , of these four conventional terminations may be calculated from

$$T_c = (1 - R_c) G R_a \quad (18)$$

where R_c is given by Eq (4),

R_a is given by Eq (7), and

G can be calculated from Eq (14).

The results of these calculations are summarized in Table IV. These results

Table IV. Passive Coupler Terminations
Optical Transmission

Nom. Size (mil)	$(1-R_c)$		G		R_a		T_c	
	-	dB	-	dB	-	dB	-	dB
46	.9433	-.26	.7924	-1.01	.8186	-.87	.6119	-2.14
$\sqrt{2} \times 46$.9433	-.26	.8098	-.92	.8186	-.87	.6253	-2.05
187	.9433	-.26	.8497	-.71	.8186	-.87	.6561	-1.84
$\sqrt{16} \times 46$.9433	-.26	.8498	-.71	.8186	-.87	.6562	-1.84

were used in the Introduction and will be used in Section III. The terms T_{46} , T_{65} and T_{180} are used in Section III to refer to the values of T_c shown in Table IV; the subscript denotes the nominal diameter of the fiber optic bundle. The value of $P=GR_a$ shown in Eq (13) gives a measured T_c value of $T_{188} = .6518$.

Two other large diameter bundles made from the 177mil diameter material had incomplete filling by the epoxy in the termination region. These two bundles used 180mil diameter ferrules and had lengths about the same as the two bundles discussed above. In this case the packing fraction is slightly worse than for the 187mil bundles; however, the transmission of both the short and long fiber bundles is slightly higher than for the 187mil bundles. Microscopic examination with transmitted light shows that the fibers that are not surrounded by epoxy are transmitting light through both the core and the cladding. Thus, the incomplete filling with epoxy at each end resulted in about an 8% increase in transmission. This result is potentially useful in

constructing passive couplers. For short distance transmission, the packing fraction of conventional terminations can be increased from about 65% to about 79% by using both the core and cladding to transmit light. This can be accomplished by using a bonding material in the terminations that has a lower index than the cladding glass ($n = 1.48$). Silicone resins such as Sylgard 182 with $n = 1.43$ and cyanoacrylate adhesives such as Rapid-Set with $n = 1.44$ are two materials which meet this requirement. Both materials are recommended for use at temperatures in excess of 125°C . Rapid-Set cures to form a clear solid; unfortunately Sylgard 182 is a gel and is not compatible with optical polishing techniques. A rigid Silicone resin has been identified; however, its index of refraction ($n = 1.47$) is too close to the cladding glass value to give useful total internal reflection at the surface of the cladding glass.

C. FIBER BUNDLE INTERFACES

Misalignment between two fiber bundles or a fiber bundle and a scrambler rod can give rise to an optical loss that is associated with the termination. Equation (19) gives an expression for the overlap area lost when two rods of equal diameter, D_r , are displaced by a small amount Δ .

$$\text{Fractional Lost Area} = \frac{2}{\pi} \left[\sin^{-1} \left(\frac{\Delta}{D_r} \right) + \frac{\Delta}{D_r} \sqrt{1 - \left(\frac{\Delta}{D_r} \right)^2} \right] \quad (19)$$

For small displacements in which

$$\Delta \leq 0.1 D_r \quad (20)$$

Eq(16) reduces to

$$\text{Fractional Lost Area} = \frac{4\Delta}{\pi D_r} = 1.273 \frac{\Delta}{D_r} \quad (21)$$

Thus, for small displacements, the lost area is linear with displacement. For a 187mil diameter, a 0.786% displacement corresponds to 1.47mil and results in a lost area of 1.0%. Equation (21) is very useful in the design of passive couplers because it sets the limits of tolerances needed to achieve adequate alignment between scrambler rods and fiber bundle terminations.

Direct butt joints between conventional terminations on 65mil diameter fiber bundles have been evaluated and compared to a fiber bundle/fiber bundle interface using a scrambler rod. The butt joints show a maximum transmission of about 55% with some rotational sensitivity. The transmission is always higher than the value expected for a worst case alignment between two highly ordered fiber arrays. This suggests that the interface between two disordered arrays of fibers will always contain regions in which the fiber/fiber alignment is good and other regions in which alignment is poor.

Use of a scrambler rod in the fiber bundle/fiber bundle interface reduces the rotational sensitivity. However, the combination of the two added front surface reflection losses and the full termination loss of the receiving fiber bundle causes the transmission to drop to 50% when the scrambler rod is added.

Several index matching fluids have been evaluated in these interfaces, both with and without scrambler rods. These matching fluids have typically been the unpolymerized resin of a Silicone or epoxy system used without adding the hardner or curing agent. The index of refraction has ranged from $n = 1.43$ for Sylgard 184 resin to $n = 1.62$ for an epoxy resin made by the Dow Chemical Co. In general, the use of a matching fluid increases the transmission and the rotational and positional sensitivity. The interface transmission without matching fluid is $T_C^2 = (1 - R_C)^2$; R_C is defined in Eq(4). With an ideal matching fluid the interface transmission is 1.0. Thus, the maximum increase in interface transmission to be expected from the use of index matching fluid is

$$\frac{1 - T_c^2}{T_c^2} (100) = 12\% \quad (22)$$

Apparent improvements both greater and less than this value (9 to 15%) have been observed. Most of this variation can be accounted for by inadequate reproducibility of the physical placement of the parts before and after the fluid is added. However, it is also probable that the measurements are further complicated by the presence of significant multiple reflection and interference effects when the matching fluid is not present.

The general form for front surface reflection for normal incidence is

$$R = \left(\frac{n_1 - n_2}{n_1 + n_2} \right)^2 \quad (23)$$

where n_1 and n_2 are the two values of index of refraction at the interface in question. When Sylgard 184 resin is used as a matching fluid for Galileo fibers, the two index of refraction values are

$$\begin{aligned} n_1 &= 1.43 && \text{(Sylgard 184)} \\ n_2 &= 1.625 && \text{(fiber core)} \end{aligned} \quad (24)$$

For this case, the front surface reflection from Eq(23) is

$$R = .0041 \quad \text{(core/Sylgard)} \quad (25)$$

Table V shows the value of front surface reflection expected for three common index matching fluids. These data indicate that the index of refraction values do not have to be closely matched to achieve a significant reduction in front surface reflection. The Sylgard 184 resin is

Table V. Front Surface Reflection With Index Matching

Matching Fluid	n_1	n_2	R
Air	1.00	1.625	.0567
Sylgard 184	1.43	1.625	.0041
Ablestik Epoxy	1.52	1.625	.0011
Dow Epoxy	1.62	1.625	2.3×10^{-6}

the most desirable index matching fluid for use in military systems. Even though this material has the greatest index mismatch, its viscosity shows very little change with temperature and its useful temperature range is -55°C to $+200^{\circ}\text{C}$. When hardner is added, the Sylgard 184 cures to form a clear resilient Silicone rubber. Thin discs of cured Sylgard 184 can also be used for index matching.

D. ETCHED TERMINATIONS

Various etching experiments to remove the cladding glass from the fibers were performed on the program. The goal of these experiments was the development of a reproducible technique for improving the transmission of fiber optic bundle terminations. While this goal was not achieved, significant progress was made. The results of these etching experiments are presented in this report to document the effort for the use of other workers in this area of technology.

Removal of the cladding glass from the glass fibers by etching would increase R_a from .8186 to 1.0 -- an increase of 22% (0.87dB) in the transmission of the termination (See Table II). The cladding must be removed only for a short length at the ends of the fiber. Thus, the attenuation of the bulk fiber between the terminations would be unaffected and the increased attenuation of the unclad region would be negligibly small due to its short length. Good control of the etch rate is required to make this technique useful. If the fibers are under-etched so that

all of the cladding glass is not removed, the full transmission improvement will not be realized. If the fibers are over-etched, the core glass will be reduced in diameter and the transmission of the termination will drop as the etched bundle diameter gets smaller than the diameter of the interfacing component. In general, controlled under-etching is always preferable to over-etching.

Due to the dissimilar characteristics of the core glass and cladding glass used in the Galileo fibers, it may be possible to formulate an etch solution that would selectively remove the borosilicate cladding without etching the lead glass core. In any case, the etched fibers will be held in place and supported in the ferrule by an epoxy. If a clear epoxy is used that has an index of refraction less than the core glass, then the epoxy will serve as a cladding layer on the unclad portion of the fibers.

A length of 150mil diameter solid clad rod was obtained from Galileo for possible use as scrambler rods in the construction of passive couplers. This solid clad rod contained the same core glass and cladding glass in the same proportion as the 2.5mil diameter fibers in the fiber optic bundles. A piece of the solid clad rod about 1.0in long was masked over half its length with black wax and then submerged in hydrofluoric acid (HF) for about 12 hours. The HF definitely etched the cladding glass and reacted with the lead glass in the core. However, the reaction with the core glass left a solid residue that was not soluble in the etching solution. This solid residue forms a rigid fossil of the core glass that can be removed from the unreacted remnant of the core. In the 12 hour etch time the HF reacted with the glass fiber to a depth of about 60mil. This left a 30mil diameter rod of unreacted core glass at the center of the rod. The depth of the reaction at the end of the rod was about the same as on the sides. This experiment shows that the cladding glass can be etched with HF and that visible solid reaction products form when the HF reaches the lead glass in the core. The solid residue is believed to be lead fluoride (PbF_2), since it is insoluble in HF, but does dissolve in dilute nitric acid.

The etch rate from this experiment is about 5.6 μ m/min. Since the thickness of the cladding glass on the 2.5mil diameter fibers is only 3 μ m, this etch rate is much too rapid for adequate process control.

Since the cladding glass is supposed to be chemically and physically identical to Corning type 7052 glass, some large diameter, thin discs of 7052 glass were obtained, so that thickness changes as a result of etching could be determined by weight changes, using a very accurate metallurgical balance. In order to use this technique, the density of the glass must be known. One published value was found, giving the density as 2.28g/cm³. A check on this value was made by measuring the diameter and thickness of one of the discs, calculating the volume of the disc, and weighting the disc. The resulting value for the density is 2.27g/cm³, less than 0.5% different from the published value.

The diameter of the disc was 1.029inches, and the thickness was 6.97mils. For a disc, the material thickness removed from all surfaces can be related to the weight change by the expression:

$$t_s = \frac{\text{Wt. Change}}{\text{Density}} \cdot \frac{1}{\pi D_d (D_d/2 + T_d)} \quad (26)$$

where t_s = thickness of material removed from each surface

D_d = diameter of the disc

T_d = thickness of the disc

For a disc with a diameter large compared to its thickness, which is the case, here, the expression reduces to

$$t_s = \frac{\text{Wt. Change}}{\text{Density}} \cdot \frac{2}{\pi D_d^2} \quad (27)$$

Using the above expression, several etching experiments were evaluated by weighing the 7052 glass disc before and after etching.

A buffered hydrofluoric acid solution was first tried at room temperature with agitation of the etchant. The etch time was 30 minutes. The etch rate was $1.7\mu\text{m/hr}$. This was considered to be too slow.

A 5% hydrofluoric acid solution yielded an etch rate of $10\mu\text{m/hr}$. A 10% solution yielded an etch rate of $18\mu\text{m/hr}$. To remove a $3\mu\text{m}$ cladding from actual fibers would require 10 minutes. A small bundle of fibers was then etched for 10 minutes in a 10% HF solution. The first observation was that the fibers became extremely fragile when immersed in the etch. Even slight agitation of the bundle caused the fibers to break, even during the first minute of etching. After 10 minutes, the remaining fibers were examined with a metallurgical microscope. Extreme differences in the degree of etching was observed among the individual fibers. Some fibers were etched to diameters of less than one mil, while other fibers appeared to have been etched only slightly or not at all. It was thought that the reaction may have been sufficiently exothermic to have caused heating near the center of the bundle, resulting in excessive etching of fibers in this location.

It was decided that an etch which required heating to achieve an acceptable etch-rate would be less likely to cause non-uniform etching due to an exothermic behavior.

The buffered hydrofluoric solution which had been too slow at room temperature was heated to 50°C , and the etch rate was determined using the 7052 glass disc. The etch rate was $917\mu\text{m/hr}$, so that removal of $3\mu\text{m}$ would require 18.5 minutes.

To further eliminate the possibility of non-uniform etching caused by bundling of the fibers, fibers were laid down side-by-side on the edge of a plate, and held in place by an inert wax. When immersed in the hot (50°C) buffered solution, the breakage problem again occurred. After etching, the fibers which were still attached to the plate were examined. Extreme differences in etch rate were again observed. Small clusters of crystalline material were also present on many fibers.

At this point it was learned that Galileo coats the glass fibers with a lubricant so that they will slide freely against each other and allow bending of the bundle without fiber breakage. A lubricant of the type used could be expected to cause problems when etching with aqueous solutions.

Some fibers from a .045in diameter Galileo bundle were cleaned in one rinse of trichloroethylene, followed by two rinses in acetone. The fibers were attached to a piece of clean silicon (which is inert to the etching solution) using black apiezon wax and were etched in hot (50°C) buffered oxide etch for 10 minutes. The resulting fibers exhibited smooth, uniform surfaces, with no evidence of crystallite clusters on the fibers as had been observed previously when etching experiments were performed on fibers which had not been solvent cleaned. However, a good method for determining the amount of cladding glass removed has not been developed. Comparison of fiber diameters between etched and unetched fibers from the same bundle is not particularly meaningful because of the variation in fiber diameter of the unetched fibers.

Solvent cleaning appears to be beneficial for uniform etching and fiber breakage was not as severe in the solvent cleaned bundle. The results look promising; however, more effort will be required to develop a technique for measuring etch rate on individual fibers.

E. COMPRESSED TERMINATION

Compression of the termination region of a fiber optic bundle to eliminate the dead space between fibers increases G from its uncompressed value to 1.0. Figure 2 and Eq(14) show that the area coverage of the fibers, G , is dependent on the ratio of bundle diameter to fiber diameter, D/d . For a fixed fiber diameter, d , Table IV shows that G has a lower value for small diameter bundles. Thus, using compressed terminations, greater improvements in G are possible for small diameter bundles because there is relatively more dead space in a small diameter bundle than a large diameter bundle of the same fibers. Combining Eq(3) with Eq(14) and the approximate formula for D/d given in Figure 2 gives an

approximate expression for G in terms of the number of fibers in the bundle

$$G \approx \frac{.907N}{\left[.895 + (N-3.7)^{\frac{1}{2}} \right]^2} \quad (28)$$

Equation (28) is accurate to better than 2% for $N \geq 19$. This expression shows that as N increases (larger bundle diameter), G approaches the limiting value of .907. From Table IV the expected improvement in T_c ranges from 26% (1.01dB) for the 46mil diameter bundle to 18% (0.71dB) for the 180mil diameter bundle.

The Galileo fiber optic bundles use two widely different types of glass for the core and the cladding. The core is a high lead glass which has a high index of refraction ($n = 1.625$), a high temperature coefficient and a low melting point. The cladding is a borosilicate glass with a low index of refraction ($n = 1.48$), a low temperature coefficient and a high melting point. One result of this is that the core glass can be liquid at a temperature at which the cladding glass is still solid or only slightly soft. The cladding glass is soft enough to deform and fuse together at 1100°F (~590°C) with pressure.

Tests were performed to soften the glass fibers by direct heat in order to determine the problems associated with forming compressed terminations. Fibers were rapidly heated both with flame and with resistance wire heaters. These rapid heating tests showed that the cladding glass tends to crack as the fibers are heated. This cracking phenomenon can be understood by considering what happens when the fibers are initially formed. As the hot clad fiber is drawn, the cladding glass solidifies and the core glass remains liquid because the cladding glass has a higher softening point temperature than the core glass. In this state, there is little or no stress induced in the glass because stress is relieved by motion of the liquid core. As the core glass cools, its shear strength increases and the stress begins to build up. Since the

fiber is cooling and the core glass has a higher expansion coefficient than the cladding glass the stress causes the core glass to be in tension and the cladding glass to be in compression. Glass is not a true solid but rather a very viscous liquid. Therefore, as it cools there is no specific temperature at which it becomes a solid. Rather, as the temperature of the glass is lowered, the viscosity and strength increase steadily. Thus, even though the fiber appears to be solid, the core continues to move within the cladding to relieve the strain induced by cooling. This process continues down to an effective strain relief temperature at which the shear strength of the core glass is sufficient to withstand the strain induced by further cooling of the fiber. Thus, the net strain in the fibers under use conditions is only due to the difference between ambient temperature and the effective strain relief temperature and the difference in the temperature coefficient between the core glass and cladding glass.

Brittle materials, like glass, are strong in compression and weak in tension. Also, glass breakage is almost entirely the result of cracks propagating into the glass from the surface. Since the surface layer (cladding) of these glass fibers is in compression, the microcracks and other flaws in the surface tend to remain closed and not propagate into the interior of the fiber. The core glass is in tension; however, it is surrounded by cladding glass and thus has no free surface at which cracks can originate. The combination of these effects results in a fiber that is quite strong and stable. If a clad fiber is to be broken with a pure tension force, that force must be sufficient to overcome the built-in compression at the surface and put the surface in tension so that cracks can propagate into the bulk from the natural flaws at the surface of the cladding glass. This same phenomenon is used in "tempering" plate glass used in store windows and glass doors. In the case of "tempered" glass the surface layer is put in compression by an ion-exchange process similar to that used in the production of some self focusing fibers.

In almost all glass forming systems there is a good correlation between optical index, temperature coefficient and melting point. Since all useful fiber optic bundles have the low index of refraction glass at the surface, all fiber optic bundles will have this compressive stress at the surface. This statement is valid for both clad fibers and unclad self-focusing fibers. Clad glass fibers with low NA will tend to be easy to break because of the close match in temperature coefficient between the core glass and cladding glass. This is at least partially offset in the case of Corning low-loss fibers by the high value of effective strain relief temperature and high inherent strength of a nearly pure quartz (SiO_2) system.

As a clad glass fiber is heated, the core expands more rapidly than the cladding; however, the surface stays in compression up to the effective strain relief temperature of the fiber. Thus, rapid heating to above the effective strain relief temperature will cause the cladding glass to crack; the fiber may break even though the core and cladding are both relatively rigid at that temperature. If a clad glass fiber is heated at a point remote from its end, the tendency to crack the fiber is even more severe. Even if the fiber is heated slowly enough for strain relief to occur, the high expansion core glass is still trapped inside a container of the more rigid and low expansion cladding glass. In this case, cracking of the cladding glass and loss of the fiber is almost inevitable. If the clad fiber is heated slowly in a relatively short region which includes the end of the fiber, the cladding glass will be much less likely to crack. These conditions tend to duplicate the conditions which occurred as the fiber cooled after being drawn. One large difference is that the surface strain is always compression when the fiber is cooled whereas the surface strain is always tension when the fiber is heated--regardless of how slowly it is heated. In any event, slowly heating a region of the fiber which includes the end offers the possibility of strain relief that is not present when the fiber is heated rapidly or when the heated region does not include the end of the fiber. This is the basic premise behind the design of the fixtures for compressing and fusing the end of the fiber optic bundle.

When a reproducible etching process is developed for removing the cladding glass from a short length near the end of the fibers, the problems associated with fusing and compressing the end of the bundle are greatly reduced. In this case only core glass is present at the end of the bundle so that heating will not produce any stress in the fibers. Also the lower deformation temperature of the core glass will allow the entire process to be performed at a lower temperature than the 1100°F required for the Galileo cladding glass. Combination of etching, compression and index matching offers the possibility of a termination with a transmission of 1.0 (0.0dB loss).

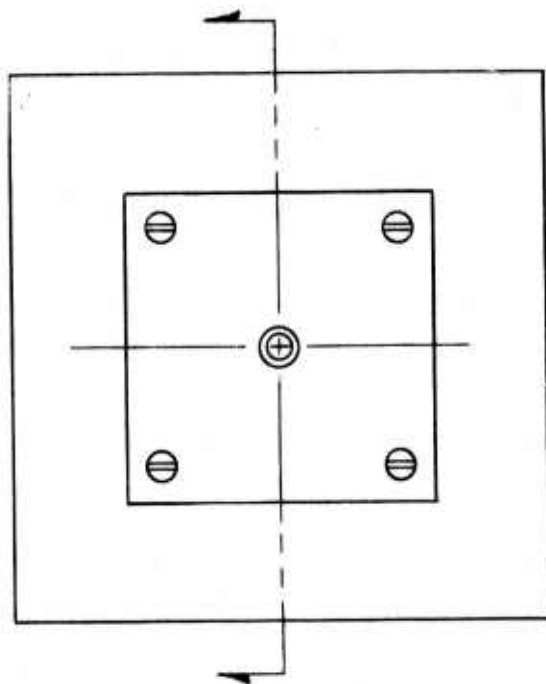
Four different styles of compression fixtures were constructed for this investigation. The first two fixtures are shown in Figure 6.

Inconel was selected as the material for these fixtures because it has a lower value of thermal expansion coefficient than the glass used in the fibers. This difference causes the glass to contract more on cooling and makes it possible to remove the finished termination from the fixture.

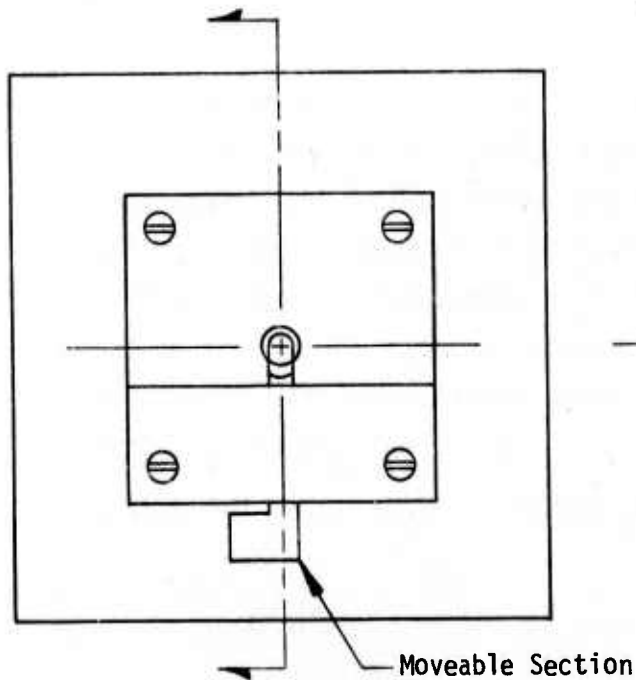
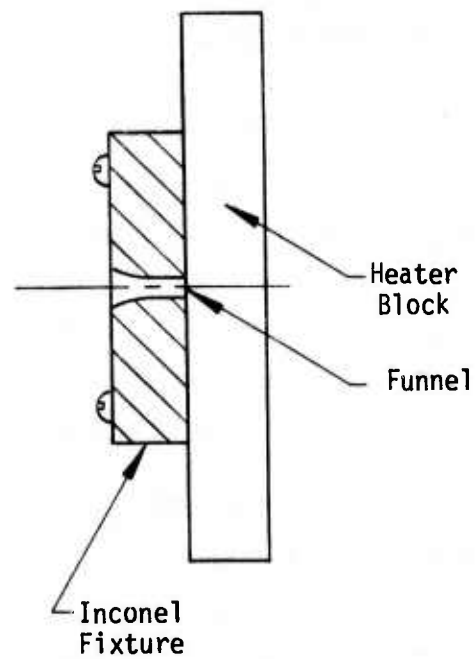
The end-push fixture is basically a funnel with an input diameter of 250mil tapering to a straight section having a diameter of 170mil. The fiber bundle is inserted into the funnel at room temperature and stops at the point at which the funnel diameter is 177mil. The fixture is then heated uniformly to a temperature of 600°C (dull red). The mechanical configuration insures that the end of the fiber bundle is heated first. When the fixture reaches 600°C the fiber bundle is slowly pushed into the funnel until it reaches the heater block.

Some of the significant results achieved with the end-push fixture are:

- Fiber bundles were heated to 600°C without excessive cracking of individual fibers.
- The bundle diameter was successfully reduced from 177mil to 170mil (see Table II).



a. End-Push Fixture



b. Side-Push Fixture

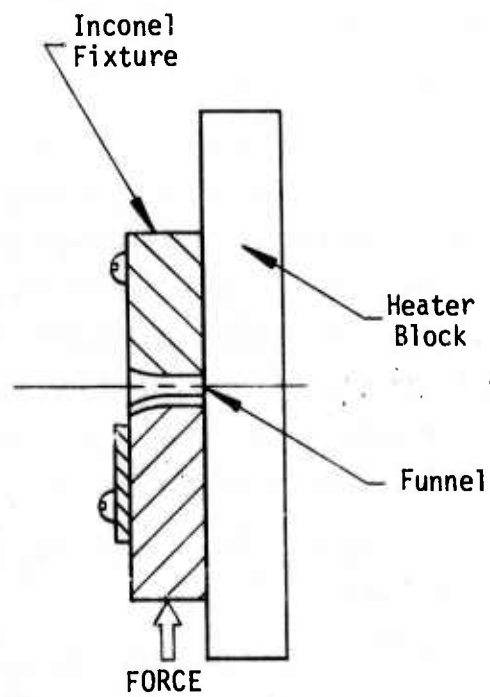


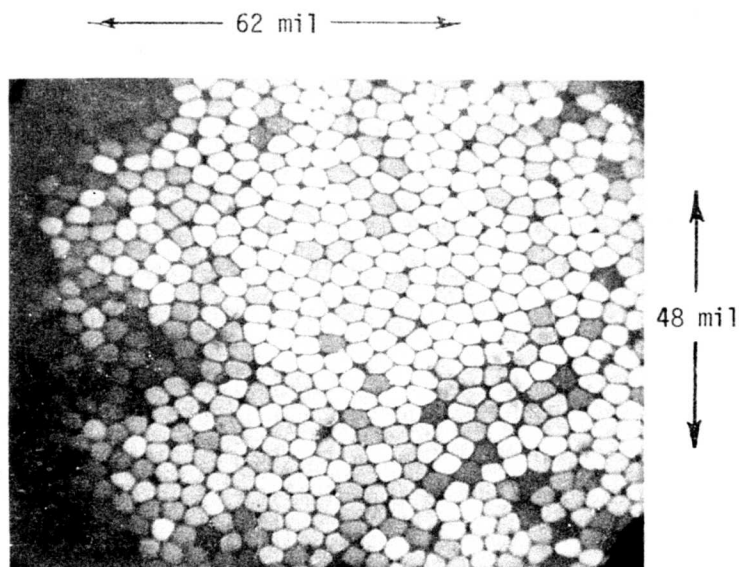
Figure 6. End-Push and Side-Push Compression Fixtures

- Deformation of the cross section of individual fibers was observed.
 - The fiber bundles do not stick to the fixture; the compressed termination can be removed when the temperature drops to 400°C.
 - No discoloration of the glass was observed.
- Thus, it appears that there is no reaction between the fixture and the cladding glass and no precipitation of lead in the core glass of the fibers.

The end-push fixture is not satisfactory for making useful compressed terminations because the required axial force causes the softened fibers outside the fixture to bend and distort during the pushing operation.

The side-push fixture shown in Figure 6 is a funnel with a movable section in one wall. With the movable section in the "closed" position, the funnel has a top diameter of 187mil tapering to an end section having a 170mil diameter. In this fixture the movable section is placed in the "open" position and the fiber bundle end is pushed into the fixture to the heater block. The fixture is then heated to 600°C; at that point the movable section is slowly pressed into the "closed" position and allowed to cool.

This side-push fixture does not cause bending and distortion of the fiber bundle outside of the funnel. Figure 7 shows a photograph of a portion of a compressed termination made with the side-push fixture. This compressed termination used one of the 177mil diameter (funnel measurement) bundles shown in Table II. Only a few fibers are broken; most of the dark fibers in the photograph are the result of non-uniform lighting and poor end finish on the other (uncompressed) end of the sample.



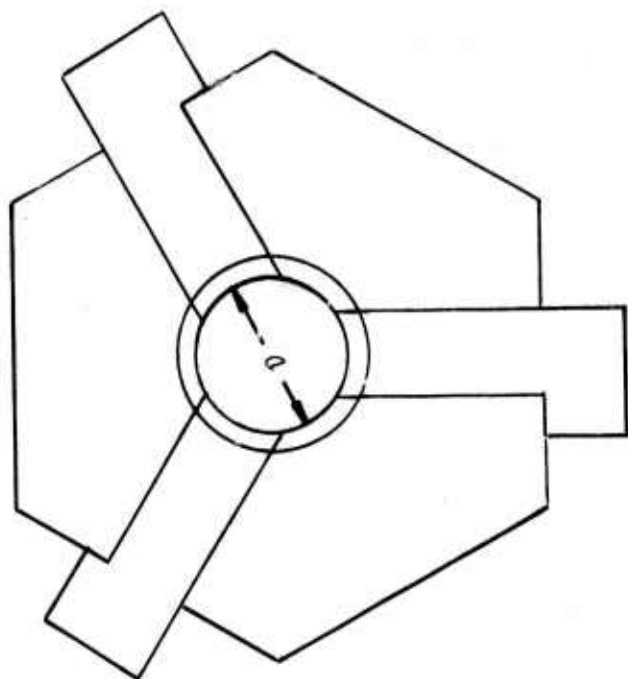
A portion of a 177mil diameter
fiber optic bundle compressed
to 170mil diameter using the
side-push fixture at 600°C.

Figure 7. Compressed Termination
Side-Push Fixture

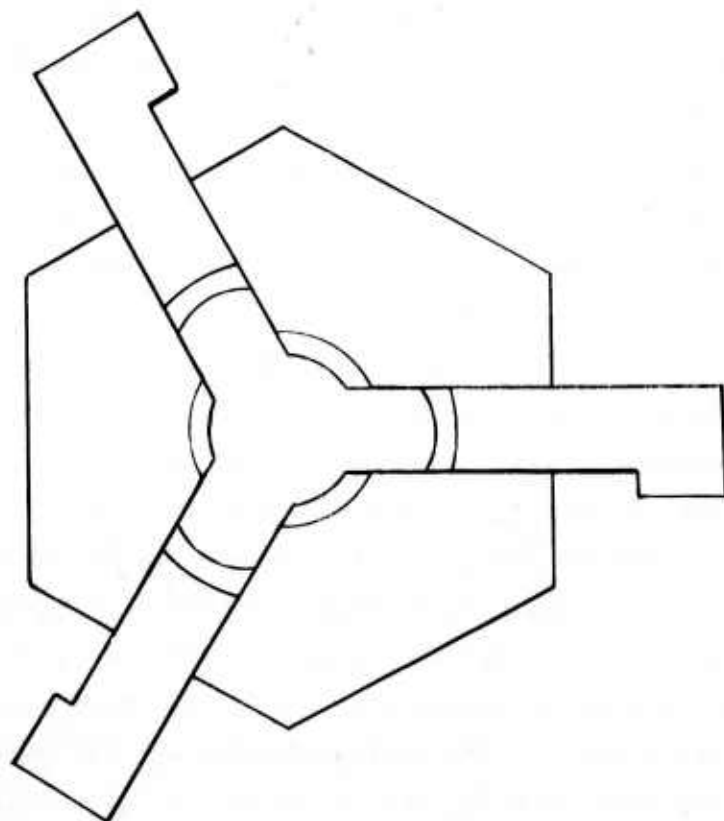
The circular border visible in the photograph is the edge of the field-of-view of the microscope and not the edge of the fiber optic bundle. The distortion in the shape of the individual fibers clearly shows that a significant improvement has been made in the transmission of the termination. However, there is still some dead space between the fibers--the dead space is most apparent in the areas where the fibers do not form a complete hexagonal pattern. In the hexagonal regions, the dead space is very low. No transmission measurements were made on this termination; however, the 4% dead space predicted from the data of Table II is consistent with the appearance of Figure 7

In the side-push fixture, all of the compression motion is exerted from one side. This one-directional compression resulted in excessive shearing of the individual fibers near the edge of the side-push fixture. Also, the moving portion of the side-push fixture formed a full one-half of the cylindrical end portion of the termination. As a result, this moving element had two knife edges that were easily bent and damaged. In order to overcome these disadvantages and obtain more uniform compression of the fiber optic bundles, two new compression fixtures were designed and constructed.

Figure 8 shows a top view of the y-push circular compression fixture. In the closed position, this fixture has the same tapered funnel cross section as the side-push fixture. In this case, the use of three moving elements gives more strength to the sharp edges by increasing the angle at the edge from zero to 60° . In the open position, the use of three moving elements means that only a small motion is required of each element to accommodate the uncompressed fiber bundle. For example, a tightly packed but uncompressed bundle of 2.6mil diameter fibers with a bundle diameter of 186mils should compress into a bundle diameter of 175mil (see Table II). A y-push fixture designed for this bundle would have a closed diameter of 175mil. The three moving elements will have to move back about 18.5mils to accommodate the uncompressed bundle. With this small displacement of the moving elements and the three-way compression, the shearing force and distortion of the individual fibers is much more uniform than in the side-push fixture.



CLOSED



OPEN

Figure 8. Y-Push Circular Compression Fixture

Figure 9 shows a y-push hexagonal compression fixture, that was designed and constructed. The philosophy and operation of the y-push hexagonal fixture is basically the same as the y-push circular fixture. For the closed position, the distance between the flats, H, is related to the compressed diameter, ϕ , by

$$H = .95232\phi \quad (29)$$

Thus, for a compressed diameter of 175mil the size of the hexagon is

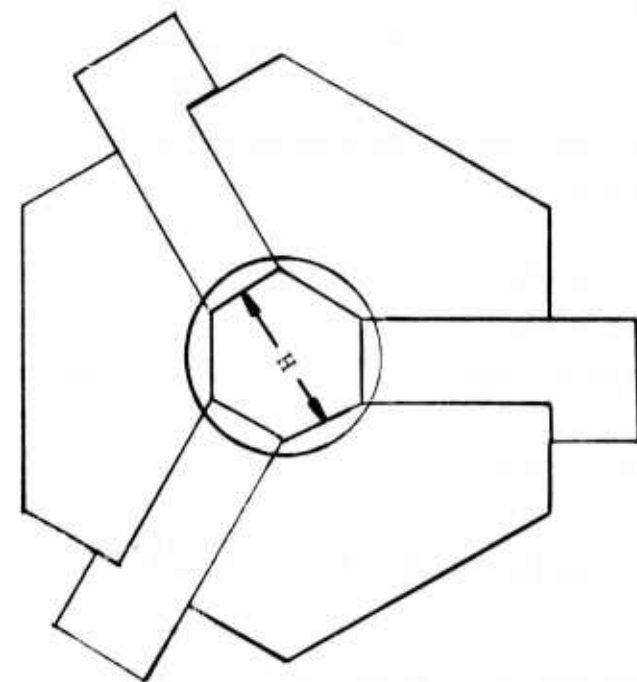
$$H = 167\text{mil} \quad (30)$$

and the moving elements will move back 11mils to accommodate the uncompressed bundle.

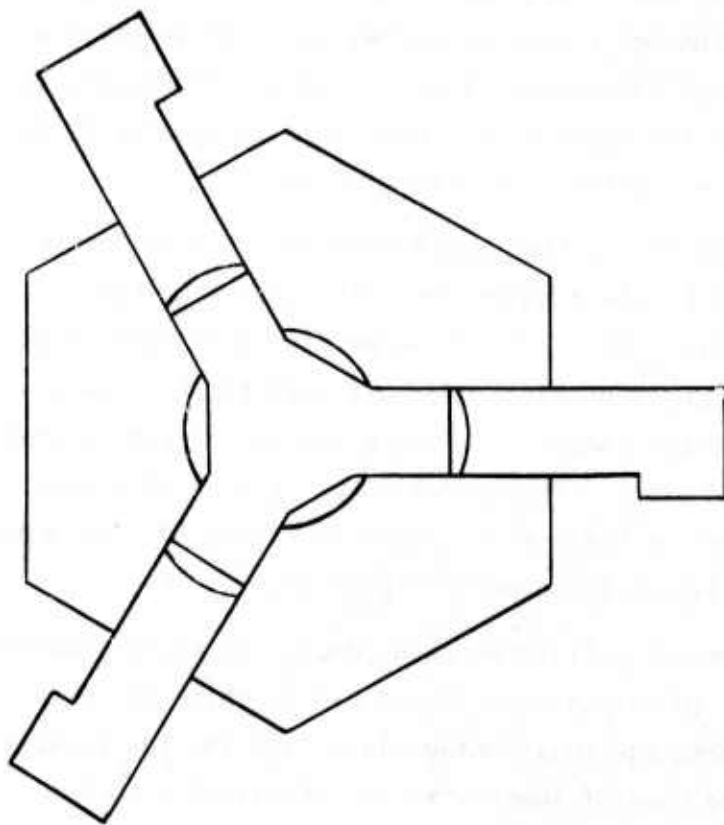
The support for the compression fixture was improved by the addition of dead weights to automatically close the y-push fixtures as the glass fibers soften. With the side-push fixture, the moving element was closed by hand after the fibers were heated to the softening point. This sudden forced motion may have contributed to fiber breakage and unnecessary distortion of individual fibers. The use of weights to allow steady closing of the fixture at a natural rate results in fewer broken fibers and a more tightly packed termination.

The improved support for the y-push compression fixtures is shown in Figures 10 and 11. The support consists of an aluminum base plate one half inch thick. Six 1/2in diameter stainless steel rods support an asbestos composition plate one half inch thick. The heater block rests on the asbestos composition plate and the y-push compression fixture rests on heater block. The heater block is made of copper. Holes for the two cartridge heaters are shown in Figure 10. The y-push circular compression fixture is shown in Figure 11.

The y-push compression fixtures each consist of eight separate pieces--three sliders, three pentagon shaped blocks which serve as the walls of the sliders, the positioning plate, and the top retaining ring. These pieces are made of invar with an industrial chromium



CLOSED



OPEN

Figure 9. Y-Push Hexagonal Compression Fixture

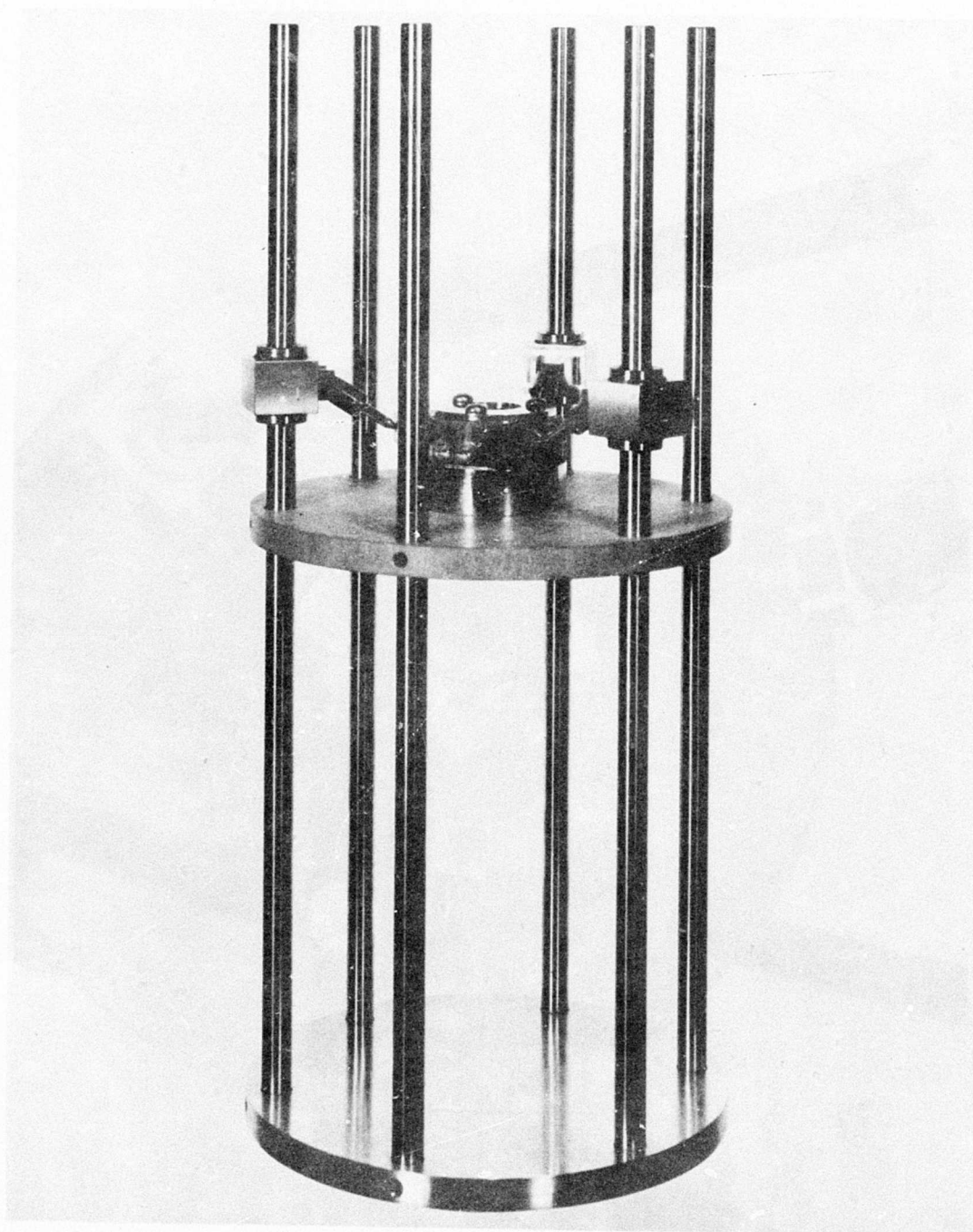


Figure 10. Y-Push Compression Fixture Support, Side View

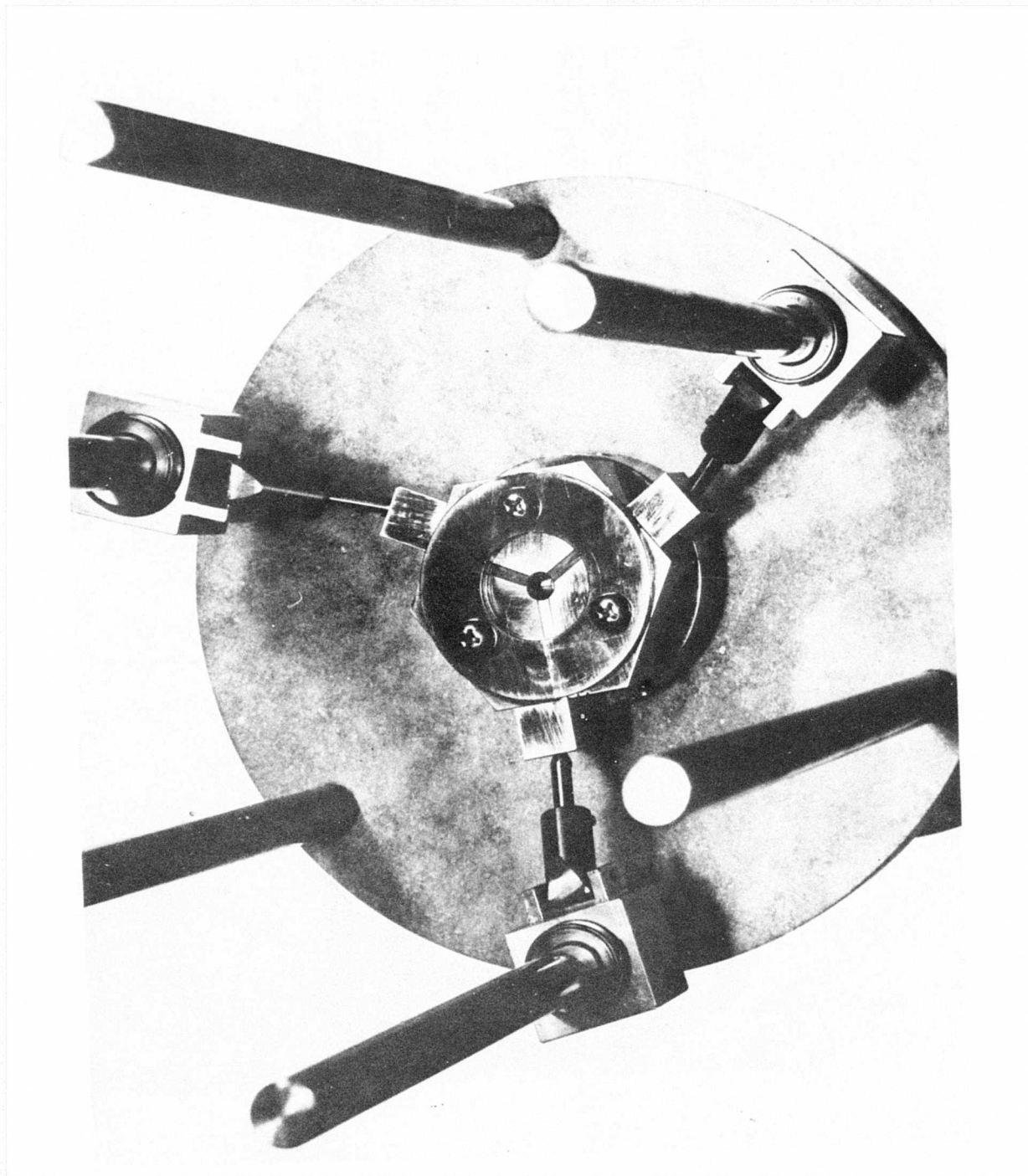


Figure 11. Y-Push Compression Fixture Support, Top View

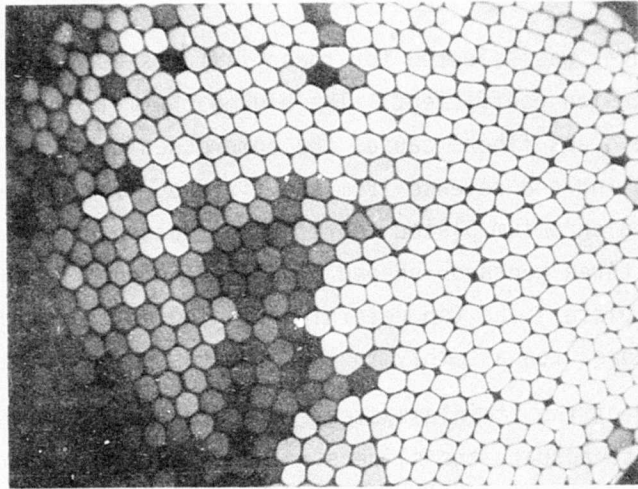
plating. Invar was selected for these fixtures because of its low thermal expansion coefficient. The higher thermal expansion coefficient of the glass fibers causes the compressed termination to contract on cooling and release from the fixture. The copper heater block is also chromium plated to retard oxidation during the heat cycle. The three pentagon shaped blocks are pinned to the bottom positioning plate. The top retaining ring holds the sliders in place and also secures the assembly to the asbestos composition plate.

Three of the stainless steel rods are used as positioning rails for weights to actuate the sliders. The weights are mounted to the rod by ballbearing assemblies. Force is transferred to the slider by means of an adjustable pin. The pin is made of stainless steel and is pointed on the end which contacts the slider in order to reduce the heat transfer during the heating cycle. The pointed end of the pin fits into a cone shaped hole in the end of the slider.

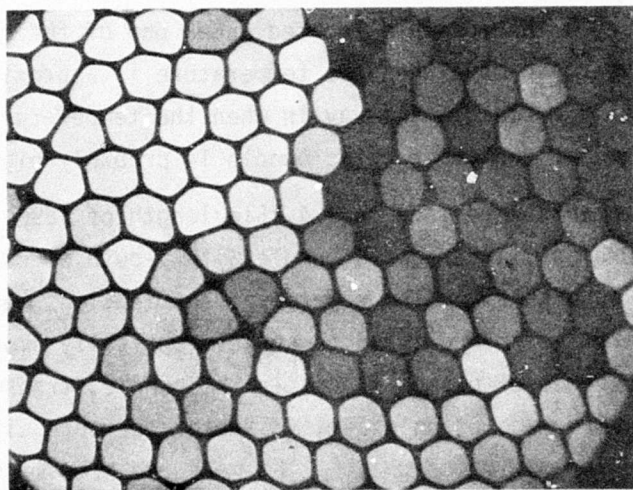
The heat cycle lasts approximately two hours. The heat-up cycle lasts approximately 15 minutes. The fiber bundle is not removed from the fixture until the temperature is below 100°C. The temperature is monitored by a thermocouple located under one of the screw heads. The sliders start to move when the temperature is approximately 580°C, and have usually moved all the way in when the temperature reaches 590°C. The temperature at the fiber optic bundle is probably higher.

Measurements were made on a 4.75in length of 189mil diameter (funnel measurement) fiber optic bundle with y-push circular compressed terminations on each end. The compressed terminations were epoxied into brass ferrules and polished to achieve optically smooth surfaces. Due to the presence of broken fibers in the bundle, transmission measurements were made using a 64mil diameter aperture with the position adjusted for maximum signal. The measured transmission was

$$T_3 = 0.7 \quad (31)$$



Low Power Magnification



High Power Magnification

Figure 12. Compressed Termination Y-Push Circular Fixture

The expected transmission for a fiber bundle with compressed terminations on each end (no dead space) is

$$T_3 = (1-R_c)^2 a R_a \quad (32)$$

The attenuation of the 4.75in length at 0.2dB/ft is

$$a = .982 \quad (33)$$

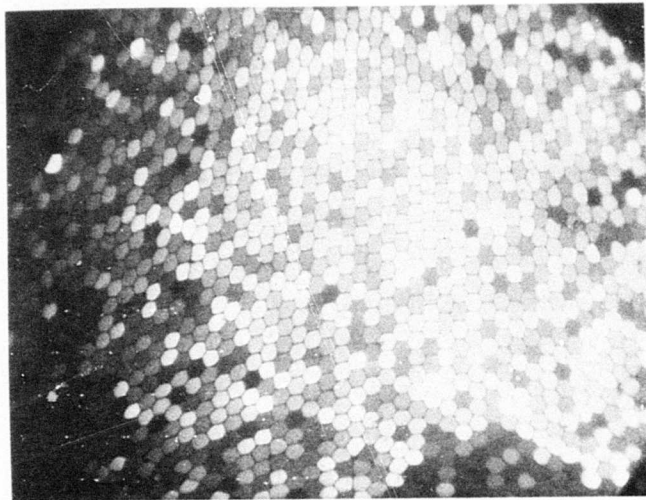
Combining Eqs (4), (7) and (32) gives the expected value of T_3

$$T_3 = 0.715 \quad (34)$$

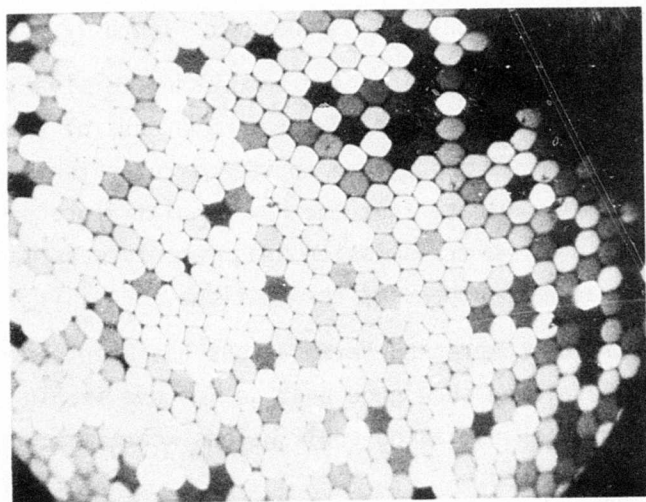
Comparing the measured and expected values of T_3 , Eqs (31) and (34), show that the measured value is 97.9% of the expected value. Thus, the dead space has been reduced to 2.1% of the area. The close packing of one of these compressed terminations is shown in Figure 12.

Figure 13 shows a portion of a compressed termination made with the y-push hexagonal compression fixture. The ends of the fibers form a more uniform hexagonal shape than in the circular termination of Figure 12. This may indicate that the hexagonal fixture produces more uniform compression. No transmission measurements were made on fiber bundles with hexagonal compressed terminations.

The effort on compressed terminations has been very successful. The techniques developed show good promise for use in high-performance optoelectronic data transmission applications where maximum termination transmission is required.



Low Power Magnification



High Power Magnification

Figure 13. Compressed Termination Y-Push Hexagonal Fixture

SECTION III

PASSIVE COUPLER DEVELOPMENT

Construction of a data bus requires the use of signal coupling devices which make it possible for each station to receive signals from the bus and transmit signals onto the bus. The vital nature of the signal transactions on an avionic data bus dictates that a strong emphasis on system reliability be used in the coupler design. In general, repeater systems are not employed in data buses because damage to one repeater would interrupt signal flow on the entire data bus.

In an optoelectronic data bus, the various stations are interconnected with flexible fiber optic bundles. The desired signal coupling device should provide the following functions:

- A portion of the optical signal should be removed from the bus for detection.
- The undetected remainder of the optical signal should be passed on for distribution to the other terminals on the bus.
- Optical signals generated in that terminal should be coupled onto the bus and distributed to the other terminals.

Meeting these requirements provides fault isolation on the optoelectronic data bus so that failure of one of the stations on the bus will affect only that station and will leave the remainder of the bus unimpaired. Two basic schemes have been reported^{1,2} for providing these functions in an optoelectronic data bus; both schemes have been investigated on this program. One approach uses an in-line configuration in which individual stations are sequentially interconnected by flexible fiber optic bundles. The other approach uses a radial configuration in which all stations are connected by flexible fiber optic bundles to a centrally located mixing point.

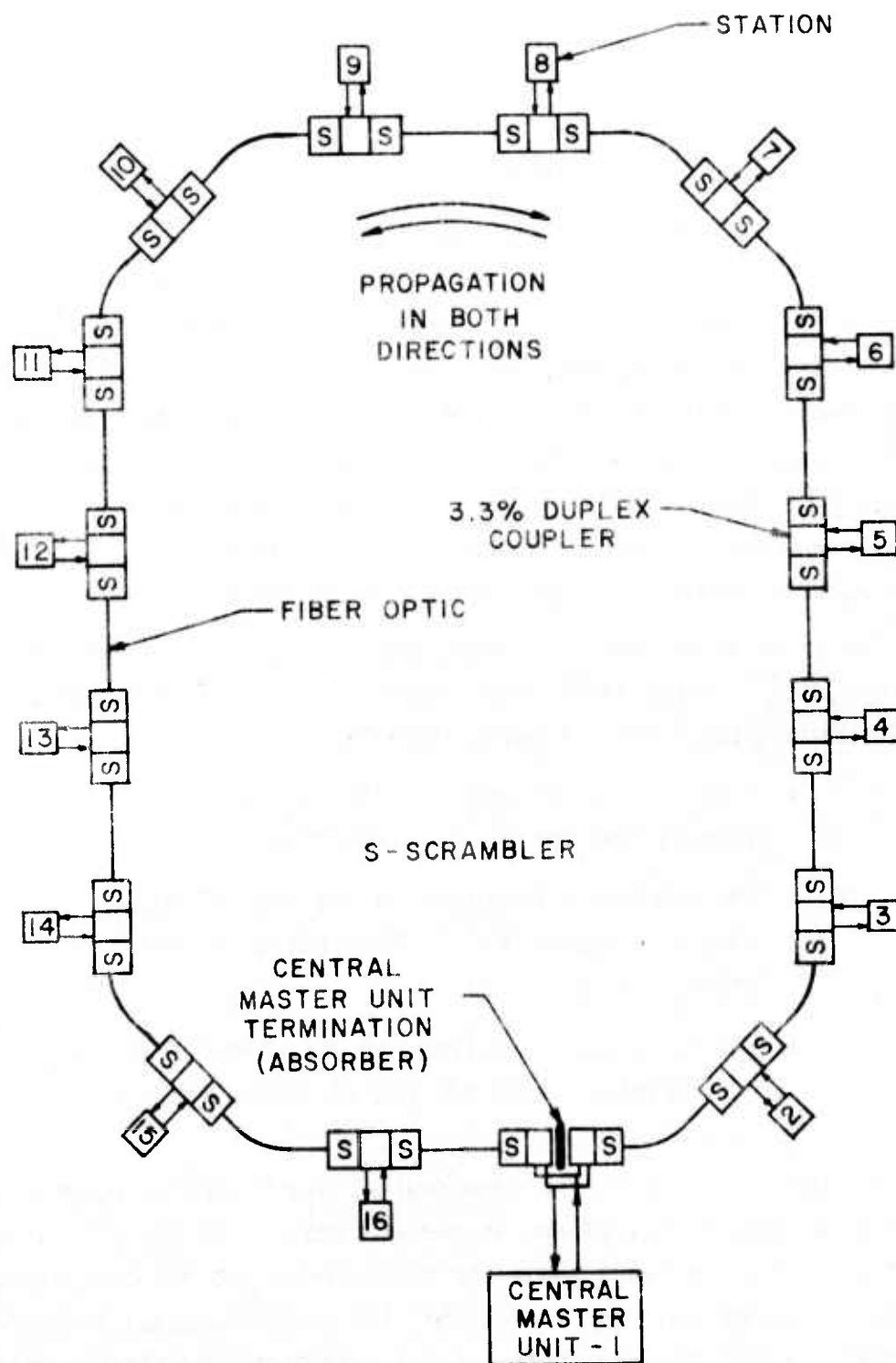


Figure 14. Uniform Duplex Data Bus Loop

A. ANALYSIS

The uniform duplex data bus loop shown in Figure 14 is an example of an in-line system. Other possible variations of this approach include simplex systems with data transmission in only one direction and tapered duplex systems in which the passive couplers are made different for each station to optimize the received signal. Any of these in-line systems can be either open ended or closed into a loop as shown in Figure 14. The passive optical couplers used with in-line systems are called T couplers; Figure 15 is a schematic representation of a duplex T coupler that could be used in the uniform duplex data bus of Figure 14. The scramblers shown in Figures 14 and 15 are short lengths of solid clad glass rod with the same diameter as the body of the coupler. The purpose of the scrambler is to uniformly distribute the optical energy entering the LED port over the area

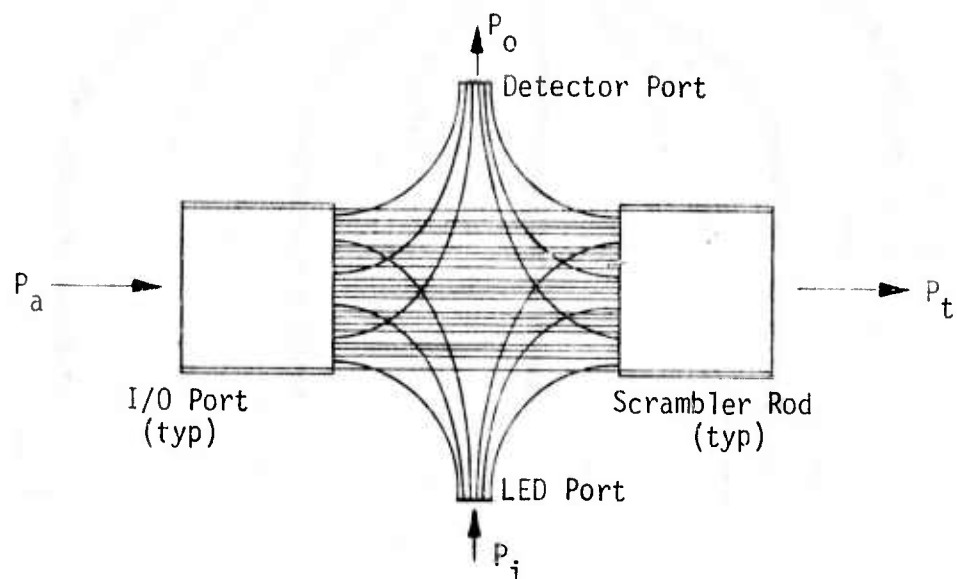


Figure 15. Uniform Duplex T Coupler

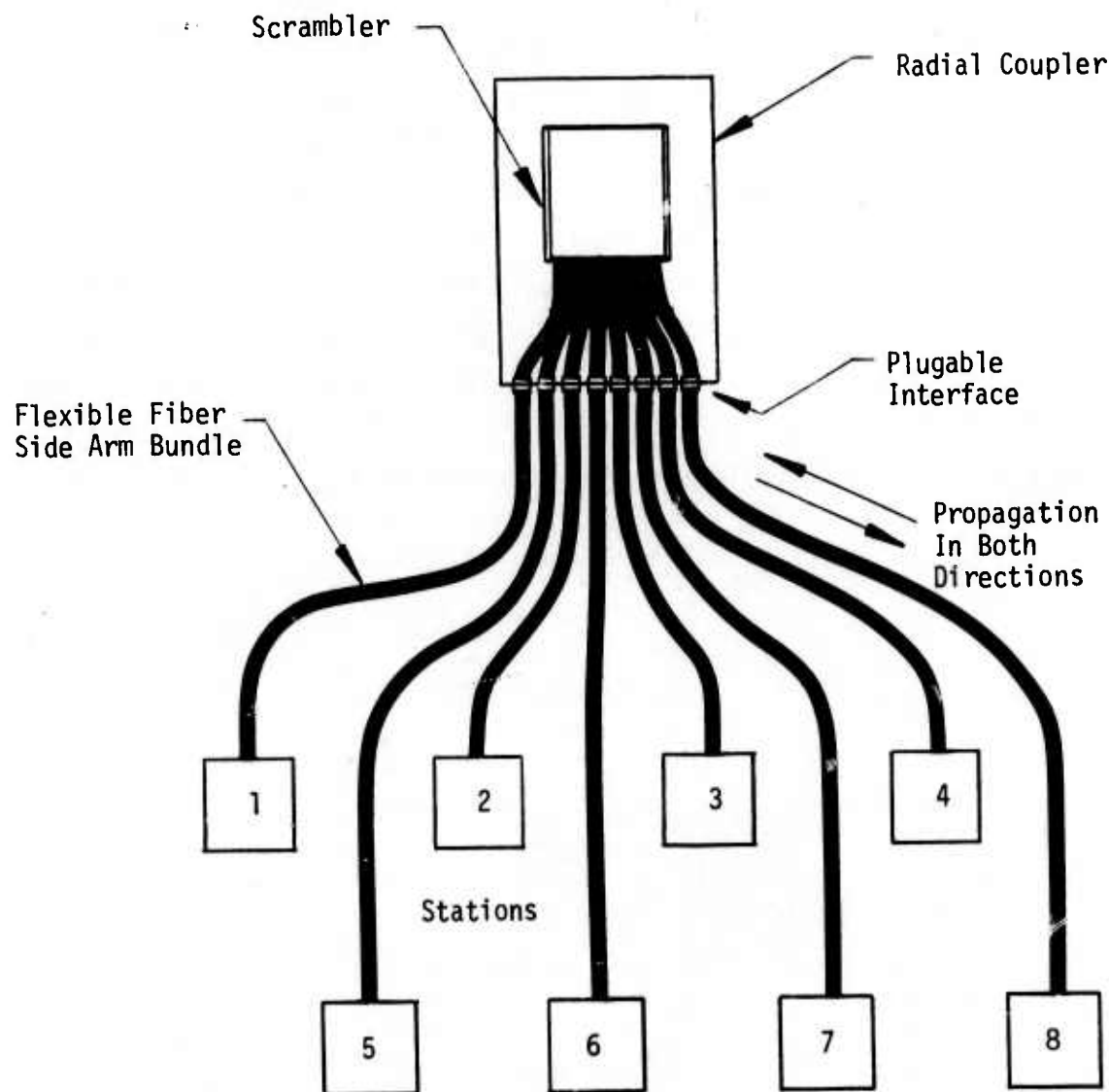


Figure 16. Radial Duplex Data Bus

of the exit port so that it will be coupled into all of the individual fibers in the fiber optic cable leading to the next station. This insures a reproducible sample of the total signal on the bus at each station.

A radial duplex data bus is shown in Figure 16. One passive coupler is required for construction of a radial data bus and that coupler need not be located at one of the stations. Figure 17 shows a schematic representation of a radial coupler. In this case, the scrambler has a diameter equal to the diameter of all of the radial arms bundled together. The mirror reflects all rays back into the scrambler so that every radial arm can couple to every other radial arm.

The performance of a passive optical coupler can be described in terms of a transmission factor, one or more quality factors and a coupling factor. In this report, T_T and C_T are used to designate the transmission factor and coupling factor for a T coupler; for a radial coupler the symbols T_* and C_* are used. The transmission factor describes the fraction of input optical power (at an input port) that is coupled to the output port. The definition of transmission factor is

$$T_T \text{ or } T_* = \frac{(\text{power at output port})}{(\text{power at input port})} \quad (35)$$

The transmission factor is always less than one because of the intentional removal of optical power at other ports and because of optical losses in the coupler. The coupling factor is basically an area ratio which describes the fraction of total power removed from the bus. The definition of coupling factor is

$$C_T \text{ or } C_* = \frac{(\text{scrambler area attributed to a detector port})}{(\text{total area of the scrambler})} \quad (36)$$

This definition of the coupling factor is very basic and general. It was chosen because it accurately represents the performance of both T and radial couplers and allows the use of common terminology in describing both types of data bus systems. The fraction of input power coupled to the detector port will always be less than predicted by Eq(36) because

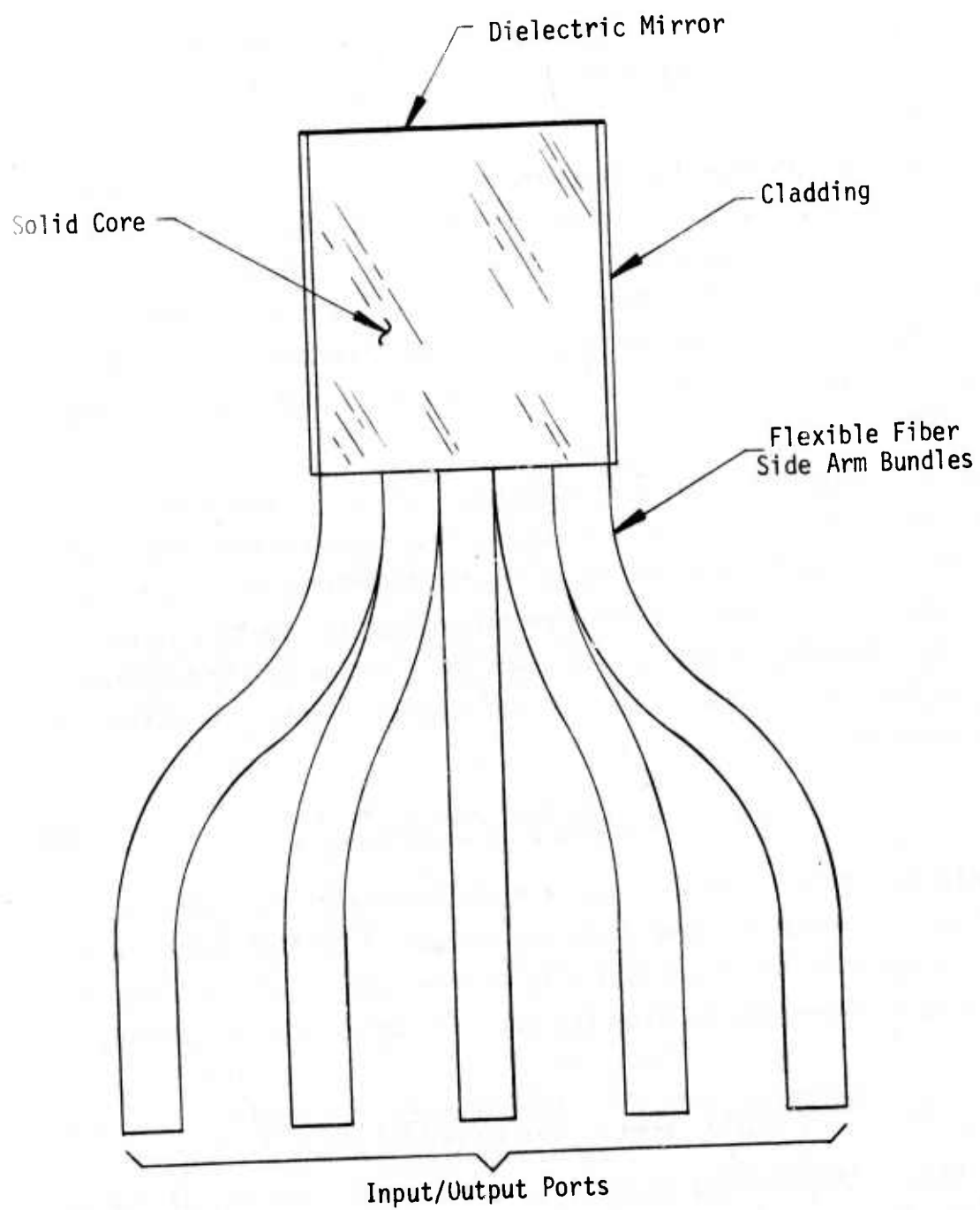


Figure 17. Duplex Radial Coupler

of reflection, packing fraction, and attenuation losses in the detector side arm. The coupling factor defined by Eq (36) cannot be measured optically on a finished coupler. However, this coupling factor has great practical value as a design parameter because it specifies the area that should be attributed to the detector port independent of the losses in the detector side arm.

1. T Coupler

Two quality factors are required to accurately represent the performance of a T coupler. A general T coupler schematic is shown in Figure 15. The transmission quality factor, m_T provides a measure of the losses in the transmission path. Using Eqs (35) and (36) and assuming equal scrambler areas attributed to LED and detector ports, the transmission quality factor is defined as

$$m_T = \frac{T_T}{1-2C_T} \quad (37)$$

which may be rearranged as

$$T_T = m_T(1-2C_T) \quad (38)$$

From Eq (37), m_T is the ratio of the power at the output port to the power into the area attributed to the output port. The coupling quality factor, m_C , provides a measure of the losses in the detector side arm; it is defined by

$$m_C = \frac{(\text{power at detector port})}{(\text{power into scrambler area attributed to detector port})} \quad (39)$$

The detector port output power P_o can now be expressed as a function of coupler output power P_a :

$$P_o = C_T m_C P_a \quad (40)$$

Due to the physical symmetry of the T coupler, it will be assumed that the coupling quality factor is the same for the LED side arm and the detector side arm. In an actual coupler, the values could be different

because of broken fibers and/or differences in packing fraction. In addition, the amount of power coupled into the LED port is strongly dependent on the radiation pattern of the LED. Losses at the LED port over and above those included in m_C should be charged against the LED and not the coupler. An LED quality factor, m_L , should be used to represent the LED-dependent losses. The definition of m_L is

$$m_L = \frac{(\text{power into area and NA of LED port})}{(\text{total output power of LED})} \quad (41)$$

Thus the product $m_C m_L$ represents the efficiency with which the total LED output power P_i is coupled to the bus.

The values of m_T and m_C can be combined to give an overall quality factor, m , for the T coupler. This overall quality factor is defined by

$$m = \frac{(\text{power sum at output, detector \& LED ports})}{(\text{power at input port})} \quad (42)$$

This factor does not appear in the system design equations; however, it is useful as a parameter to assess the quality and perfection of the technology used to construct a coupler. The value of m can be obtained from Eq (42) using Eqs (35) and (36).

$$m = T_T + 2m_C C_T \quad (43)$$

Combining Eq (43) with Eq (38) to eliminate T_T gives

$$m = m_T \left[1 - 2C_T \left(1 - \frac{m_C}{m_T} \right) \right] \quad (44)$$

If the coupling factor, C_T , is small, Eq (44) shows that the overall quality factor is about equal to m_T . In fact, if $m_C = m_T$, the overall quality factor is equal to m_T for all values of C_T . In general, quality

factor is a transmission parameter which designates the complement of the attenuation or loss; when losses are zero, quality factor has its maximum value of one.

A serious effort has been made to define parameters that describe the performance of T couplers without resorting to any particular technology or construction technique. Because of this, Eqs (35) through (44) have relied heavily on general word definitions rather than schematics or pictures of a specific type of T coupler. This general T coupler model is used in Appendix II in the analysis of an in-line data bus. Section III.B. considers specific coupler structures in detail and identifies the physical characteristics that contribute to the various performance factors.

The analysis of an in-line data bus presented in Appendix II shows that the worst case signal transfer occurs when the station at one end of the bus is communicating with the station at the other end of the bus. For an N station bus, the worst case power ratio, R_{PT} , is

$$R_{PT} = \frac{P_{ON}}{P_{i1}} = \left[\frac{a_0 T_C T_C m_L m_C^2 C_T}{2} \right] \left[a_0 T_C T_C m_T (1 - 2C_T) \right]^{N-2} \quad (45)$$

where P_{ON} is the output power at the detector port of station N, and P_{i1} is the input power at the LED port of station 1.

The term a_0 represents the average attenuation between adjacent stations and is defined in Eq (164) of Appendix II.

Equation (45) shows the relative importance of the parameters of the T coupler in determining overall system performance. The transmission quality factor, m_T , appears with the exponent N-2; whereas, the coupling quality factor, m_C , appears with the exponent 2 independent of the

number of stations on the bus. Thus, m_T has much greater significance than m_C in determining system performance and the greatest emphasis should be placed on increasing the value of m_T . The worst case power ratio can be maximized by setting the derivative of Eq (45) with respect to C_T equal to zero, and solving for the optimum value of C_T . This operation gives (see Appendix II for derivation)

$$C_{opt} = \frac{1}{2(N-1)} \quad (46)$$

From Eq (46), the optimum value of C_T is dependent only on the number of stations on the bus. Specifically, this means that C_{opt} is independent of quality factor and fiber optic attenuation; this is a very general result with no limiting assumptions or approximations. Thus, Eq (46) and Eq (36) combine to specify the fraction of the area of the scrambler that should be used for the detector port. For equal areas attributed to the LED port and detector port this area ratio becomes

$$\frac{(\text{Scrambler area attributed to LED \& detector ports})}{(\text{Area of scrambler})} = \frac{1}{N-1} \quad (47)$$

Note that this area ratio is independent of the value of m_C associated with the LED and detector side arms.

The maximum value of the worst case power ratio for the duplex bus is calculated by substituting Eq (46) into Eq (45). This operation gives

$$R_{PT}|_{max} = \left[\frac{a_o T_c T_c m_L m_C^2}{4(N-1)} \right] \left[\frac{a_o T_c T_c m_T (N-2)}{(N-1)} \right]^{N-2} \quad (48)$$

Referring again to the in-line data bus analysis presented in Appendix II, the worst case dynamic range when the coupling factor is equal to C_{opt} is given by

$$D_{RT}|_{opt} = \left[\frac{1}{a_o T_c T_c m_T} \frac{N-1}{N-2} \right]^{N-2} \quad (49)$$

2. Radial Coupler

Due to the symmetry of the radial coupler, only one quality factor, m_* , is required to describe its performance. A radial coupler is shown in schematic form in Figure 17. The quality factor, m_* , is defined by

$$m_* = \frac{(\text{sum of output power at all ports})}{(\text{power in at input port})} \quad (50)$$

This is similar to the overall quality factor of the T coupler given in Eq (43). For the radial coupler there is no possibility of optimizing the coupling factor because the area ratio is uniquely determined by the geometry. For an N-station radial duplex bus there are N input/output ports all of the same area. Therefore, the total area of the composite fiber optic bundle at the scrambler rod must be N times the area of each input/output port. From Eq (36) the coupling factor for the radial coupler is

$$C_* = \frac{1}{N} \quad (51)$$

From Eq (51) the coupling factor is again seen to be independent of the quality factor or fiber optic attenuation. A complete analysis of a radial duplex data bus is presented in Appendix III. Equations (36) and (51) combine to specify the fraction of the area of the scrambler that should be used for the detector (input/output) port.

$$\frac{(\text{Area attributed to one input/output port})}{(\text{Area of scrambler})} = \frac{1}{N} \quad (52)$$

When power is coupled into any one LED port of a radial data bus, all N detector ports receive power. In the ideal case of uniform power distribution in the scrambler the transmission factor of the radial coupler is the same for all stations and is given by

$$T_{\star} = m_{\star} C_{\star} \quad (53)$$

Combining Eqs (51) and (53) gives

$$T_{\star} = \frac{m_{\star}}{N} \quad (54)$$

If the longest transmission path is between stations k and N and station k is transmitting, then the worst case fractional power ratio is given by

$$R_{p\star} = \frac{P_{oN}}{P_{ik}} = \frac{m_L a_m T_{\star} T_{fk} T_{fN}}{2} \quad (55)$$

where m_L is the LED quality factor, Eq (40)

T_{fk} and T_{fN} are the transmission factors for the plugable interfaces at the input/output ports of the radial coupler, and a_m is the maximum fiber optic attenuation

The value of a_m is given by

$$a_m = \exp [-\alpha L] \quad (56)$$

where L is the total length of the data bus, and α is the loss coefficient of the fiber optic bundle.

Comparing Eq (56) with Eq (164) of Appendix II shows that

$$a_m = a_o^{N-1} \quad (57)$$

Using Eqs (54) and (57), the worst case fractional power ratio for the radial data bus is

$$R_{p*} = \frac{m_L m_c^* T_c T_{fk} T_{fN} a_o^{N-1}}{2N} \quad (58)$$

From Appendix III the worst case dynamic range, D_{R*} , for the radial system can in theory be reduced to 1.0 (zero dB) by including equal attenuation in each radial arm. In practice, the radial coupler will always give a small dynamic range at the various detector ports because of nonuniform spreading of the light by the scrambler.

3. T/Radial Comparison

The worst case fractional power ratios for the in-line and radial data bus systems are given in Eqs (48) and (58) respectively. Comparison of these expressions shows that fiber optic attenuation (a_o^{N-1}) is the same for both systems. However, for everything except fiber optic attenuation, the radial coupler gives superior performance. The ratio of worst case detector power for the two systems can be obtained by dividing Eq (58) by Eq (48). This operation gives

$$\frac{R_{p*}}{R_{PT}} = \frac{2m_c^* T_c T_{fk} T_{fN}}{m_c^2 T_c T_c (m_T T_c T_c)^{N-2}} \left(\frac{N-1}{N} \right) \left(\frac{N-1}{N-2} \right)^{N-2} \quad (59)$$

For an 8-station system this ratio becomes

$$\frac{R_{p*}}{R_{PT}} = \frac{4.41 m_c^* T_c T_{fk} T_{fN}}{m_c^2 T_c T_c (m_T T_c T_c)^6} \quad (60)$$

This expression can be further simplified by comparing specific systems. The T_c in the numerator of Eq (60) arises at the LED/fiber optic interface in the radial data bus and is therefore about equal to m_c in the denominator which arises at the LED/fiber optic interface in the in-line data bus. For a solid side arm radial coupler and a split-rod T coupler $T_{fN} \approx T_c$ and $T_{fk} \approx T_c$. With index matching materials used at the internal interfaces in the two couplers, typical values of the quality factors are $m_* = .848$ and $m_c = .558$. Using these approximations, Eq (60) reduces to

$$\frac{R_{p*}}{R_{pT}} = \frac{6.7}{(m_T T_c T_c)^6} \quad (61)$$

With no index matching at the plugable interface, m_T is about equal to T_c^2 . For lead glass fiber $T_c \approx .94$ and from Table IV a typical value of T_c is .656. Using these values Eq (61) shows that the minimum detector power in the radial system is about 256 times larger (24dB) as compared to the minimum signal power for the in-line data bus. Even with index matching and perfect terminations ($m_T T_c T_c = 1$) the radial system is better than the in-line system by a factor of 6.7 (8.26dB).

The optimum value of dynamic range for an in-line data bus, D_{RT} , is given by Eq (49) and the expected value of dynamic range for a radial data bus about 2.0. Thus, the ratio of dynamic range for the two systems is

$$\frac{D_{RT}}{D_{R*}} = \frac{1}{2} \left[\frac{1}{a_0 m_T T_c T_c} \left(\frac{N-1}{N-2} \right) \right]^{N-2} \quad (62)$$

For an 8-station data bus this ratio becomes

$$\frac{D_{RT}}{D_{R*}} = 1.26 \left[\frac{1}{a_0 m_T T_C T_C} \right]^6 \quad (63)$$

The factor $m_T T_C T_C$ appears in both Eq (62) and Eq (63); the typical values given above result in $m_T T_C T_C = .545$. For a 100ft data bus using Galileo fiber at 0.2dB/ft the value of a_0 is -2.5dB (0.562). Substituting these values into Eq (63) gives

$$\frac{D_{RT}}{D_{R*}} = 1526 \quad (31.8\text{dB}) \quad (64)$$

Pilkington fiber optic bundles (65 μm fibers) at 100dB/km give $a_0 = 0.435\text{dB}$ (0.905) and $m_T T_C T_C = .548$ which gives

$$\frac{D_{RT}}{D_{R*}} = 87.5 \quad (19.4\text{dB}) \quad (65)$$

Perfect terminations, $m_T T_C T_C = 1.0$, and Pilkington fiber optic bundle, $a_0 = .905$, gives

$$\frac{D_{RT}}{D_{R*}} = 2.29 \quad (3.6\text{dB}) \quad (66)$$

A radial data bus always has a better (lower) dynamic range than a corresponding in-line data bus.

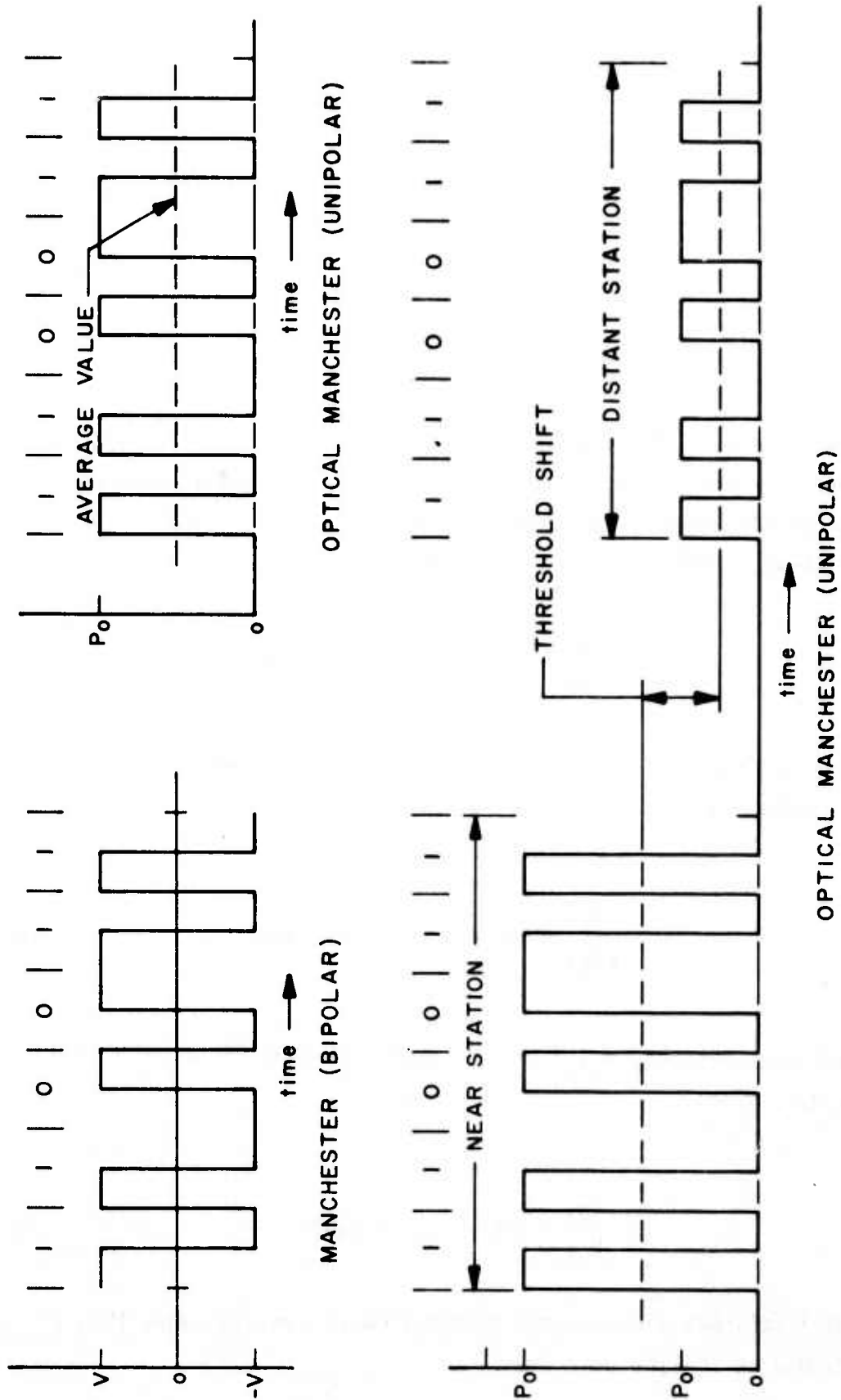


Figure 18. Bipolar and Unipolar Manchester

Preliminary design effort has been completed on the sync recovery circuits for use in the data bus to be constructed on this program. This design effort has shown that the performance of the bus is significantly reduced when the receivers must operate with a large dynamic range. The dynamic range sensitivity in an optoelectronic data bus is the result of a combination of effects related to the unipolar nature of the optical signal^{3,5} and the drift/noise characteristic of the preamp in the receiver. The temperature related drift in the output voltage of a well designed, photodiode/preamp will be about $25\mu\text{V}/^\circ\text{C}$ ⁵. For the temperature range -54°C to $+125^\circ\text{C}$, the dc output voltage will drift by about 4.5mV. For a data rate of 10Mbit/s the required preamp bandwidth will be of the order of 10MHz and the total rms noise voltage at the output of the preamp will be about 0.4mV. Thus, in a 10Mbit/s system the preamp drift is 11 times greater than the rms noise. The effects of drift can be overcome by using Manchester coded optical signals and ac coupling in the receiver. A comparison of conventional and optical Manchester signals is shown in Figure 18. The unipolar Manchester signal has a constant duty cycle of 0.5. Therefore, the average value is independent of data content and no information is lost by using an ac coupled receiver.

With an ac coupled receiver and Manchester coded signals, the error rate is determined entirely by the rms noise and is independent of the drift. However, the dynamic range of received signals can cause a severe problem that is illustrated in the lower half of Figure 18. For a transaction with a near station the signal is large and the coupling capacitor charges up to the average value of the signal. If this is followed by a transaction with a distant station, the signal is small and has a small average value. The coupling capacitor must discharge to this new average value before the small signal can be properly decoded. This change in average value between transactions has the same effect as a shift in threshold; it occurs only in

a data bus where each station communicates with every other station on the bus.

When the dynamic range is small (2-4) as in a radial data bus, the coupling capacitor value can be selected to achieve discharge during the dead time between transaction. When the dynamic range is large (500-1000), as in an in-line data bus with Galileo fibers, the dead time between transactions required for coupling capacitor discharge is long and the data bus efficiency is lowered. Special circuits to clamp (discharge) the coupling capacitors at the end of each transaction can be used. This approach maintains the data bus efficiency at the expense of the added cost and complexity of the discharge circuit and the logic needed to actuate it.

A direct coupled receiver requires more optical power at the detector than an ac coupled receiver because of the presence of both noise and drift as possible sources of error. Figure 19 shows

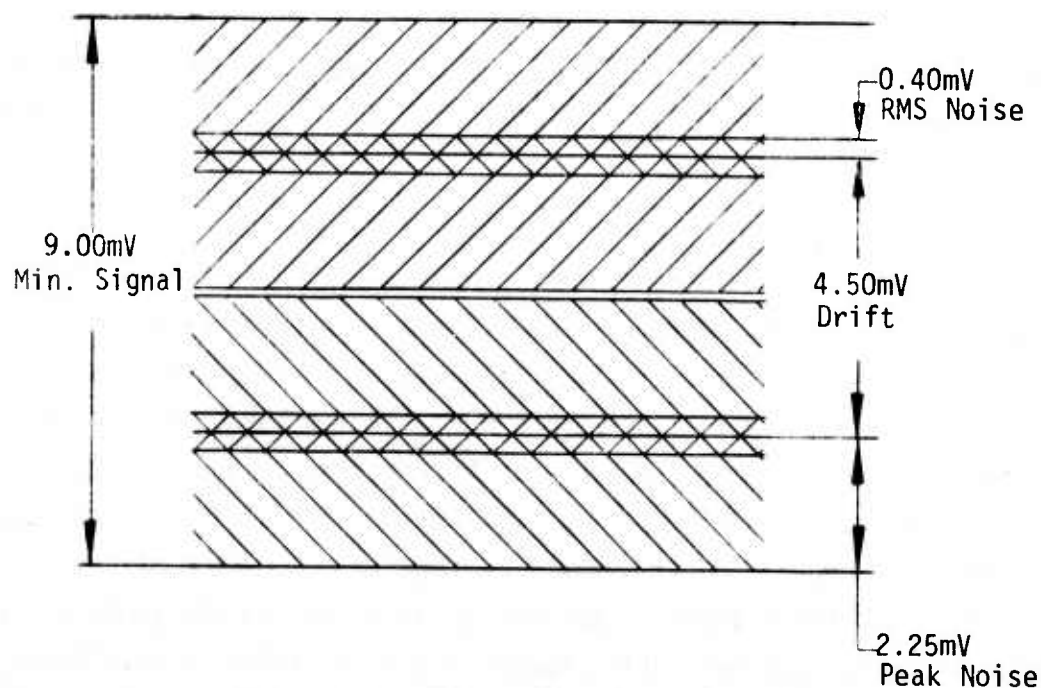


Figure 19. Effect of Noise and Drift

the relative effects of noise and drift for an optimized 10MHz preamp. A random noise error rate of one error in 10^8 bits is achieved with a peak/rms ratio of 5.62^3 ; this gives a peak noise band of $(0.4\text{mV})(5.62) = 2.25\text{mV}$ on each side of the output. Thus, in the direct coupled receiver the minimum peak-to-peak signal is 9mV; in the corresponding ac coupled receiver the minimum peak-to-peak signal is 4.5mV. The use of a direct coupled receiver requires 2 times (3dB) more minimum optical power on the detector than is required with an ac coupled receiver with the same bandwidth.

Dynamic range in a direct coupled receiver causes a different problem than was described above for the ac coupled receiver. Figure 20 shows typical waveforms for a weak signal and a strong signal. These waveforms are typical for 10Mbit/s with a system

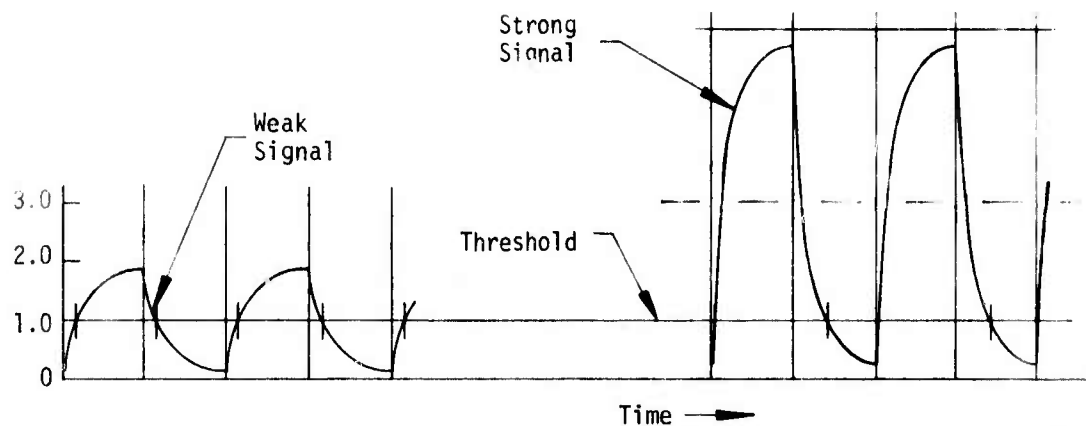


Figure 20. Signals in a Direct Coupled Receiver

bandwidth (3dB) of 10.0MHz. The threshold is set to properly detect the weak signal; however, a strong signal that is 3 times larger than the weak signal is not symmetrical about the threshold. For a dynamic range of 12.5, no portion of the strong signal waveform will fall below the threshold level. This deficiency can be overcome by increasing the system bandwidth to give faster rise and fall time on the signal waveforms. With faster rise time the signal will come closer to the steady-state "on" or "off" level during each half bit time and more dynamic range can be accommodated. However, optimized preamps have an equivalent input noise current that is proportional to bandwidth. For a constant error rate the required signal power on the detector is proportional to the amplifier bandwidth. Thus, in a direct coupled system, dynamic range can be accommodated only at the expense of receiver sensitivity.

This discussion has shown that large dynamic range in an optoelectronic data bus can be achieved. However, if a large dynamic range must be accommodated, one or more of the following must be employed in the receiver design.

- increased preamp bandwidth (this increases noise),
- longer dead time between transactions on the bus (this lowers the data bus efficiency),
- special circuits to discharge the coupling capacitors (this increases circuit complexity).

The small dynamic range offered by the radial data bus is a very desirable feature.

Considering both the worst case power ratio and the dynamic range, the radial data bus is superior to the in-line data bus. Based on this superiority, the radial configuration has been selected for the 8-station data bus to be constructed on this contract.

B. SCRAMBLER DESIGN

Passive couplers for both in-line and radial data buses require the use of scramblers. Figure 15 shows a T coupler for use in a uniform duplex bus (in-line) which requires two scramblers. Figure 17 shows a radial coupler for use in a radial bus which requires one scrambler. The purpose of a scrambler in a passive coupler is to accept light from a small number of fibers and spread that light as uniformly as possible over the area of the scrambler without altering the axial angular distribution of the light. This function can be performed by an optically smooth glass rod that is mirrored on the external surface but not on the ends as shown in Figure 21. The optical function of a scrambler is much the same as that of each fiber in a fiber optic bundle.

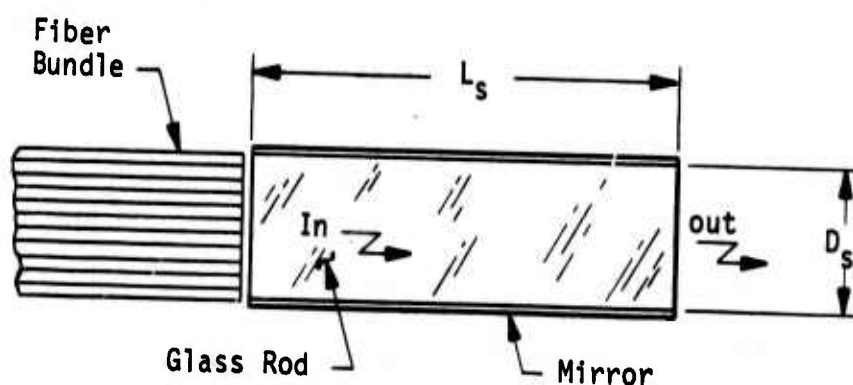


Figure 21. Scrambler Rod

As described in Appendix I, the mirror on the external surface should be provided by total internal reflection. The total internal reflection phenomenon produces a 100% reflective mirror while a metal mirror reflects only 97-98% of the incident light. This 100% reflective mirror

can be achieved by using a high-index glass rod similar to the core glass of the fibers and cladding it with a lower index material. An all-glass rod with a high-index core and low-index cladding can be used for the scrambler. However, it is difficult to obtain a clad glass rod with adequate precision of the core diameter. It is usually more expedient to use a low-index Silicone or epoxy resin for the cladding layer. This makes it possible to grind and polish the glass rod to close mechanical tolerances and provide a good optical quality finish on the external surface of the rod. The plastic cladding layer can also serve as the mounting medium which properly positions the scrambler rod and anchors it to the coupler housing. Many useful plastic materials have greater optical attenuation than glass. However, the length of a scrambler is not more than a few inches and the resulting loss due to absorption in the cladding layer is negligible.

In order for the scrambler rod to support all of the rays coupled into it, there must be an adequate change in index of refraction at the core/cladding interface. The limiting numerical aperture, NA_s , of the acceptance cone of a scrambler is (see Appendix I)

$$NA_s = (n_2^2 - n_3^2)^{\frac{1}{2}} \quad (67)$$

where n_2 is the index of the core, and
 n_3 is the index of the cladding.

Numerical aperture is defined by

$$NA = n_1 \sin \theta_1 \quad (68)$$

where θ_1 is the angle to the normal of any ray measured in a medium having an index of n_1 . When the external medium is air, then $n_1 = 1$ and NA_s specifies the maximum half angle of the acceptance cone. Due to the form of Eq (68) and Snells law,³ the value of NA is the same

inside and outside the scrambler.

$$NA = n_1 \sin \theta_1 = n_2 \sin \theta_2 \quad (69)$$

In some data bus systems, the NA_ϕ of the light input to the scrambler will be known and Eq (67) can be used to determine the minimum index difference in the scrambler. In many cases it will be adequate to make the NA_s for the scrambler equal to the NA of the fiber bundle being used. This will insure that the scrambler will support any ray that will propagate on the fiber optic bundle.

The length and diameter of the scrambler rod are also important parameters in the design and construction of passive couplers. This is true for both radial and T couplers. The scrambler should be long enough that light exiting any individual fiber in the input bundle spreads out to fill the entire bundle at the exit surface. Ideally, the scrambler should be short enough that no meridional ray reflects from the clad surface more than one time. Figure 22 shows a scrambler for a radial coupler. In this case, the length, L_s , is 2 times the physical length of the rod due to the mirror at the open end of the scrambler. The dashed lines indicate the mirror image of the radial coupler in the end mirror. For a T coupler, the physical length of the scrambler rod is the full length, L_s . The diameter of a scrambler must be equal to the diameter of the composite fiber optic bundle used in the data bus. The mirror over the flat end of the scrambler should ideally be a multi-layer dielectric coating similar to that used on laser mirrors. Again, the dielectric mirror will produce a higher reflectivity ($\sim 100\%$) than can be achieved with a metal mirror. Figure 22 shows optical output from two typical fibers -- one at the center and one at the edge of the composite bundle. The optimum length is seen to be dependent on the NA_ϕ of the light from the optical fibers. From Figure 22 the length and diameter are related by

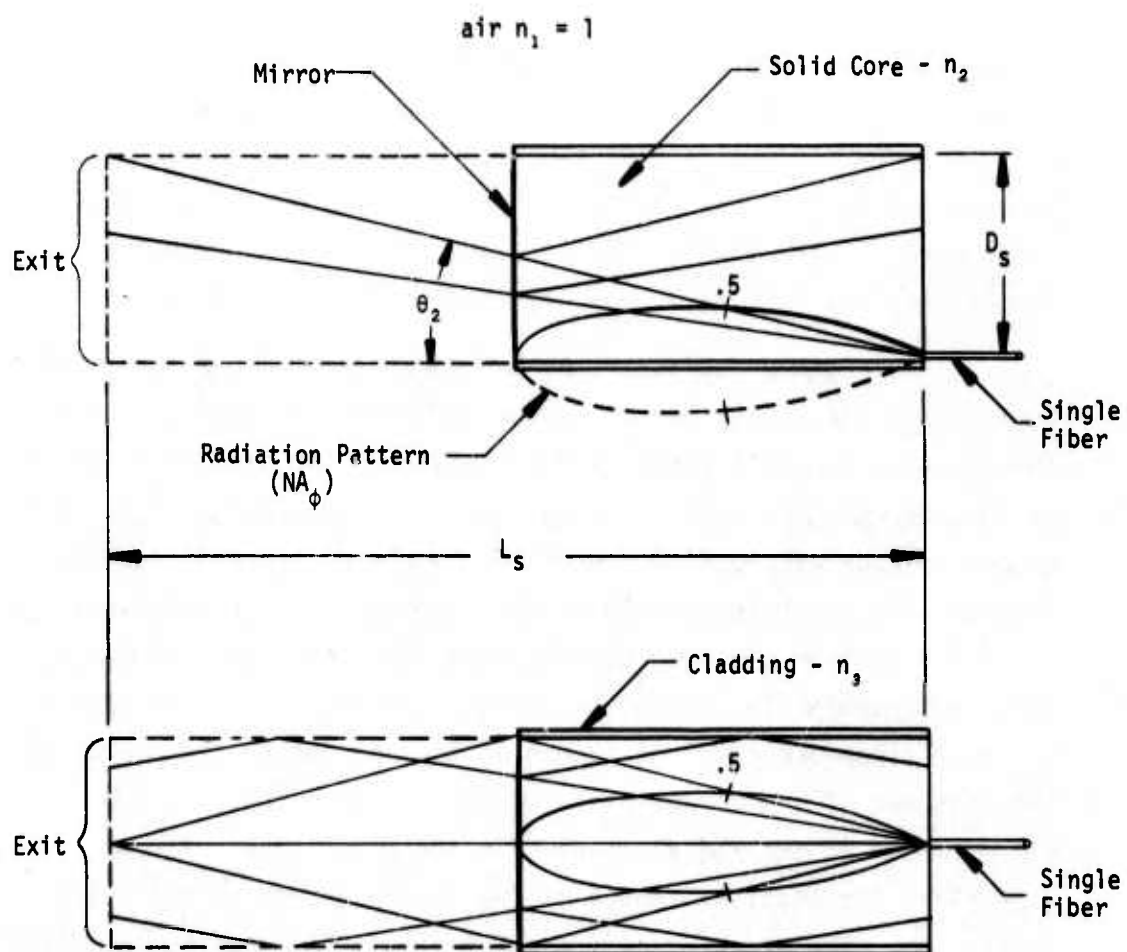


Figure 22. Scrambler Rod Operation

$$L_s = \frac{D_s}{\tan \theta_2} \quad (70)$$

The angle θ_2 should be selected such that

$$NA_\phi = n_2 \sin \theta_2 \quad (71)$$

then

$$\cos \theta_2 = (1 - \sin^2 \theta_2)^{\frac{1}{2}} \quad (72)$$

$$\cos \theta_2 = \frac{1}{n_2} (n_2^2 - NA_\phi^2)^{\frac{1}{2}}$$

and

$$\tan \theta_2 = \frac{\sin \theta_2}{\cos \theta_2} = \frac{NA_\phi}{(n_2^2 - NA_\phi^2)^{\frac{1}{2}}} \quad (73)$$

Substituting Eq (73) into Eq (70) gives the desired relationship between L_s and D_s in terms of the angular distribution of the light entering the scrambler

$$\frac{L_s}{D_s} = \frac{(n_2^2 - NA_\phi^2)^{\frac{1}{2}}}{NA_\phi} \quad (74)$$

Measurements performed on long (150ft) Galileo fiber optic bundles show that the equilibrium angular distribution of the light at the exit end of the fiber is described by

$$NA_\phi = .24 \quad (75)$$

For

$$n_2 = 1.625 \quad (76)$$

Eq (74) becomes

$$L_s = 6.70 D_s \quad (\text{Galileo}) \quad (77)$$

If Corning low loss fibers are used the typical parameters are

$$NA_\phi = 0.14 \quad (78)$$

$$n_2 = 1.5$$

and Eq (74) becomes

$$L_s = 10.7 D_s \quad (\text{Corning}) \quad (79)$$

A comparison of Eqs (77) and (79) shows the effects of NA_ϕ on scrambler length. If $D_s = 0.187\text{in}$, the T coupler scrambler for the Galileo fiber has a length of 1.25in whereas L_s for the Corning fiber is 2.0in. For radial couplers these lengths should be halved.

Equation (74) results from a very simple model of the scrambler and for that reason should be considered only as an approximate expression. In order for Eq (74) to give a useful result, it is necessary to properly interpret the value of NA_ϕ . Figure 22 implies that the half angle of the launch cone is associated with the half power point of the radiation pattern. This is not a valid assumption for all radiation patterns. A more detailed analysis that includes the shape of the radiant intensity distribution at the exit end of the fiber optic bundle could give the optimum scrambler

length for any given application.

Figure 22 and the preceding discussion represent the scrambler as having a circular cross section. A circular scrambler has many advantages such as ease of fabrication, good mechanical tolerance, and ease of alignment. However, the circular scrambler inherently gives nonuniform power distribution at the exit face because of skew rays that can not be shown in the axial plane representation shown in Figure 22. Both skew rays and meridional rays are shown in Figure 23 along with photographs showing the uniformity of power distribution over the end of a cylindrical scrambler rod. The light from the on-axis fiber shown in the upper part of Figure 23 is uniformly distributed because all rays are meridional. Off-axis light introduced at the edge of the scrambler is not uniformly distributed because many of the rays make a small angle with the clad surface. These small angle rays (skew rays) describe a helical trajectory made up of many reflections that keep the ray always close to the outside surface of the scrambler. Some of the off-axis light is spread over the end of the scrambler; however, most of it stays near the edge. Thus, a scrambler with circular cross section tends to give nonuniform power distribution with the highest power density at the edge of the scrambler and the lowest power density in the center. Even with the noted deficiencies in the model, Eq (74) gives a good approximation for the best scrambler length.

In a radial coupler, uniform power distribution can be achieved by uniformly distributing the fibers from the various radial arms over the entire area of the composite bundle. Another approach uses a hollow glass tube for the scrambler⁶ so that all fibers are near the edge of the scrambler. In a T coupler, the use of the split-rod construction shown in Section III.D insures a representative sampling of all signals on the data bus.

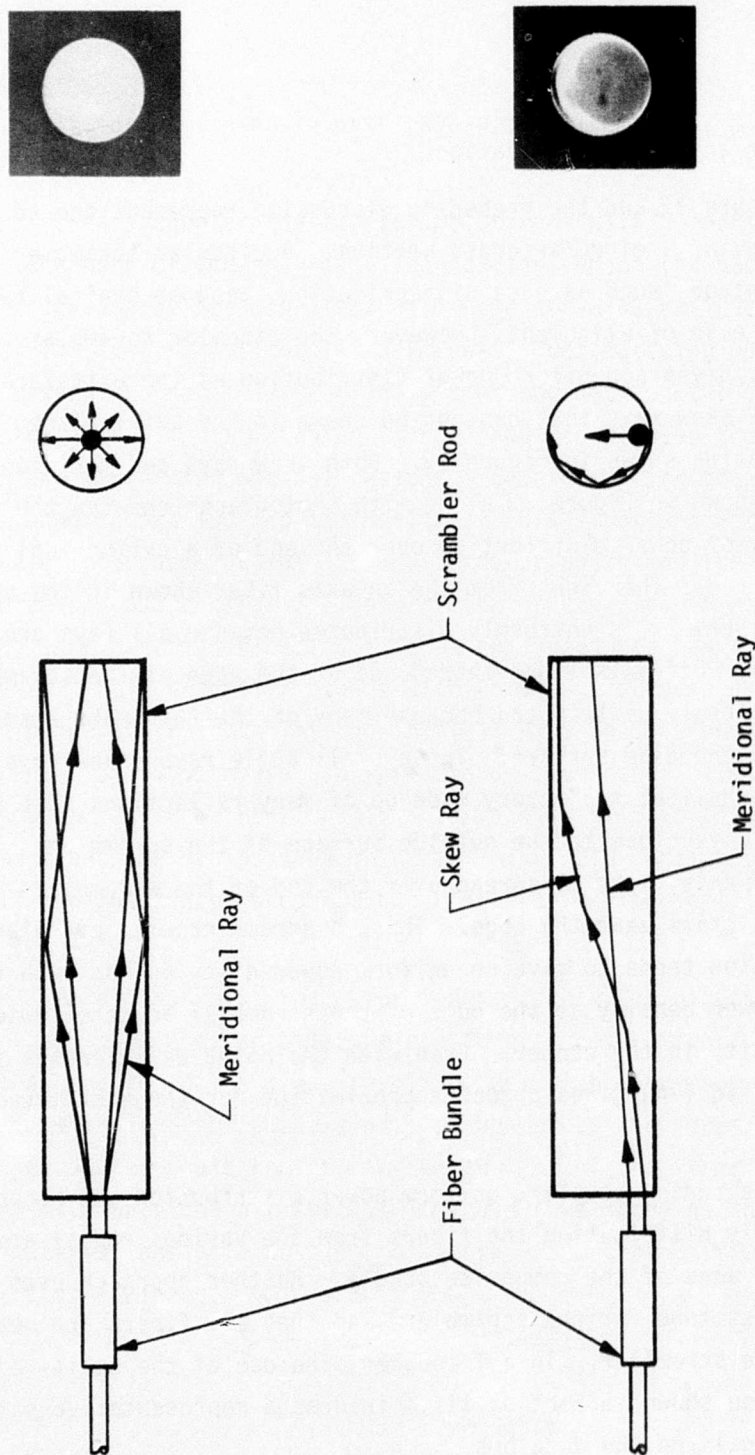


Figure 23. Power Distribution in a Cylindrical Scrambler Rod

A very simple structure which gives uniform power distribution is the rectangular scrambler shown in Figure 24. The four orthogonal faces of the rectangular rod act as plane mirrors very much like a child's kaleidoscope. Each point on the exit end of the scrambler sees the input fiber and 8 virtual images (reflections) for all positions of the input fiber. Figure 24 shows a centrally located input fiber and its reflections on the left and an off-center input fiber and its reflections on the right. Light from each input fiber is distributed uniformly over the exit face of the scrambler.

Equation (74) gives a good length for a rectangular scrambler rod if D_s is interpreted as the diagonal of the rectangular cross section; again, NA_ϕ must be properly interpreted to achieve the best result.

There are various types of fiber optic bundles that are commercially available or will be available before the end of 1975. The high NA fiber is made by Galileo (NA = 0.66), American Optical (NA = 0.66), Rank (NA = 0.58), and Pilkington (NA = .5). These products have lead glass core and borosilicate glass cladding. Because of the glass composition these fibers are not suitable for use in a nuclear environment; the lead glass core develops color centers at low dose levels. A dose of 52.6 Rad ^{60}Co -Gamma adds 0.1dB/m attenuation⁵. Also, the boron in the cladding glass has a high cross section for thermal neutrons. The Galileo fiber is low cost and readily available; the attenuation is 590dB/km and the core/fiber diameter ratio is 19/21. American Optical fiber bundles have 400dB/km attenuation and core/fiber diameter ratio of 17/19. Rank fiber optic bundles have 400-420dB/km attenuation and core/fiber diameter ratio of 9/10; this product is available from stock in England. The Pilkington fiber is moderately priced and is also available from stock in England; the attenuation is less than 100dB/km and the core/fiber diameter ratio is 17/20. The characteristics of the fiber optic bundles discussed here are shown in Table VI.

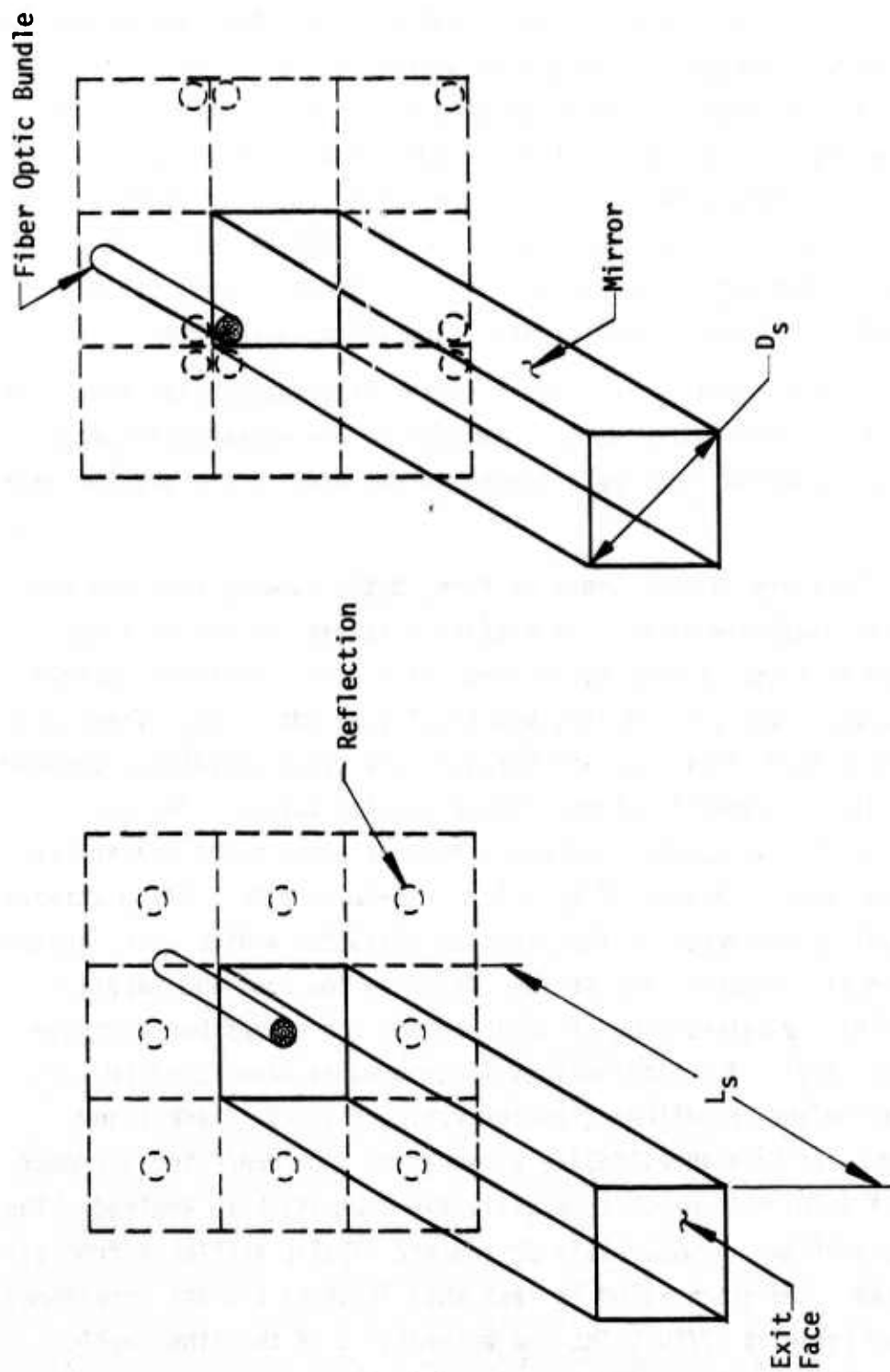


Figure 24. Power Distribution in a Rectangular Scrambler Rod

Table VI. Fiber Optic Bundles

Manufacturer	Core	Clad	NA	Core/fiber dia. ratio	Attenuation	Radiation Tolerance
Galileo	lead glass	borosilicate	0.66	19/21	<590dB/km	poor
American Optical	lead glass	borosilicate	0.66	17/19	<400dB/km	poor
Rank	lead glass	borosilicate	0.58	9/10	<420dB/km	poor
Pilkington	lead glass	borosilicate	0.50	17/20	<100dB/km	poor
Vaitec, ITT (and others)	SiO ₂	plastic (>125°C)	0.3-0.4	4/5-20/23	<100dB/km	good
Corning	SiO ₂ :Ge	SiO ₂	0.14	3/5	<30dB/km	moderate
Bell Northern	graded	SiO ₂	0.25	5/6	<8dB/km	moderate

Fiber optic bundles with pure fused silica (SiO_2) core and plastic cladding are under development in several laboratories in the United States. Valtec has announced prototype fiber bundles and ITT is working with single fibers. These fibers are expected to have $\text{NA} = 0.3\text{-}0.4$, core/fiber diameter ratios between 4/5 and 20/23, and attenuation less than 100dB/km. Since the SiO_2 core contains no doping impurities and the cladding layer is plastic these fibers are expected to have excellent characteristics in a nuclear radiation environment. The maximum operating temperature for the plastic clad-fused silica fibers will be greater than 125°C. The limited data available suggests that these plastic clad-fused silica fiber bundles will be the dominant type of fiber optic bundle used in optoelectronic data transmission and data bus applications for lengths up to 300ft. Low-loss fiber optic bundles are sold by Corning Glass. These fibers have a doped SiO_2 core and pure SiO_2 cladding. The characteristics in a nuclear environment are better than the lead glass fibers but not as good as the expected performance of the plastic clad fused silica fibers mentioned above. The Corning fibers have a core/fiber diameter ratio of 3/5, $\text{NA} = 0.14$, and attenuation of less than 30dB/km; this fiber bundle is readily available but the cost is high. Bell Northern Research of Ottawa Canada and a number of other companies are developing low-loss, graded index single fibers for long distance optical transmission ($\geq 1.0\text{km}$); because of the intended application, these graded index fibers are usually not available in bundles. It is expected that in the future bundles of 19 or more graded index fibers will find application in high-speed data buses ($\geq 100\text{Mbit/s}$). The characteristics of the Bell Northern fibers are shown in Table VI.

The key parameters of the fiber optic bundle which have the greatest impact on the design of passive couplers are the NA_ϕ and bundle diameter. The effect of these two parameters on the required length of the scrambler rod is shown in Eqs (77) and (79). In order

for a scrambler rod to give the same performance whether the light reaching it has traversed a long fiber bundle or a short fiber bundle, the NA_{ϕ} must be the same in all parts of the data bus.

Scattering and mode mixing in a fiber optic bundle changes the exit end radiation pattern (NA_{ϕ}) as a function of length. In particular, the exit end radiation pattern for long fibers approaches an equilibrium shape that is independent of launch conditions. The length required to reach this equilibrium value of NA_{ϕ} is dependent on the strength of the scattering in the particular fiber optic bundle. Due to the large amount of scattering in the Galileo fiber, the equilibrium value of $NA_{\phi} = 0.24$ is reached in about 150ft⁵. Therefore, the use of Galileo fiber in a 100ft data bus requires that the scrambler rods and LEDs both have radiation patterns characterized by $NA_{\phi} = 0.24$.

The Pilkington fiber and plastic clad-fused silica fiber both have attenuation of less than 100dB/km and most of the attenuation at 900nm wavelength is due to absorption in the core glass. Thus, these fiber types have very weak scattering; and at a length of 100ft are expected to preserve the NA_{ϕ} of the LED at the exit end of the fiber. The scrambler rods to be used with these two types of fiber optic bundle should be designed for the NA_{ϕ} of the LED. The LED planned for use on this program is the SPX 1775 edge emitter developed for the Naval Avionics Facility at Indianapolis under contract N00163-73-C-0544. The numeric aperture of the SPX 1775 is $NA_{\phi} = 0.21$.

The Corning fiber also has very weak scattering; at 100ft length, it is expected to preserve the launch angles at the exit end of the fiber. In this case, the fiber bundle has a lower value of NA than any available LED. Therefore, a data bus built with Corning low-loss fiber optic bundles will require scrambler rods designed for $NA_{\phi} = 0.14$ regardless of what LED is used.

The fiber optic bundle diameter selected for the LED/fiber optic interface (and the detector/fiber optic interface) also has an important effect on the design of passive couplers. For an in-line data bus Eq (47) gives the expression for the area of the scrambler rod in terms of the area of the LED and detector ports and number of stations; Eq (51) is the comparable expression for the radial coupler. For an 8-station in-line data bus Eq (47) gives a scrambler rod area that is 7 times the scrambler area attributed to the LED and detector or 7 times the area of the detector port alone. This corresponds to a scrambler diameter that is $\sqrt{7} = 2.65$ times the fiber bundle diameter at the detector port. From Eq (51) an 8 station radial coupler requires a scrambler rod diameter that is 4 times the fiber bundle diameter at the detector/fiber optic interface. Thus, for 46mil Galileo fiber optic bundles at the LED and detector interfaces, the scrambler rod diameter, D_s , is 122mil for a T coupler and 184mil for a radial coupler. If Corning low-loss fiber optic bundles are used, the 19 fiber bundle has a diameter of 25mil; therefore, D_s is 66mil for a T coupler and 100mil for a radial coupler. The Pilkington fiber optic bundles are supplied with fiber diameters of 85 μ m and 65 μ m. The 85 μ m fibers are available in a 30mil diameter bundle which gives a D_s value of 79mil for a T coupler and 120mil for a radial coupler. The 65 μ m Pilkington fibers are available in 22.8mil diameter bundles which give a D_s value of 60mil for a T coupler and 91mil for a radial coupler. The plastic clad-fused silica fibers will probably be supplied in the form of 19 fiber 25mil diameter bundles similar to the Corning low-loss fiber discussed above. In a radial coupler built with a rectangular scrambler rod, the cross sectional area of the rectangular scrambler rod is the same as the corresponding cylindrical scrambler rod. For equal cross sectional areas the diagonal of the rectangular rod (Figure 24) is 1.25 times the diameter of the corresponding cylindrical rod. From Eq (74) rectangular rods are required to be 25% longer than the corresponding cylindrical rods.

The dimensions of these coupler designs are summarized in Table VII; NA and bundle diameter are the two most important parameters of fiber optic bundles that affect the design of passive optical couplers. A different coupler design is required for each type of fiber optic bundle. A significant loss in performance can be expected if a coupler is used with a fiber bundle type other than the one for which it was designed.

C. GENERAL CONSIDERATIONS

The passive couplers constructed during the phase of the contract effort covered by this report have all been based on the use of Galileo fiber optic bundles. Working with a single type of fiber optic bundle simplified the logistics of the development effort and made it possible to put maximum emphasis on the development of construction techniques and mathematical models and their verification through evaluation and testing. Even though Galileo fiber was the only type used, the construction techniques and mathematical models are general and are applicable to all types of fiber optic bundles. The data bus performance will, of course, vary depending on the characteristics of the type of fiber optic bundle used in the system. This section will summarize some of the general coupler system characteristics associated with different types of fiber optic bundles.

1. Radiation Resistance/EMI/EMP

Passive optical couplers will typically use scrambler rods made from the same type of glass as the core glass of the fiber optic bundles used in the system. Flexible side arms in the couplers will employ the same type fiber optic bundle as is used in the system. With the construction technique developed on this contract, the passive couplers use unclad solid glass scrambler rods that are surrounded and held in place by a low-index Silicone or epoxy resin which also acts as a cladding layer. Based on this approach, the nuclear radiation

Table VII. Coupler Designs For 8 Station Data Bus

Fiber Optic Det. Port Bundle	Dia.	Scrambler NA_{ϕ}	Cylindrical Scrambler		Rectangular Scrambler	
			T dia.	T length * dia. * length	T diag.	T length * diag. * length
Galileo	46mil	.24 ⁽¹⁾	122mil	.82in 184mil .62in	153mil 1.03in	231mil .77in
Corning	25mil	.14 ⁽²⁾	66mil	.71in 100mil .54in	83mil .89in	125mil .67in
Pilkington (85 μ m)	30mil	.21 ⁽³⁾	79mil	.61in 120mil .46in	99mil .76in	150mil .58in
Pilkington (65 μ m)	22.8mil	.21 ⁽³⁾	60mil	.46in 91mil .35in	75mil .58 in	114mil .44in

(1) Equilibrium NA_{ϕ} of Galileo fiber

(2) Limiting NA of Corning low-loss fiber

(3) NA_{ϕ} of SPX 1775 LED

resistance of the passive coupler is expected to be equal to or better than an equivalent length of the corresponding fiber optic bundle. With the lead glass/borosilicate glass fibers (Galileo, Rank, American Optical and Pilkington) the plastic cladding used in the coupler will give superior performance to the borosilicate glass used in the fiber optic bundles. This same situation applies to couplers made for Corning low-loss fiber. With the plastic clad-fused silica fibers, the couplers and fiber optic bundles should have equivalent radiation resistance. Since these fibers and couplers use undoped SiO_2 , they are expected to give the best radiation resistance of any of the approaches considered. All-plastic fiber bundles and couplers based on DuPont's Crofon fibers will provide even better nuclear radiation resistance than the plastic clad-fused silica fibers. This approach has not been considered because plastic fiber optic bundles require LEDs with a wavelength of less than 700nm and high-performance LEDs in this wavelength range are not available. Basic material limitations seem to indicate that a suitable plastic-fiber LED will not be achieved.

The passive parts of an optoelectronic data bus (the coupler and fiber optic bundles) consist of glass and plastic insulators that are immune to electromagnetic interference (EMI) such as ground loops, cross talk, and radio frequency interference (RFI). The term electromagnetic pulse (EMP) covers a wide range of electromagnetic phenomena associated with nuclear blasts; the passive parts of the optoelectronic data bus will withstand all levels of EMP that are not mechanically or thermally damaging to the aircraft.

2. Thermal

In the all-glass fiber systems, the fibers themselves are not damaged by temperatures of several hundred centigrade degrees ($^{\circ}\text{C}$); the Corning fibers being almost pure SiO_2 will withstand the

highest temperature. However, the jacketing material used by most fiber bundle manufacturers is polyvinyl chloride or PVC which carries a recommended temperature range of 0-80°C. Other jacketing materials are available on special order. The two most promising materials are Teflon and Kynar. Both of these materials cover the full MIL-E-5400P Class 4 temperature range from -54°C to +125°C.

The plastic clad fused silica fibers are limited by the maximum temperature of the plastic cladding material. The composition of the cladding material is proprietary and the same material is probably not being used by all of the laboratories engaged in the development of this type of fiber. However, the operating temperature range of the plastic clad-fused silica fiber is expected to be -54°C to +125°C or greater. Again, an appropriate jacket material such as Teflon or Kynar is required to achieve this temperature range with fiber optic bundles.

The DuPont Crofon fiber has a core made of polymethyl methacrylate which is also known by the trade names Lucite and Plexiglass. This common plastic has a heat distortion temperature of 100°C; however, DuPont recommends that the intermittent maximum temperature not exceed 95°C and that the continuous maximum temperature not exceed 80°C. The recommended minimum temperature for Crofon is -40°C. Crofon fiber optic bundles are not recommended for military data bus use and are only mentioned here because of their radiation resistance.

Fiber optic terminations usually employ a precision piece part called a ferrule and a suitable cement to bond the fiber optic bundle and jacket to the ferrule. Acceptable optical transmission for the termination requires that the end of the fiber optic bundle be perpendicular to the axis of the ferrule and polished with an optical quality finish. Thus, the ferrule material and cement

must both be compatible with the optical polishing procedure. The fiber optic terminations made at Spectronics, Inc. have typically employed brass ferrules and epoxy resins with heat distortion temperatures of 150°C. These materials are compatible with the optical polishing techniques used at Spectronics and operate over the -55°C to +125°C temperature range. The Silicone elastomers such as Sylgard 182 and 184 have excellent high-temperature characteristics but are not used in terminations because they can not be polished. Cyanoacrylate adhesives, such as Rapid-Set, cure to form a clear transparent solid, and are recommended for use at temperatures above 125°C. A rigid curing Silicone resin has also been identified which has excellent high temperature characteristics. Both of these materials show promise as suitable cements for -54°C to +125°C terminations. No work has been done on this program on insulating ferrules. However, several dimensionally stable filled plastic materials are available that are compatible with optical polishing techniques and operate over the required temperature range -54°C to +125°C. Insulating plastic ferrules can be made by molding and/or machining.

Some of the passive optical couplers constructed on this program and described in Section III.D were mounted in clear Plexiglass housings to display their internal geometry and the construction techniques used in their manufacture. The use of Plexiglass limits these units to a maximum temperature of 80°C. However, there is no temperature limit imposed by the construction techniques and proper selection of materials should result in a coupler that will operate over the temperature range -54°C to +125°C. Acceptable housing materials are brass, aluminum and high-temperature filled plastics.

The passive optical couplers built and evaluated on this program were all designed for compatibility with lead glass fiber optic bundles (Galileo) and therefore used lead glass scrambler rods.

The high index of refraction ($n = 1.62$) of these scrambler rods makes it possible to use high-temperature epoxies having index of refraction values in the range $n = 1.52$ to $n = 1.56$ as both cladding and cement. Thus, the required -54°C to $+125^{\circ}\text{C}$ temperature range can be achieved in couplers designed for lead-glass fibers.

In order to equal the radiation resistance of the plastic clad-fused silica fibers, a passive coupler must use scrambler rods made from fused silica. The low index of refraction of fused silica ($n = 1.45$) severely limits the number of cements that can be used in coupler construction. The best candidates are the Silicone elastomers Sylgard 182 and 184 with $n = 1.43$; from Eq (67) these materials on fused silica give a numeric aperture of $\text{NA}_s = 0.24$. This value of NA_s is marginally adequate for use with the SPX 1775 LED which has a radiation pattern characterized by $\text{NA}_\phi = 0.21$. The preferred approach, in this case will be to clad the fused silica scrambler rod with the same proprietary plastic used on the fibers. With a plastic clad scrambler rod there is no index of refraction restriction placed on the cement used in the construction of the passive coupler.

In summary, all of the glass and plastic clad-fused silica fiber optic bundles discussed in this section are suitable for operation over the MIL-E-5400P Class 4 temperature range of -54°C to $+125^{\circ}\text{C}$ provided a high-temperature jacketing material is used. Ferrule and housing materials and cements are available for constructing compatible terminations and passive optical couplers which will operate over the full temperature range.

3. Mechanical

No investigations of the mechanical strength of fiber optic bundles have been performed on this program. However, the reported data indicate that fiber optic bundles are compatible with the altitude,

shock, vibration, and acoustic noise specifications set forth in MIL-E-5400P Class 4.

Passive optical couplers will be constructed such that all voids are filled with an appropriate epoxy or casting resin. No critical mechanical or environmental limitations are anticipated for these parts.

The greatest potential for mechanical damage to the components of an optoelectronic data bus will occur during installation in the aircraft. Tensile strength and flexure tolerance data show that fiber optic bundles are about as rugged as copper wire. It is felt that techniques can be developed which will insure damage free installation of optoelectronic data bus components.

4. Index Matching

Index matching can be used to good advantage in the construction of passive optical couplers to reduce the front surface reflection loss at the various interfaces. For Galileo fiber optic bundles and related scrambler rods the theoretical improvement in the transmission of an interface is 12% as given in Eq (22). In order for this degree of improvement to be realized, two requirements must be met

- the interface in question must be experiencing the full theoretical front surface reflection loss without index matching, and
- the material used for index matching must have an index of refraction equal to that of the glass on each side of the interface.

It is possible to observe less than full front surface reflection loss at a glass/air/glass interface when interference effects between the two surfaces are significant. With visible light, interference effects are significant only when the separation between the two surfaces is very small -- about $1\mu\text{m}$ or less. However, the narrow band of 900nm light from a GaAs LED is relatively more coherent than white visible light and significant interference effects can occur when the two surfaces are separated by as much as $30\mu\text{m}$ (1.2mil). When two flat and parallel glass surfaces are separated by an integral number of half wavelengths of the LED light and where the maximum separation is less than $30\mu\text{m}$, some degree of index matching will occur even though the glass surfaces are separated by air. When the same surfaces are separated by an odd number of quarter wavelengths of the LED light, no matching occurs. In a practical coupler, the surfaces are neither ideally flat nor parallel. Therefore, any given physical spacing of the interface will include regions that are spaced at all fractions of the LED wavelength. Some regions will appear to have the full calculated front surface reflectivity and some regions will have less reflectivity than the calculated value. Based on this discussion, the reflectivity values calculated in Section II.B are worst case values that may be reduced somewhat by interference effects. The presence of interference at the glass/glass interfaces in a passive coupler produces both desirable and undesirable effects. It is desirable that the interference effects in general tend to reduce the front surface reflection loss. It is undesirable that this reduction is very position sensitive and difficult to reproduce.

When the material used for index matching has the same index of refraction as the glass on each side of the interface, then the interface disappears and no reflection or interference effects are observed. If the index matching material has a different

index than the glass, then part of the reflection effects remain. The data presented in Table V provide a measure of the reduction in front surface reflection provided by different materials. Equation (25) shows that Sylgard 184 ($n = 1.43$) on lead glass ($n = 1.62$) reduces the front surface reflectivity from 5.67% to 0.41% -- this is a very significant reduction of 13.8 times even though the index values are not well matched.

Experimental evaluation of index matching is presented in Section II.C. These tests were performed with the unpolymerized resin of a Silicone or epoxy system used without adding the hardner. For a fiber bundle/fiber bundle interface using two 65mil diameter bundles, the observed improvement with index matching was between 9% and 15%. This compares favorably to the theoretical improvement of 12% presented by Eq (22). Index matching tests were also performed on the split rod T coupler described in Section III.D. These measurements were made using Sylgard 184 resin as the matching fluid in the scrambler rod/slotted rod interfaces. Transmission improvements were observed but were typically lower than expected -- performance within 8 % of the expected value were obtained. This discrepancy is believed to be the result of the interference effects discussed above. These effects would cause the transmission to be higher than expected without the index matching material and would, therefore, give an improvement less than the expected value.

In addition to reducing front surface reflection losses, the use of index matching materials also stabilizes coupler performance and fills voids in the optical path that might become contaminated with dust or other foreign substances. The passive couplers constructed on this program used a modular approach which allowed independent testing of subassemblies and removal and replacement of the scrambler rods. As a result, the index matching tests used only liquids that are referred to elsewhere in the report as index matching fluids. Passive

couplers built for use in an avionic data bus will employ a different fabrication strategy.

In a T coupler the two scrambler rods will be permanently bonded to the body of the coupler. The bonding cement (probably a Silicone or cyanoacrylate adhesive) will also serve as an index matching material. In a radial coupler permanent index matching bonds will be used between the scrambler rod and mirror and between the scrambler rod and side arms. Index matching is not required between the scrambler and mirror for optical reasons. However, a permanent bond should be used to preclude contamination of this important interface. The plugable interfaces at the LED and detector ports and the input/output ports can use a clear Silicone grease or the resin of Sylgard 182 or 184 as a matching fluid. Silicone compounds of this type exhibit very little viscosity change with temperature and should remain in place after installation. A fluid also has the advantage that it can be easily removed and replaced as a means of eliminating foreign substances from the plugable interface. This can also be a disadvantage because fluids tend to capture and hold foreign substances if the interface is opened under adverse environmental conditions.

An alternate approach for index matching in plugable interfaces is the use of a cured Silicone elastomer. Both Sylgard 182 and Sylgard 184 cure to form a clear resilient gel with a dry non-tacky surface. A thin layer of cured elastomer bonded to the input/output port of the coupler would conform to the surface of the fiber optic bundle and eliminate the air space. It would thus serve as an index matching material and as a cushion to separate and protect the polished glass surfaces.

D. EVALUATION

Both T couplers and radial couplers were designed, constructed and evaluated on this program. Two or more couplers of each type were constructed and representative units supplied to the Avionics Laboratory as working models. These prototype couplers have been configured to interface with the 10-Channel Data Bus Demonstrator as a working demonstration.

In an in-line data bus the T couplers are connected with flexible fiber optic bundles. In a radial data bus flexible fiber optic bundles are used for the connections between the stations and the radial coupler. In both systems the optical signal must pass through several fiber optic terminations. Thus, the transmission of the terminations is an important parameter in determining system performance. The worst case power ratio expressions for the two systems are given in Eqs (48) and (58). In these two expressions the performance factors representing the passive couplers and fiber optic terminations are included explicitly as separate terms. This approach was used in the analysis so that the effects of the various parts of the system on overall system performance could be illustrated.

All of the passive couplers constructed in this R&D phase of the program have used Galileo fiber optic bundles with conventional epoxy filled terminations and matching lead glass scrambler rods with length appropriate to $NA_{\phi} = 0.24$. However, the physical structures used can be adapted for use with compressed and/or etched terminations as described in Section II of this report. Other types of fiber optic bundles can also be used provided the appropriate dimensional changes are made as outlined in Table VII.

1. T Coupler

Figure 15 shows a T coupler for a uniform duplex data bus. This figure implies that both the through transmission path and the side arms are made from fiber optic bundles. This construction

technique was investigated early in the program. Transmission through the coupler in either direction encounters a full termination loss due to the packing fraction of the fiber optic bundle used in the coupler body. The transmission of these internal terminations can be maximized by using etched and compressed terminations and index matching. However, the use of these techniques increases the complexity of coupler fabrication and offers no performance advantage over the use of a solid glass rod as the coupler body. Thus, the construction technique for T couplers illustrated in Figure 15 has been abandoned. Fiber optic bundles have continued to be used in the LED and detector side arms. This is a practical expedient in that it offers a means of getting light on and off the main bus while maintaining the NA_ϕ constant in all parts of the system. As discussed in Appendix I, the fiber optic bundle can bend on a radius as small as 20 times the core diameter of an individual fiber without significantly affecting the NA_ϕ of the light being transmitted. The fiber optic bundle termination also offers a convenient plugable interface for the LED and detector. The basic concept of a solid glass rod coupler body with fiber optic bundle side arms is compatible with Eq (48). This expression for the worst case power ratio of an in-line data bus shows that the transmission quality factor m_T is encountered $N-2$ times whereas the coupling quality factor is encountered only 2 times. Thus, m_T has much greater significance than m_C in determining system performance and the greatest emphasis should be placed on maximizing m_T .

A uniform duplex coupler for a 17 station data bus was selected for evaluation. This particular form of T coupler was selected because it can be constructed using standard fiber bundle diameters. Also, a T coupler designed for 17 stations could be used in the 8 station data bus to be constructed on this program to provide for expansion of the system by adding more stations.

From Eq (46) the optimum value of C_T for a 17 station coupler is

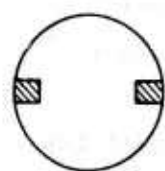
$$C_{opt} = \frac{1}{2(17-1)} = \frac{1}{32} \quad (80)$$

and from Eq (47) the area of the scrambler should be 16 times greater than the area attributed to the LED and detector ports. The general construction of this uniform duplex T coupler is shown in Figure 25. The proper area ratio is obtained when the interconnecting fiber optic cables have a nominal 187mil diameter and the LED and detector ports each form a nominal 46mil diameter bundle. Table III shows that the appropriate scrambler diameter is 180mil. Light entering the coupler is transmitted from the fiber optic bundle into the scrambler and on to the solid rod body and exit scrambler without a packing fraction loss. Light going out of the coupler in either direction encounters one termination loss when it is transmitted into the fiber optic bundle. This termination loss is important in calculating system performance but is not charged against the T coupler.

The first T coupler designed and constructed on this program used a slotted glass rod body shown in Figure 26 and two 180mil diameter scrambler rods. Each of the slots will hold one half of the fibers in a 46mil diameter bundle; each slot has a cross sectional area that is 1/30 of the area of the full 180mil diameter rod. Thus, C_T is 1/30 in reasonable agreement with Eq (80) and the slot area attributed to the LED and detector ports is 1/15 of the area of the scrambler rod in reasonable agreement with Eq (47).

A versatile set of precision termination hardware was developed to facilitate the construction of all of the passive couplers built on this program. A typical set of this hardware is shown in Figure 27. The fiber optic ferrule has a 180mil diameter bore to form a conventional termination on the fiber optic bundle.

COUPLER PARAMETERS		
Symbol	Defining Equation	Typ. Value (8 sta)
C	(see illustration)	-14.8dB
m_C^C	P_o/P_a	-18.2dB
T_T	P_t/P_a	-1.6dB
m_C	$P_o/(C_T P_a)$	-3.4dB
m	$(P_t + 2P_o)/P_a$	-1.5dB



$$C_T = \frac{\text{area of one slot}}{\text{scrambler area}}$$

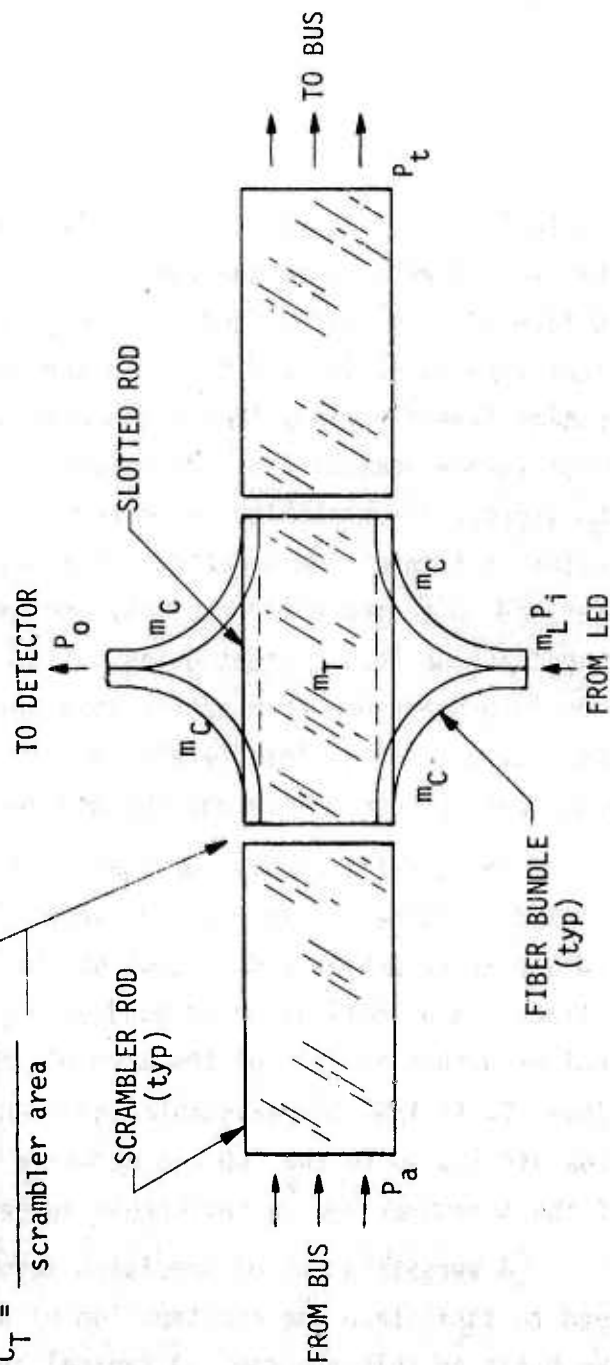
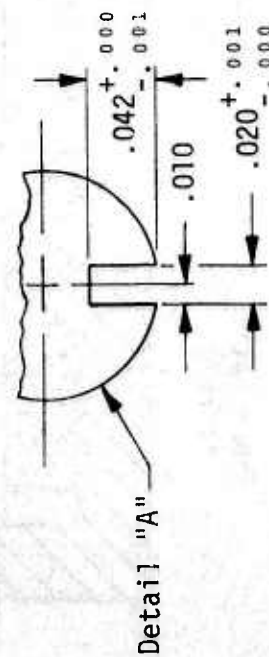
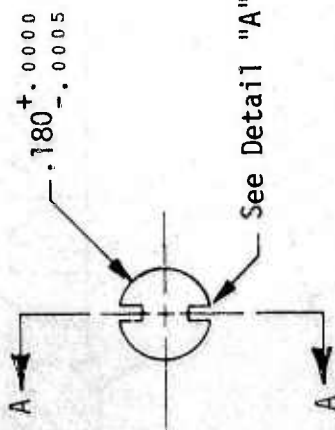
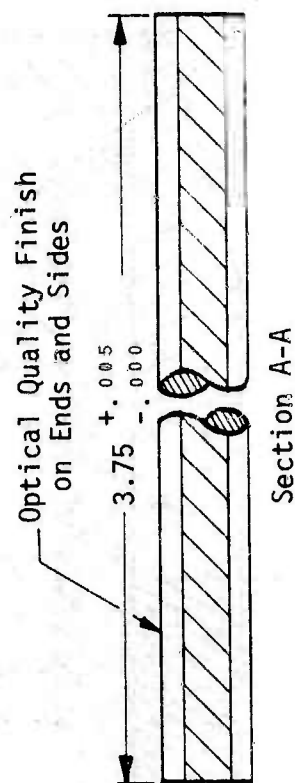


Figure 25. Optical Layout of T Coupler



Lead Glass
 $n = 1.62$

Figure 26. Slotted Glass Rod Coupler Body

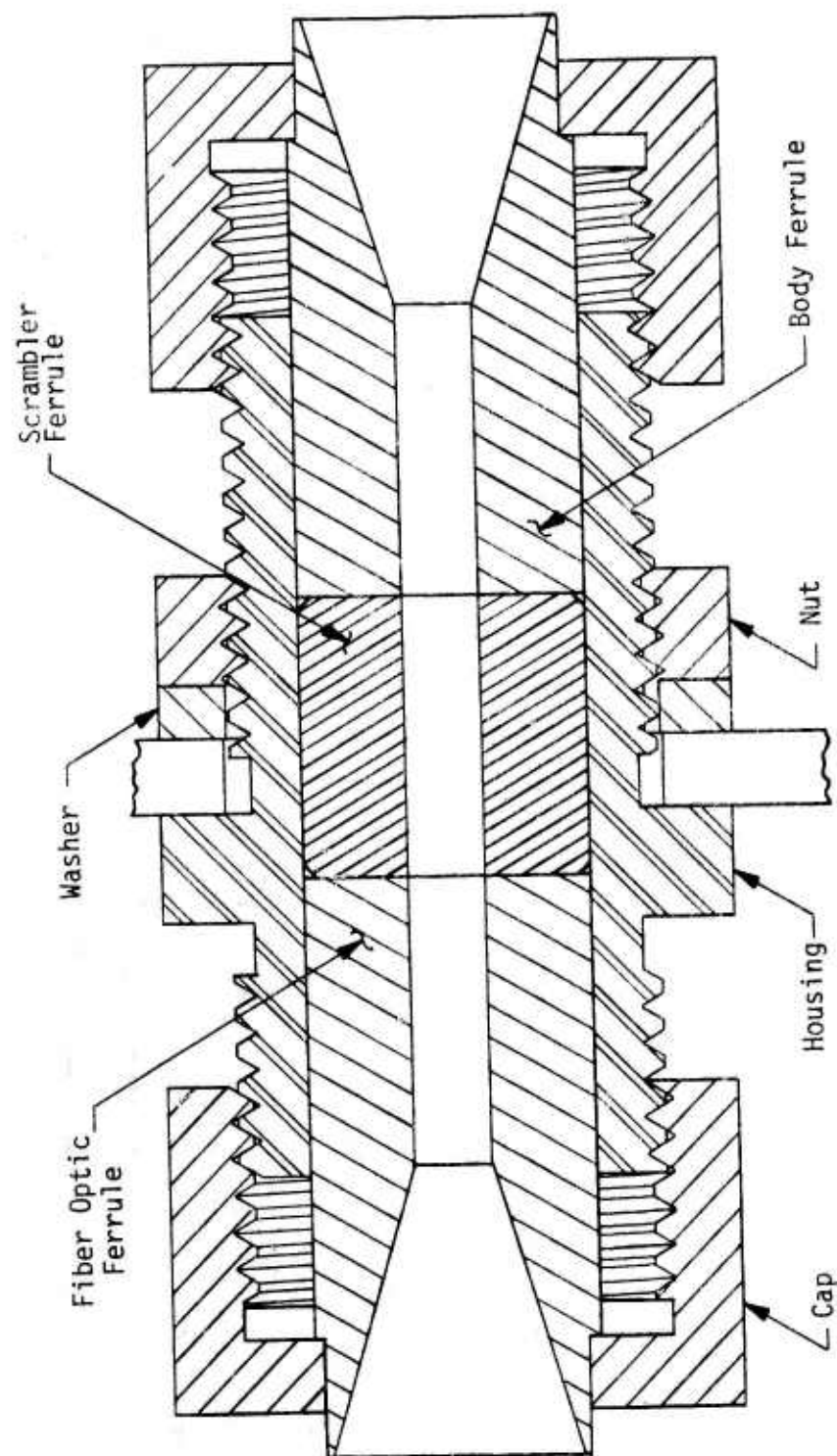


Figure 27. Coupler Termination Hardware

The scrambler ferrule supports and positions the 180mil diameter scrambler rod. The body ferrule supports one end of the slotted rod with flexible fiber optic bundles in the slots for the LED and detector side arms. There is a body ferrule on each end of the slotted rod; two complete sets of this termination hardware are required to construct a T coupler. The mechanical tolerances of the outside diameter of the ferrules and the inside diameter of the housing are held to $\pm 0.2\text{mil}$. This insures good centering and alignment of the various optical interfaces. Referring to Eq (21), the termination hardware of Figure 27 has a probable misalignment at each interface of about $\Delta = 0.7\text{mil}$. This gives a fractional lost area of about 0.48%.

Two views of the first slotted rod T coupler are shown in Figures 28 and 29. The coupler was built in a metal box with clear inserts in the top and bottom to allow observation of the construction details. The dimensions of this coupler are approximately 6in x 3in x 3in.

Transmission measurements made on this coupler at the Avionics Laboratory gave

$$\begin{aligned} C_T &= 3.3\% & (-14.77\text{dB}) \\ m_C C_T &= 0.56\% & (-22.44\text{dB}) \\ m_C &= 17.1\% & (-7.66\text{dB}) \\ T_T &= 61.5\% & (-2.11\text{dB}) \\ m &= 62.6\% & (-2.03\text{dB}) \end{aligned} \tag{81}$$

The symbols used here are defined in detail in Section III.A and indicated schematically on Figure 25. The term C_T is given by the physical area ratio of the slotted rod according to Eq (36). The factor $m_C C_T$ is the measured power at the detector port divided by the total power at the input port. The coupling quality factor m_C , Eq (39), is calculated from C_T and $m_C C_T$ and recorded here for comparison purposes. The transmission of the T coupler, T_T , is measured power at the output port

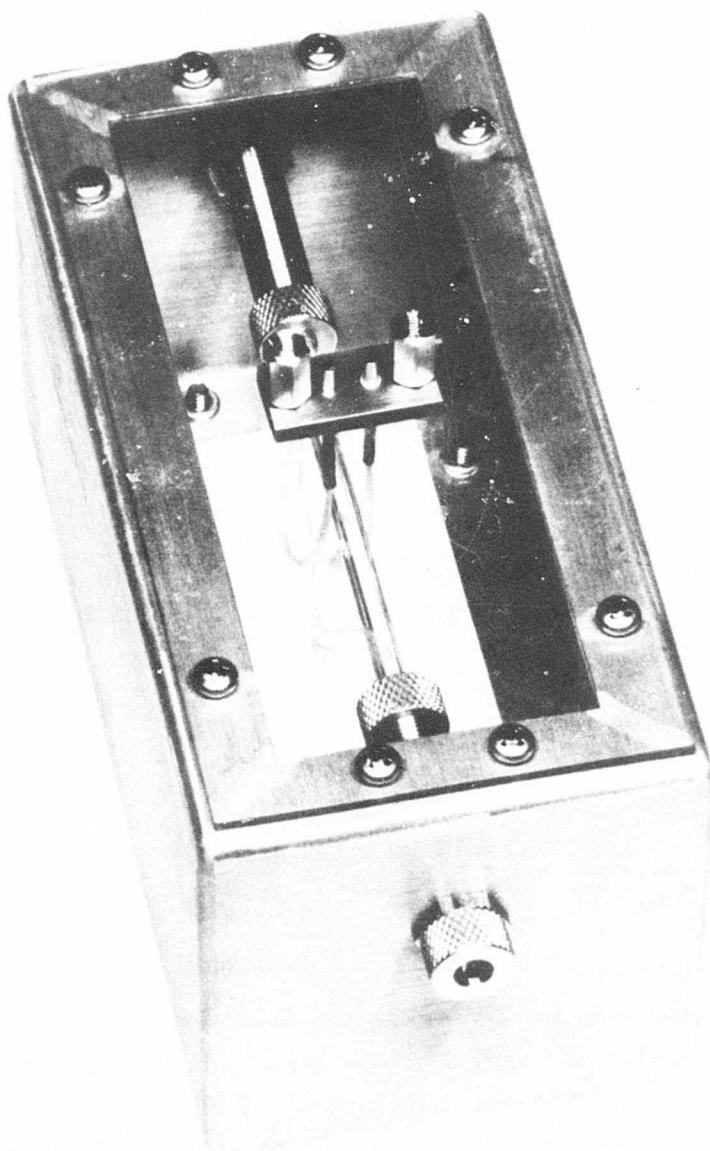


Figure 28. Experimental T Coupler

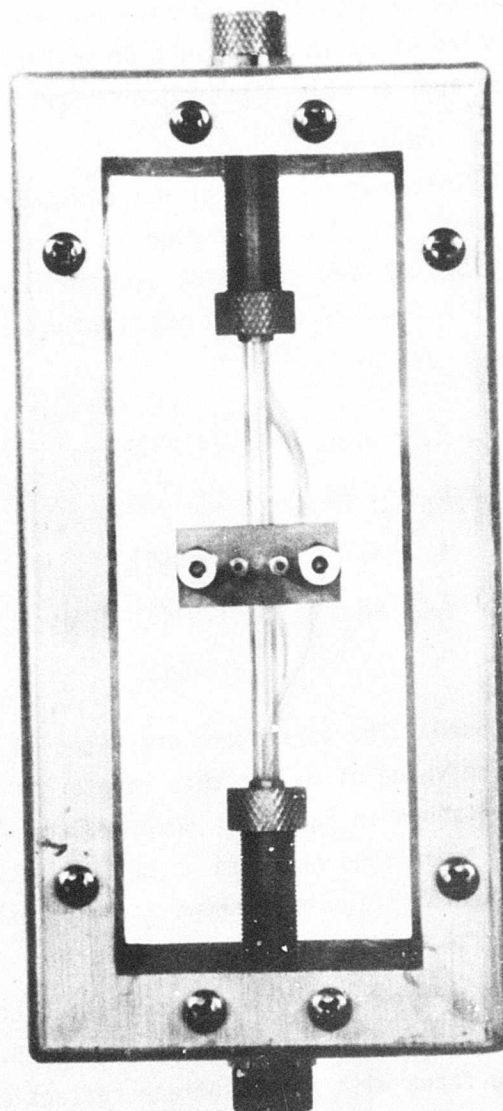


Figure 29. T Coupler, Top View

divided by the total power at the input port. The overall quality factor, m , is calculated from Eq (43) and recorded here for comparison purposes. The low value of m_C is the result of broken fibers in the LED and detector side arms on this first experimental coupler; no index matching was used.

A second slotted rod T coupler was constructed and evaluated at Spectronics, Inc. This T coupler used a shorter slotted rod than the first one. This allowed the total package size to be reduced to 4.25in x 1.25in x 1.0in. Transmission measurements on this unit gave

$$\begin{aligned}
 C_T &= 3.3\% & (-14.77\text{dB}) \\
 m_C C_T &= 1.5\% & (-18.16\text{dB}) \\
 m_C &= 45\% & (-3.39\text{dB}) \\
 T_T &= 68.5\% & (-1.64\text{dB}) \\
 m &= 71.5\% & (-1.46\text{dB})
 \end{aligned} \tag{82}$$

No index matching was used. The parameters evaluated in Eq (82) are shown in Figure 25. The value of m_C for this coupler is considerably improved over the value shown in Eq (81). However, the 45% value of m_C shown in Eq (82) is lower than expected which indicates the presence of some broken fibers. Figure 30 shows a photograph of the polished end of the slotted rod used in this coupler.

The expected performance of a slotted rod T coupler can be calculated using the optical layout shown in Figure 25. The through transmission has six surfaces with front surface reflection. The front surface reflection for an air interface can be calculated from Eq (23) for $n_1 = 1.0$ and n_2 for the various glass parts. The slotted rod and scrambler rods have $n_2 = 1.62$ which gives

$$R_S = .0560 \tag{83}$$

The reflection loss at the exit end of the input fiber optic bundle is included in the system equations as T_c and should not be charged against the coupler. From the dimension of the slots, 1/15 of the

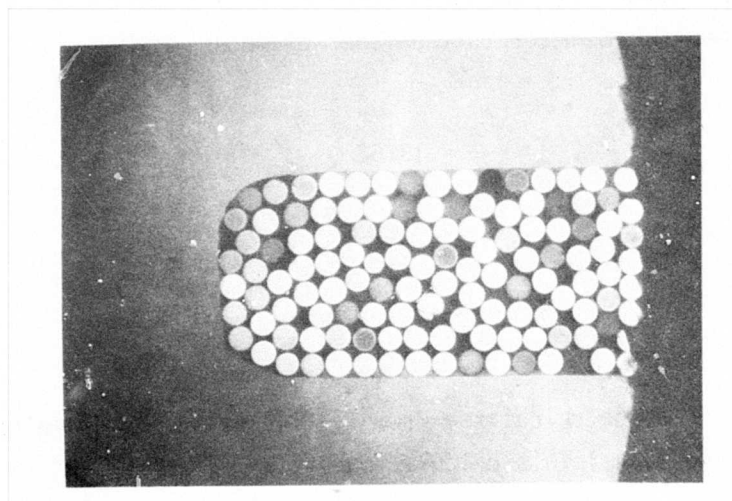


Figure 30. T Coupler Slotted Rod, End View

through transmission is removed for the side arms. The expression for the through transmission is

$$\begin{aligned}
 T_T &= (1 - R_s)^6 \quad (14/15) \\
 &= (1 - .056)^6 \quad (14/15) \quad (84) \\
 &= 0.660 \text{ or } 66.0\% \text{ } (-1.80\text{dB})
 \end{aligned}$$

The side arm output starts with the light falling on each of the slots which is 1/30 of the total. This value is further reduced by two front surface reflections and the packing fraction loss of the side arm fiber. Calculation and graphical layout have shown that the packing density of circular fibers in a rectangular slot is equal to or better than the packing density of those same fibers into the circular arrangement shown in Figure 2. The equivalent circular arrangement will be used for calculating a limiting value of m_c .

From Figure 2, interpolation for $N = 142$ gives a diameter ratio of 13.35. The discussion associated with Table II shows that this diameter ratio should be increased by 2% to obtain the ratio of the equivalent ferrule diameter to the fiber diameter; thus,

$$\frac{D_f}{d} = 13.62 \quad (85)$$

and

$$\frac{D}{d} = \sqrt{142} = 11.92 \quad (86)$$

The value of G may be calculated from Eq (14) using the diameter ratios in Eqs (85) and (86). This calculation gives

$$G = \left(\frac{11.92}{13.62} \right)^2 = 0.766 \quad (87)$$

The packing fraction, P , for this coupler is

$$\begin{aligned} P &= G R_a \\ &= (0.766)(0.8186) \\ &= 0.627 \end{aligned} \quad (88)$$

where R_a for the Galileo fiber optic bundles is given by Eq (7). Combining this packing fraction with the four front surface reflections gives

$$\begin{aligned} m_c &= (1 - R_s)^2 (1 - R_c)^2 P \\ &= (.944)^2 (.9433)^2 (.627) \\ &= 0.497 \text{ or } 49.7\% \text{ } (-3.03\text{dB}) \end{aligned} \quad (89)$$

Combining Eq (89) with the area ratio gives

$$\begin{aligned} m_C C_T &= (0.495)(1/30) \\ &= 0.0166 \text{ or } 1.66\% \text{ } (-17.81\text{dB}) \end{aligned} \quad (90)$$

The transmission quality factor for the slotted rod T coupler can be calculated from Eq (37)

$$\begin{aligned} m_T &= \frac{0.660}{1 - \frac{2}{30}} \\ &= 0.707 \text{ or } 70.7\% \text{ } (-1.50\text{dB}) \end{aligned} \quad (91)$$

The overall quality factor can be obtained from Eq (43)

$$m = 0.693 \text{ or } 69.3\% \text{ } (-1.59\text{dB}) \quad (92)$$

The calculated and measured performance parameters of the slotted rod T couplers are compared in Table VIII . Coupler No. 2 performance is close to the calculated values on all parameters.

Table VIII. Slotted Rod T Coupler Performance Comparison

Parameter	Coupler No. 1	Coupler No. 2	Calculated Values
C_T	3.3%	3.3%	3.3%
m_C	17.1%	45.0%	49.7%
$m_C C_T$	0.57%	1.5%	1.66%
T_T	61.5%	68.5%	66.0%
m	62.6%	71.5%	69.3%

The greatest deviation is the 10% difference between the measured and calculated values of m_C . This deviation can be accounted for by a detailed inspection of Figure 30. This photograph shows only 124 fibers which is 12.7% less than the assumed count of 142. The loss of 18 fibers would not of itself reduce m_C by 10%; however, the relatively poor packing density of the remaining 124 fibers and the number of dead fibers shown in the photograph do adequately account for the loss in m_C . A smaller deviation ($\sim 3\%$) is also noted for the measured and calculated values of T_T and m . However, the measured values are higher than the calculated values. This result demonstrates the presence of the interference effects discussed in Section III.C.4.

Due to the close index of refraction match between the scrambler rods and Galileo core glass the use of an index matching fluid will essentially eliminate front surface reflection. Based on Table V the Dow epoxy is an ideal matching fluid. The calculated performance of a slotted rod coupled with index matching is shown in Eq (93).

$$\begin{aligned}
 C_T &= 3.3\% & (-14.77\text{dB}) \\
 m_C &= 59.1\% & (-2.28\text{dB}) \\
 m_C C_T &= 1.97\% & (-17.05\text{dB}) \\
 T_T &= 93.4\% & (-0.297\text{dB}) \\
 m &= 97.3\% & (-0.117\text{dB})
 \end{aligned}
 \tag{93}$$

This calculation assumes the use of conventional terminations on the fiber optic bundles.

Measurements have been made using Sylgard 184 resin as the matching fluid in the scrambler rod/slotted rod interfaces. Transmission measurements within 8% of the expected value have been observed. Failure to observe the full calculated performance is believed to be the result of multiple reflection and interference effects and small unidentified

losses. When no index matching is used, these two effects tend to compensate and measured performance is close to the calculated value. When the index matching fluid is introduced, only the losses remain and the expected performance is not achieved. The measurements indicate the presence of -0.337dB of unidentified losses in the slotted rod T coupler. When no matching fluid is used, the multiple reflection and interference effects improve the transmission by 0.499dB. The loss in the slotted rod could be the result of scattering from the imperfectly polished sides of the slots. Further study is required to finally resolve this difference between measured and calculated performance.

An improved T coupler was designed using a split rod for the coupler body. The split rod is made of two of the halves shown in Figure 31. This configuration is more desirable than the slotted rod because the flat face of the rod can be easily polished whereas polishing the inside of the slots is more difficult. Also, the split rod construction spreads out the side arm fibers across a diameter of the scrambler rod. This gives a more reliable sampling of the total optical power. One split rod coupler was constructed using the termination hardware shown in Figure 27. Two different views of the coupler are shown in Figures 32 and 33. This unit was assembled in clear plastic to give visibility to the construction details; the package size is 4.25in x 1.25in x 1.0in. Using the nominal dimensions shown in Figure 31 to calculate the area ratio, the split rod T coupler has a coupling factor of

$$C_T = 3.18\% \quad (-14.98\text{dB}) \quad (94)$$

The other measured parameters are

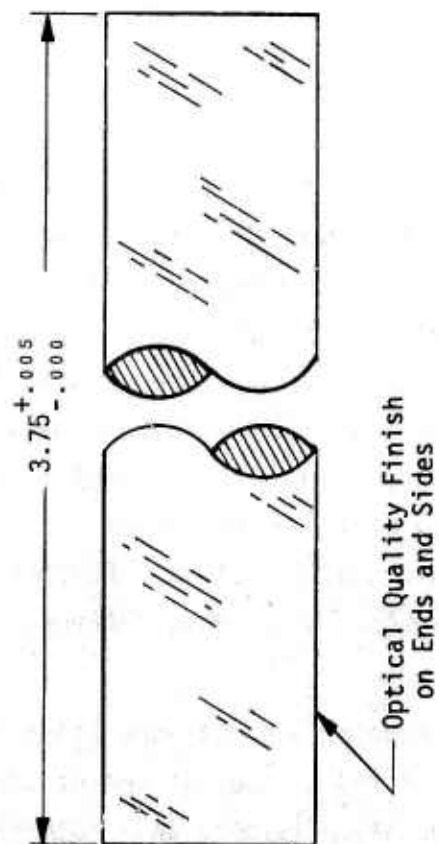
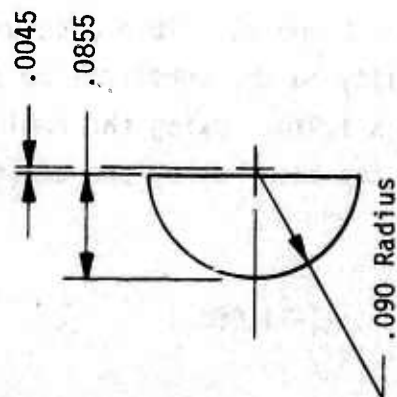


Figure 31. Split Rod Coupler Body

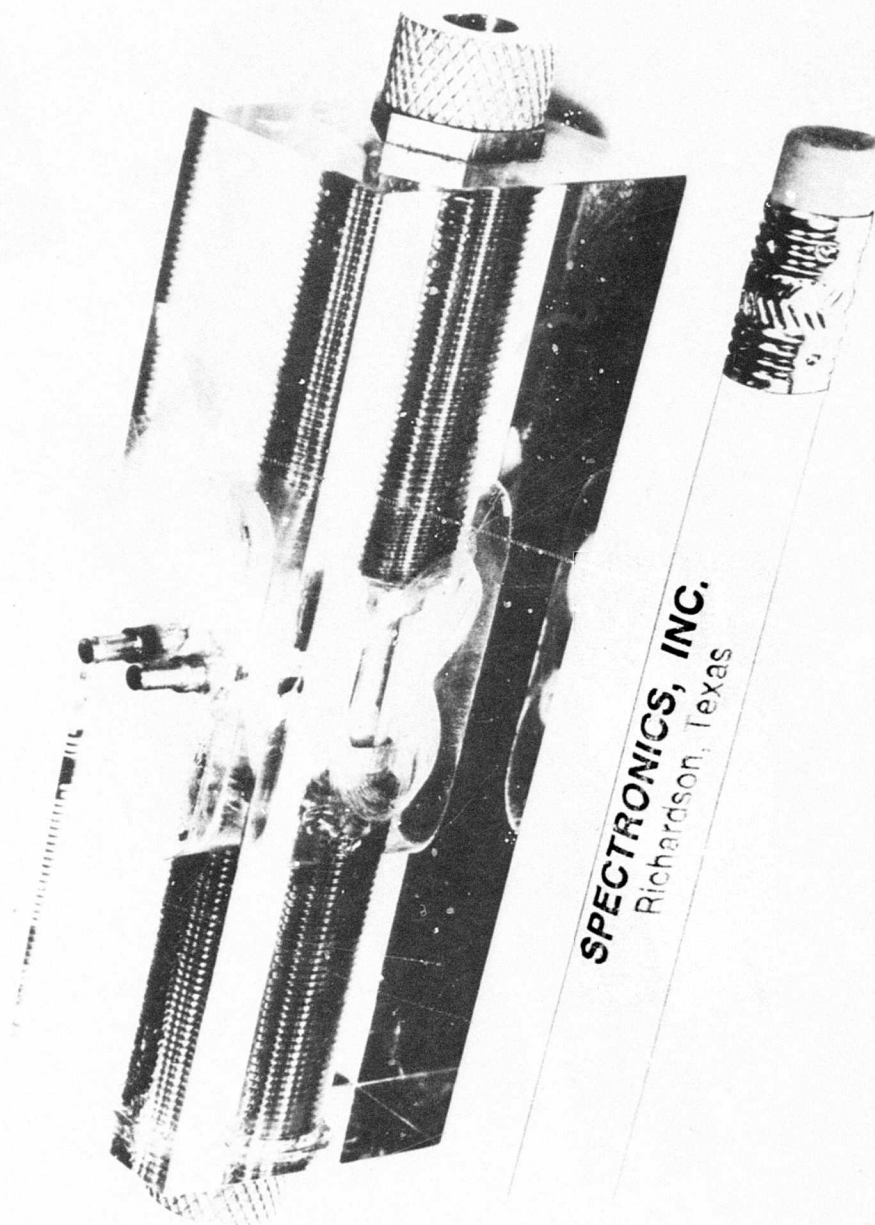
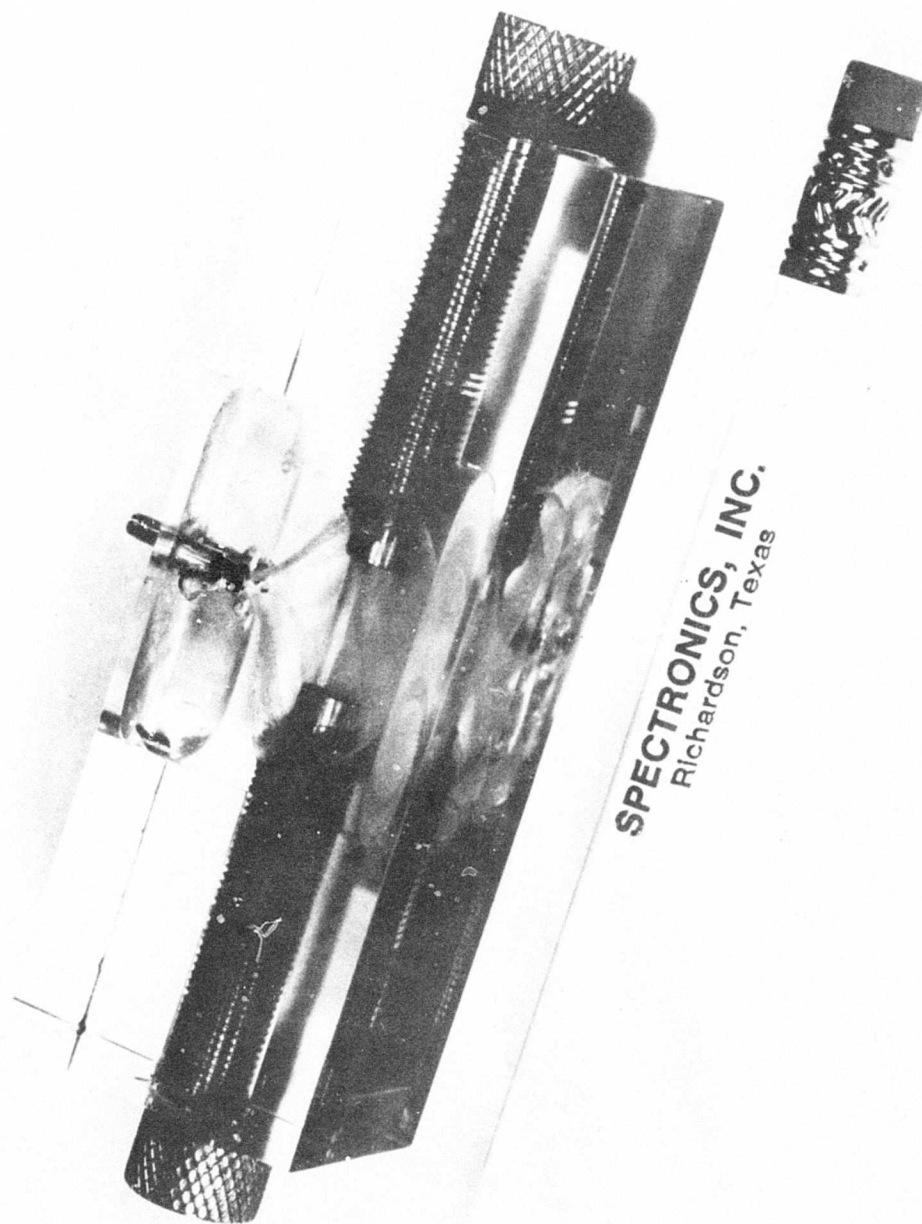


Figure 32. Split Rod T Coupler, Top View



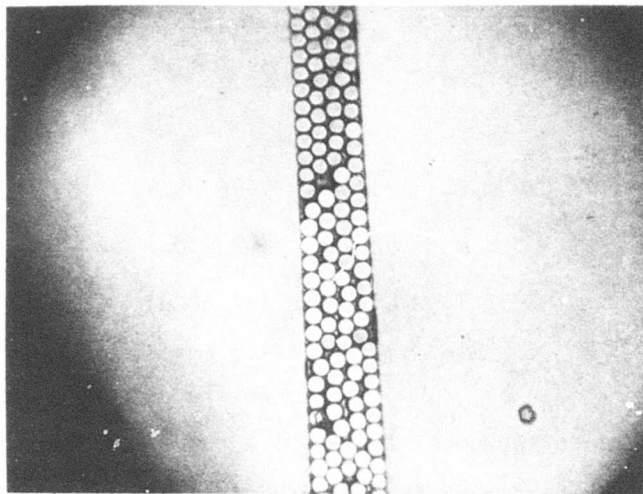
SPECTRONICS, INC.
Richardson, Texas

Figure 33. Split Rod T Coupler, Side View

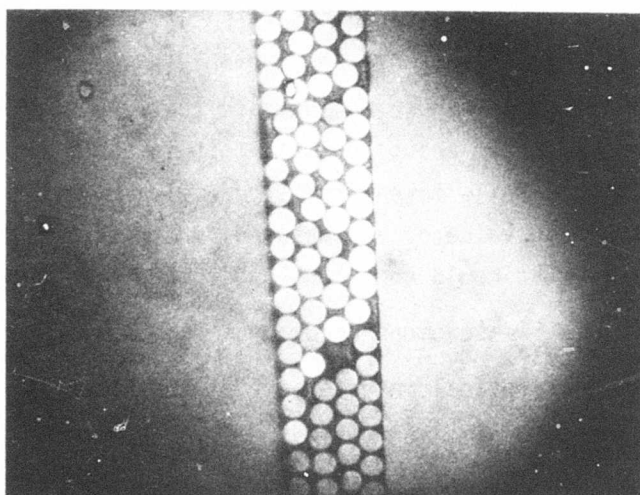
$$\begin{aligned}
 m_C C_T &= 2.0\% & (-16.99\text{dB}) \\
 m_C &= 62.9\% & (-2.01\text{dB}) \\
 T_T &= 68.5\% & (-1.64\text{dB}) \\
 m &= 72.5\% & (-1.40\text{dB})
 \end{aligned}
 \tag{95}$$

The theoretical performance of the split rod T coupler is essentially the same as the calculated values shown in Table VIII for the slotted rod T coupler. Comparison of Eq (95) and Table VIII shows that this coupler meets or exceeds the calculated values of transmission and quality factors. The small difference in C_T values results from the design dimensions for the two configurations. The major difference between measured and calculated performance is the coupling quality factor. The measured value of m_C (62.9%) is 27% higher than the calculated value. Figure 34 shows that the split rod construction essentially eliminates broken fibers in the side arms. Physical measurements taken from Figure 34 indicate that the slot is tapered with an average width of about 10.5mil; this is about 17% higher than the design width of 9mils taken from Figure 31. However, this does not explain the high value of m_C measured for this coupler. Some possible effects that could contribute to this discrepancy are

- measurement accuracy,
- optical interference at the glass/glass interfaces,
- multiple reflections in the coupler and the test equipment, and
- significant optical transmission in the cladding glass of the side arm fibers.



Low Power Magnification



High Power Magnification

Figure 34. T Coupler Split Rod, End View

Further study is required to resolve these final differences. The calculated performance of a split rod T-coupler with index matching is essentially the same as for the slotted rod T-coupler shown in Eq (93). No index matching measurements were made on this coupler.

2. Radial Coupler

An eight station radial coupler was selected for construction and evaluation. Two 46mil diameter bundles were used to form each side arm; this results in a 65mil diameter bundle that is indicated by $\sqrt{2} \times 46$ in Table III. At the station end of the fiber optic cable (see Figure 16), the fibers are again split into two bundles -- the two 46mil bundles are used to form the LED/fiber optic interface and the detector/fiber optic interface. When the eight side arms are brought together a composite bundle with a diameter of about 180mil is formed; this bundle is equivalent to sixteen 46mil diameter bundles and is indicated by $\sqrt{16} \times 46$ in Table III.

The construction details of the radial coupler are shown in Figure 35. The coupler termination hardware shown in Figure 27 was used in the construction of the radial coupler. One set of hardware was used for the coupler body and eight sets for the fiber/fiber plugable interfaces on the eight side arms. The radial coupler was housed in a metal case for ease in demonstration and display. Front panel and exposed rear views of the demonstration coupler are shown in Figures 36 and 37.

Three radial couplers were constructed and evaluated. The first two used conventional Galileo fiber optic bundles in the side arms; the third unit used special unclad fibers. The third unit was not successful and will be discussed separately.

The first step in constructing a radial coupler is the formation of the fiber bundle structure with polished conventional terminations on the eight 65mil diameter bundles and the 180mil diameter composite

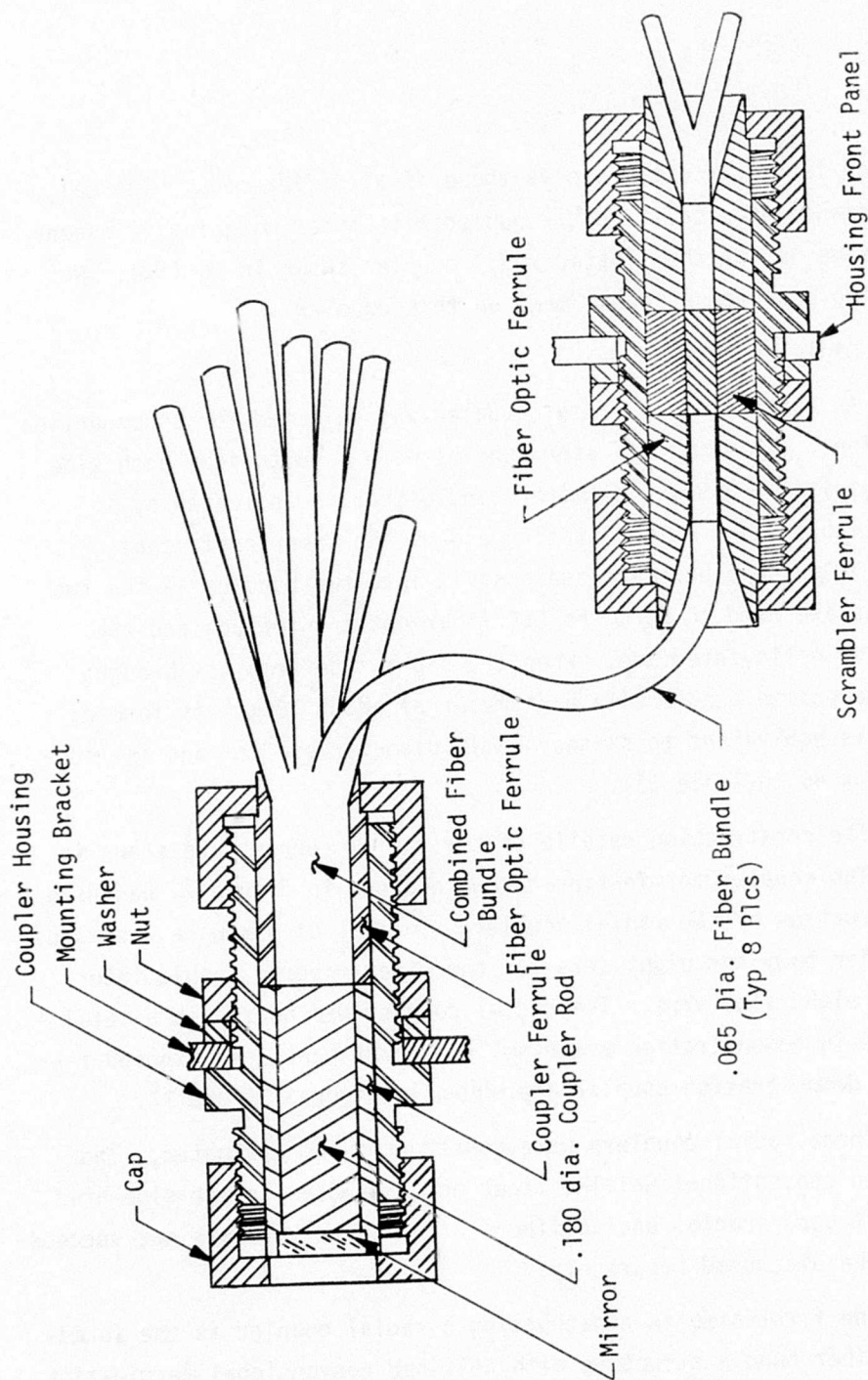


Figure 35. Fiber Optic Radial Coupler

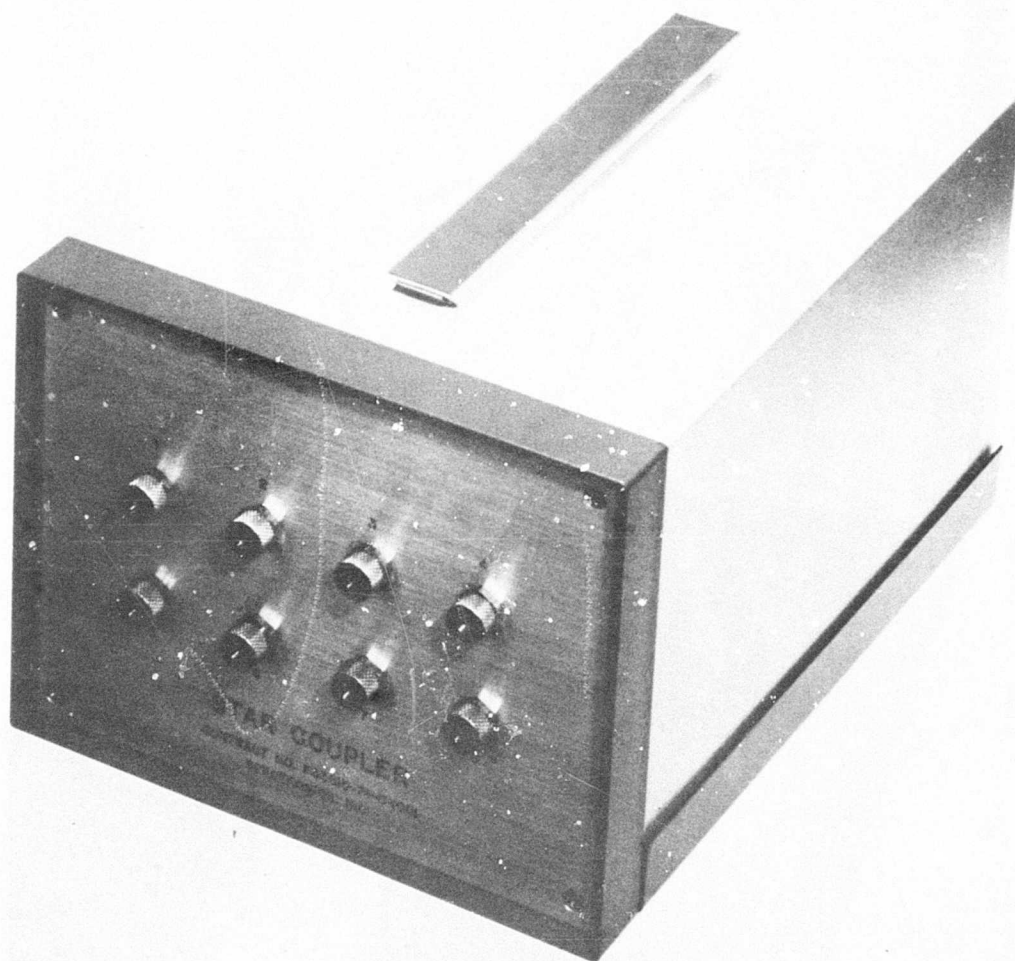


Figure 36. Radial Coupler, Front View

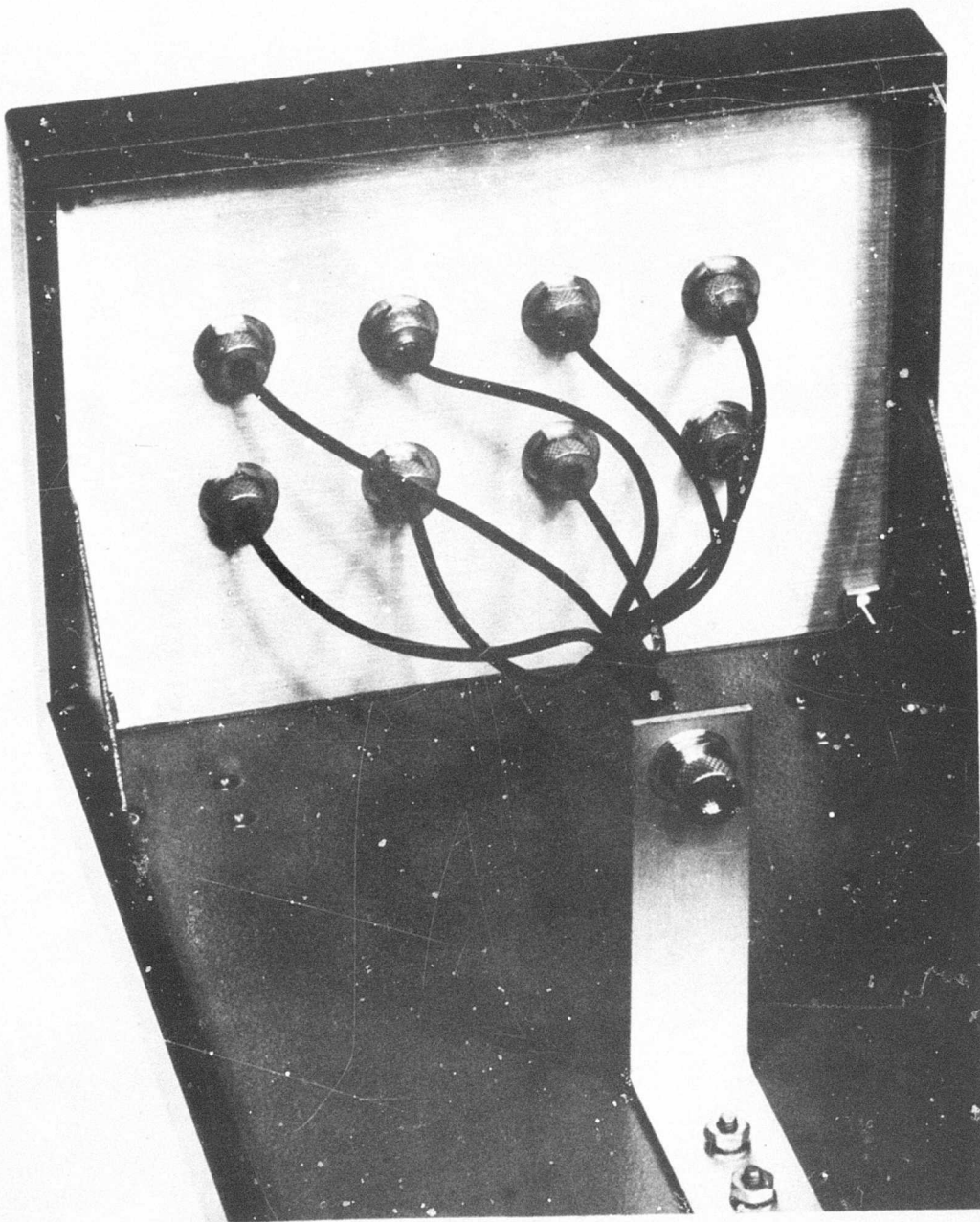


Figure 37. Radial Coupler, Exposed View

bundle. The transmission of the side arms of the fiber bundle structures for couplers 1 and 2 were measured at the subassembly level shown in Figure 38. The results of these measurements are presented in Table IX. The measurements were made with the aid of a special illuminator assembly employing a GaAs dome LED and having a 65mil diameter aperture. A reference level was established first by detecting the total illuminator output. Output from the 180mil bundle was then measured with a 65mil side arm bundle positioned at the illuminator aperture. The low transmission in arms 2 and 8 of Coupler No. 1 was due to broken fibers. A considerable improvement in construction technique was achieved on Coupler No. 2; this is evidenced by the consistency of the transmission data shown in Table IX.

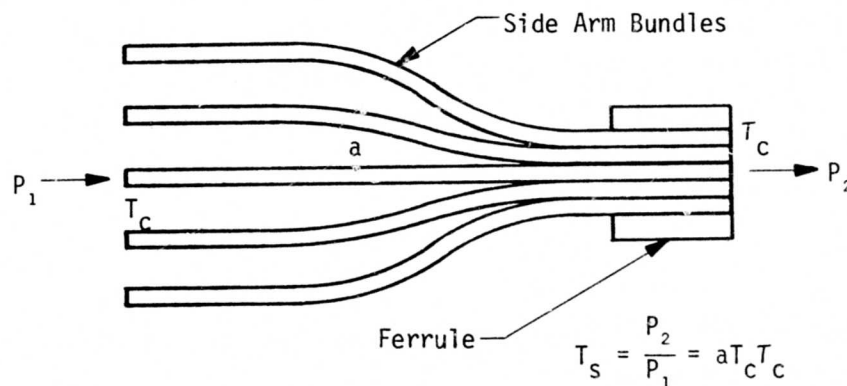


Figure 38. Side Arm Assembly

Table IX. Radial Coupler Side Arm
Transmission

Arm No.	Transmission, T_s	
	Coupler No. 1	Coupler No. 2
1	53%	55%
2	48%	52%
3	55%	52%
4	57%	54%
5	50%	52%
6	50%	55%
7	52%	52%
8	40%	54%
Average	51%	53%

As shown in Figure 38, the transmission of the side arm bundles involves the transmission of the input termination, T_c given by Eq (18), the attenuation of the side arm bundle, a , and the transmissivity of the core/air interface at the exit end, $T_c = (1 - R_c)$; R_c is given by Eq (4). Thus, the expected transmission of each one of the 8 side arm bundles is given by

$$T_s = a(1 - R_c)T_{66} \quad (96)$$

The length of the 65mil diameter bundles is 8in; at 0.2dB/ft this gives an attenuation of

$$a = -0.133\text{dB} \quad (0.97) \quad (97)$$

The calculated value of T_{66} from Table IV can not be used in Eq (73) because the fiber optic ferrules made for the radial arm terminations have an inside diameter of 66mils which is slightly larger than the D_f value used in Table III. From Table III the value of D for two

46mil diameter bundles is 58.8mil. Using this value with the actual ferrule diameter, $D_f = 66\text{mil}$, in Eq (14) gives

$$G_{66} = \left(\frac{D}{D_f}\right)^2 = \left(\frac{58.8}{66}\right)^2 \quad (98)$$

$$G_{66} = 0.794$$

The transmission of the 66mil termination, T_{66} can be calculated from Eq (18) using the value of G_{66} from Eq (98) with the value of R_a from Eq (7) and the value of R_c from Eq (4)

$$T_{66} = (1 - R_c)G_{66}R_a$$

$$= (.9433)(.794)(.8186) \quad (99)$$

$$= .613 \text{ or } 61.3\%$$

Using Eq (97) and (99) with the value of R_c from Eq (4) gives a calculated value of T_s from Eq (96)

$$T_s = (0.97)(0.9433)(0.613) \quad (100)$$

$$= 0.56 \text{ or } 56\%$$

This calculated value is only 5% greater than the average transmission of Coupler No. 2 shown in Table IX.

The couplers were next assembled without matching fluid using a 180mil diameter scrambler rod and a dielectric mirror. A multilayer dielectric mirror was selected because it gives a higher reflectivity, $R_m = 0.996$ than a metal mirror such as aluminum or gold.

$R_m = 0.98$. Another important property of the dielectric mirror is that it is transparent to visible light. This allows the inside of the radial coupler body to be observed after the unit is fully assembled. However, it also limits the useful wavelength of the coupler. The mirrors used in these couplers are optimized for a wavelength of 907nm. From Eq (51) the coupling factor of the two radial couplers is

$$C_{\star} = \frac{1}{8} = 0.125 \quad (101)$$

The value of T_{\star} was measured by successively coupling light into each of the polished side arm terminations and individually reading all of the light output at the other seven polished terminations. This measurement is schematically indicated in Figure 39. Table X shows representative values of T_{\star} for Coupler No. 1; Table XI shows similar data for Coupler No. 2. In each case, the data shown includes the highest average transmission, lowest average transmission, highest individual transmission and lowest individual transmission; the indicated limiting values are underlined. The average of all transmission measurements for Coupler No. 1 is 0.030 (3%); for Coupler No. 2 the overall average is 0.034 (3.4%).

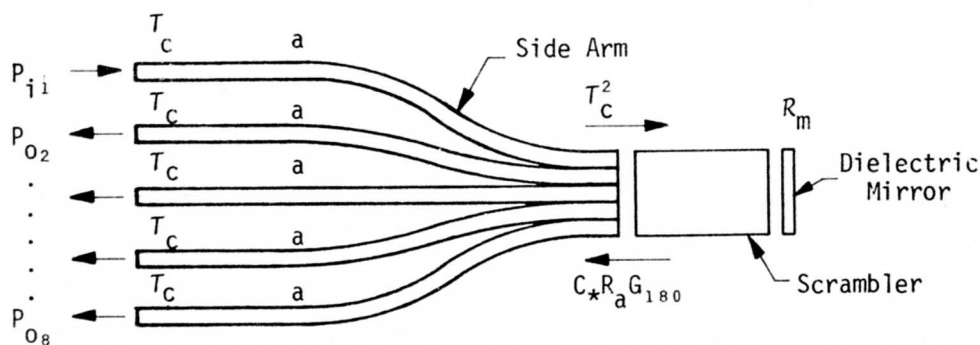


Figure 39. Measurement of T_{\star}

Table X. Measured T_* For
Radial Coupler No. 1

Arms	T_*	Arms	T_*	Arms	T_*
1-2	.020	2-1	.015	8-1	.028
1-3	.050	2-3	.015	8-2	.024
1-4	.040	2-4	.018	8-3	.028
1-5	.039	2-5	.040	8-4	.022
1-6	.046	2-6	<u>.010</u>	8-5	.030
1-7	.019	2-7	<u>.074</u>	8-6	.020
1-8	.028	2-8	.031	8-7	.030
Avg.	<u>.034</u>	Avg.	.029	Avg.	<u>.026</u>

Overall Average T_* = .030

Table XI. Measured T_* For
Radial Coupler No. 2

Arms	T_*	Arms	T_*	Arms	T_{*p}
3-1	.037	4-1	.039	6-1	.025
3-2	.047	4-2	.023	6-2	.053
3-4	.024	4-3	.034	6-3	.032
3-5	<u>.020</u>	4-5	<u>.058</u>	6-4	.025
3-6	.031	4-6	.048	6-5	.039
3-7	.050	4-7	0.24	6-7	.027
3-8	.037	4-8	.034	6-8	.025
Avg.	.035	Avg.	<u>.037</u>	Avg.	<u>.032</u>

Overall Average T_* = .034

The expected value of T_* can be calculated by referring to Figure 39. Input power incident on port No. 1 first encounters the termination transmission T given by Eq (99). As the light transits side arm No. 1 it is attenuated by the factor a given by Eq (97). At the scrambler end of side arm No. 1 the light is attenuated by $T_C = (1 - R_S)$ as it leaves the fiber optic bundle. It is then attenuated by $T_S = (1 - R_S)$, see Eq (83), as it enters the

scrambler. After entering the scrambler, the light is reflected from the dielectric mirror with a reflectivity $R_m = .996$. As the light exits the scrambler it is coupled into a 180mil diameter termination which has a transmission of $G_{180}R_a$ where G_{180} and R_a are given by the bottom line in Table IV. The fiber bundle splits into the 8 side arms so that the light in any one side arm is determined by C_* given in Eq (101). As the light transits any exit side arm it is again attenuated by the factor a given by Eq (97). At the exit end of the exit side arm, the light is attenuated by the core/air transmissivity $T_C = (1 - R_C)$. When all of these factors are combined, the resulting expression for T_* is

$$T_* = C_* R_m a^2 T_C^2 T_S T_{66} G_{180} R_a \quad (102)$$

In the development of Eq (102), front surface reflection losses were counted at the input to the scrambler but not counted at the dielectric mirror or the exit face of the scrambler. Reflections at the input to the scrambler cause the light to be reflected back to the LED and lost; these reflections must be counted. Reflections at the scrambler surface in front of the dielectric mirror do not cause a loss as shown in Figure 40. Considering only the first order reflections for simplicity, Figure 40 shows that the front surface reflection, R_s , only reflects a portion of the light that would have been reflected by the mirror anyway. If all multiple reflections are considered the total reflectivity, R_T , of this interface is given by

$$R_T = R_s + \frac{(1-R_s)^2 R_m}{1 - R_s R_m} \quad (103)$$

For $R_s = .056$ and $R_m = 0.996$ the value of R_T is

$$R_T = .99600095 \quad (104)$$

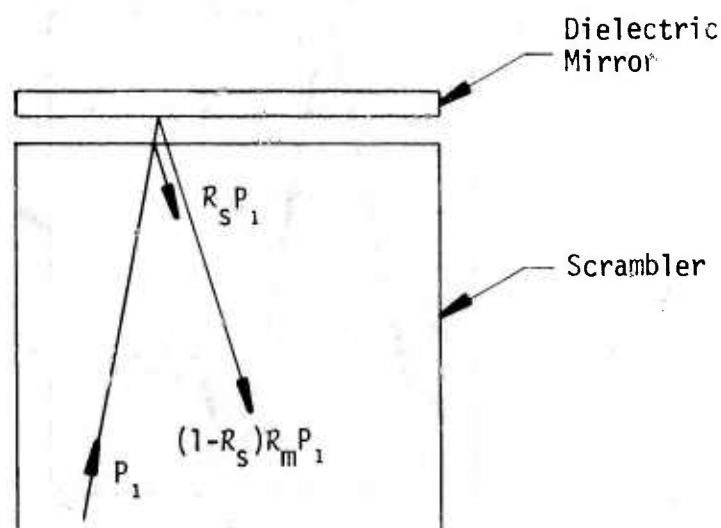


Figure 40. Front Surface Reflection at Mirror

which is essentially equal to R_m .

The nature of front surface reflections at the exit surface of the scrambler can be understood from Figure 41. A portion of every exit ray is reflected as shown by the arrow labeled $R_S R_m P_1$. However, each one of these reflected rays is acted on by the scrambler and returned to some other point on the exit surface on the second reflection. Since the scrambler is essentially lossless, all of the light coupled into the scrambler must come out somewhere on the exit face. In general, each of the side arm fibers receives just enough second second reflection light from the other 7 side arms to make up for its one reflection loss at the exit surface. Thus, reflection at the exit surface of the scrambler or the scrambler end of the side arm bundles should not be counted as an optical loss.

Equation (102) is a correct and general expression for calculating a theoretical value of T_* . However, it is not in a

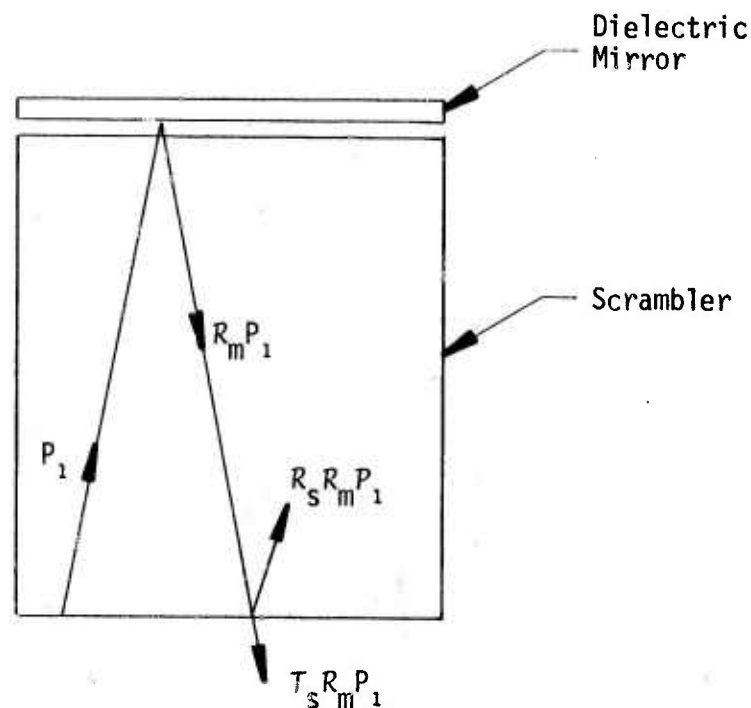


Figure 41. Front Surface Reflection at Scrambler Exit

convenient form to use the measured values of T_s recorded in Table IX to calculate the expected value of T_* . Referring to the expression for T_s given in Eq (96) and Figure 38, the terms in Eq (102) can be rearranged as

$$T_* = C_* R_m (a T_C T_{66})^2 \frac{T_s G_{180} R_a}{T_{66}} \quad (105)$$

$$T_* = C_* R_m T_s^2 \frac{(1-R_s) G_{180} R_a}{T_{66}}$$

From Eq (18)

$$G_{180}R_a = \frac{T_{180}}{(1-R_c)} \quad (106)$$

Substituting Eq (106) into Eq (105) gives

$$T_{\star} = C_{\star}R_mT_s^2 \frac{(1-R_s)T_{180}}{(1-R_c)T_{66}} \quad (107)$$

where T_{66} is given by Eq (99),

T_{180} is given on the bottom line of Table IV,

R_s is given by Eq (83),

R_c is given by Eq (4),

R_m is .996,

C_{\star} is given by Eq (101), and

T_s is the average value in Table IX.

Notice that the factor $(1-R_c)$ in the denominator of Eq (107) also is present implicitly in T_{180} in the numerator; similarly the term T_{66} in the denominator is also present implicitly in one of the T_s factors of the numerator.

No scattering loss or absorption loss in the scrambler has been included in the development of Eqs (102) and (107). This approach has been used so that values of T_{\star} calculated from Eqs (102) and (107) will represent the maximum achievable performance. On this basis, scattering and absorption losses in the scrambler are included with broken fibers and other undesirable losses as effects which must be eliminated to achieve the highest coupler performance. The deviation

of experimental performance from values calculated with Eqs (102) and (107) provides a measure of the undesirable losses.

From Eq (107), the expected value of T_* for coupler No. 1 is

$$T_* = .035 \quad (-14.56\text{dB}) \quad (\text{No. 1}) \quad (108)$$

and for coupler No. 2 the expected value is

$$T_* = .036 \quad (-14.44\text{dB}) \quad (\text{No. 2}) \quad (109)$$

If the calculated value of T_s in Eq (100) is used in Eq (107) the result is the theoretical or ideal value of T_* for the configuration

$$T_* = .042 \quad (-13.77\text{dB}) \quad (\text{Ideal}) \quad (110)$$

From Table X the average value of T_* for coupler No. 1 is 14% less than the expected value shown in Eq (108) and 29% less than the ideal value shown in Eq (110). From Table XI the average T_* for coupler No. 2 is 8.1% less than the expected value in Eq (109) and 19% less than the ideal value shown in Eq (110).

The values of m_* can be calculated using Eqs (53) and (101)

$$m_* = .240 \quad (-6.20\text{dB}) \quad (\text{No. 1}) \quad (111)$$

$$m_* = .272 \quad (-5.65\text{dB}) \quad (\text{No. 2}) \quad (112)$$

$$m_* = .336 \quad (-4.74\text{dB}) \quad (\text{Ideal}) \quad (113)$$

The performance of the two radial couplers and the ideal performance for the radial configuration employed in this effort are summarized in

Table XII. The quality factor of coupler No. 2 is within less than 1dB of ideal performance.

Table XII. Radial Coupler Performance Summary

Coupler	C _*		T _*		m _*	
		dB		dB		dB
No. 1	.125	-9.03	.030	-15.23	.240	-6.20
No. 2	.125	-9.03	.034	-14.69	.272	-5.65
Ideal	.125	-9.03	.042	-13.77	.336	-4.74

Another very important characteristic of the radial coupler is the dynamic range of the output signals. The ideal performance of a radial coupler calls for input light to be uniformly distributed to all of the radial arms. If this condition is achieved, then dynamic range problems can be eliminated by fixing the attenuation of the fiber optic cables at a constant value independent of cable length. In this case, each station would receive the same signal regardless of which station was transmitting.

Inspection of Tables X and XI show that the input light is not uniformly distributed. Furthermore, the coupling between arms is not symmetrical in every case; arm 1 couples more light to arm 2 than arm 2 couples to arm 1. The dynamic range of coupler No. 1 is defined by the minimum and maximum values of T_{*} -- arms 2-6 and 2-7 respectively.

$$D_{R*} = \frac{.074}{.010} = 7.4$$

$$= 7.4 \text{ (8.69dB)}$$

(No. 1) (114)

For coupler No. 2 the uniformity is much better; the limiting arms are 2-5 and 4-5.

$$\begin{aligned} D_{R*} &= \frac{.058}{.020} \\ &= 2.9 \quad (4.62\text{dB}) \end{aligned} \qquad \begin{array}{l} \text{(No. 2)} \\ \text{(115)} \end{array}$$

This observed nonuniformity of power distribution is the result of the cylindrical shape of the scrambler. A cylindrical scrambler is ideal for distributing light introduced in a small aperture on the axis of the cylinder. However, light introduced near the edge of the cylinder results in a large fraction of the power in the skew rays that undergo a large number of small angle reflections and remain near the edge of the scrambler. This tends to develop a characteristic nonuniform light distribution which shows weak coupling to the on-axis fibers when light is introduced at the edge of the scrambler but uniform coupling to all fibers when light is introduced on axis. This subject is discussed in Section III.B and the effect is illustrated in Figure 23.

The dynamic range of coupler No. 2 is adequate for most systems applications. Since this is an experimental ratio, continued small improvements may be expected as the construction techniques improve. However, a dramatic reduction in D_{R*} requires a basic change in the physical configuration of the radial coupler. For example, uniform coupling could be achieved by mixing up the fibers from the radial arms so that fibers from each arm are scattered over the entire composite bundle. Another configuration which has been proposed⁶ uses a hollow tube for the scrambler. This approach completely removes the center of the scrambler and puts all of the light near the edge of the scrambler. The approach proposed by Spectronics as a result of this coupler development effort is based on the use of a scrambler

with square cross section and solid, rectangular cross section side arms. Figure 42 shows the construction of this improved radial coupler.

One of the principal advantages of this configuration is the elimination of the skew ray problem. In a rectangular scrambler, each of the flat sides acts as a plane mirror. Therefore, at the input/output face of the scrambler each arm sees multiple mirror images of every other arm as shown in Figure 24. This leads to more uniform power distribution and a smaller total number of reflections at the scrambler surfaces. Another advantage of the rectangular configuration is the elimination of packing fraction loss at the interface between the side arms and the scrambler; this interface is now ideal for use of an index matching material to eliminate reflection. The solid glass side arms also give a dramatic improvement in the transmission of the plugable interfaces as compared to a fiber bundle/fiber bundle interface.

As shown in Figure 42, the interconnecting fiber optic bundles between the radial coupler and the stations must interface with the 2/1 rectangular shape of the solid side arm. While the individual fibers are round, the total bundle of fibers can be formed into any convenient shape such as square, rectangular, or hexagonal. All that is required is to be able to form the hole in the ferrule in the desired shape with close mechanical tolerances. Figures 30 and 34 are photographs of rectangular arrays of fibers used in the T couplers built on this contract. Figure 43 shows a simple numerical example of 43 fibers with diameter d fitted into a 2/1 rectangle of $4.5d \times 9.1d$. The area of all of the fibers in Figure 43 is

$$\text{Area of Fibers} = (43) \left(\frac{\pi}{4} \right) (d)^2 = 33d^2 \quad (116)$$

and the area of the rectangular ferrule is

$$\text{Area of Ferrule} = (4.5d)(9d) = 40.5d^2 \quad (117)$$

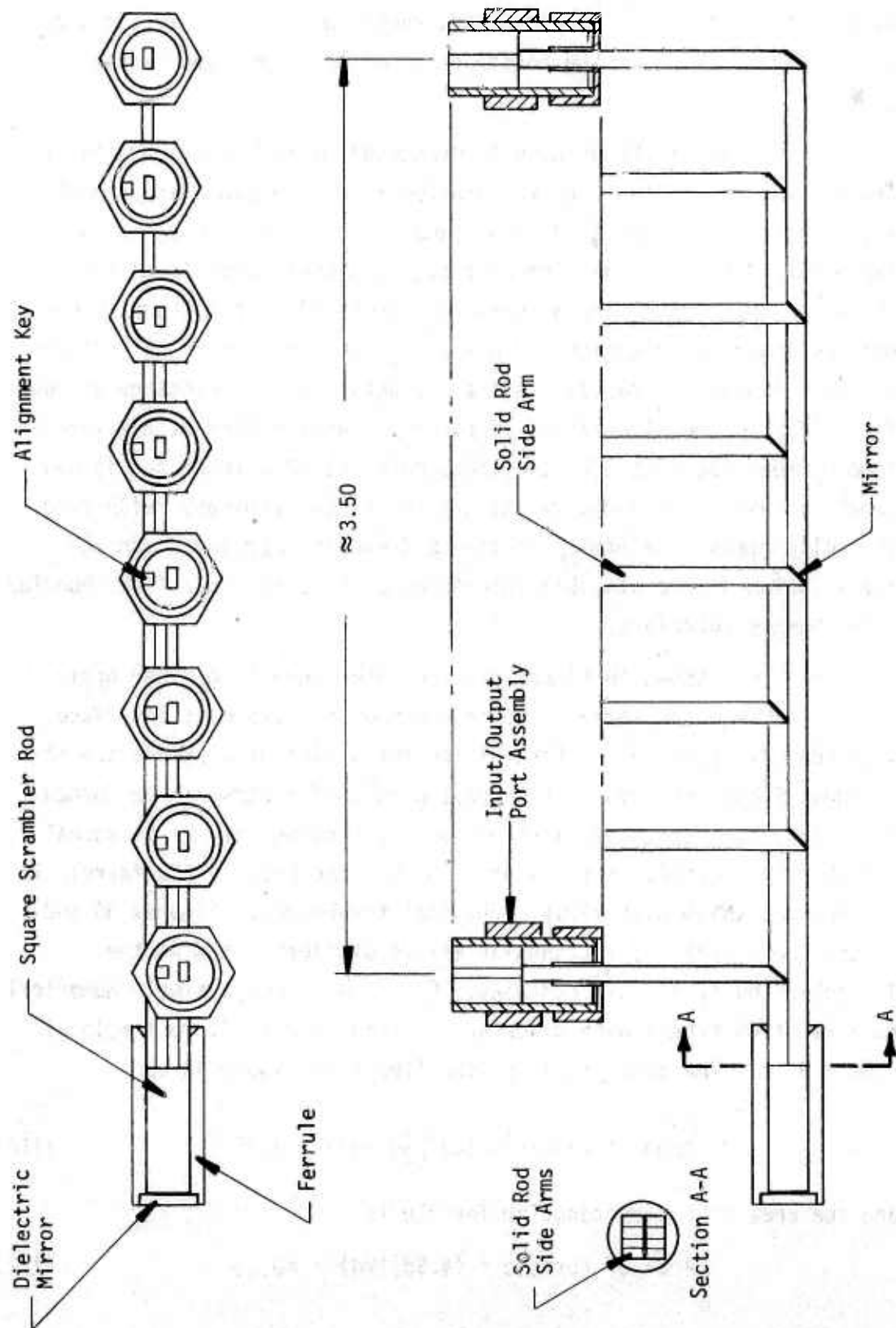


Figure 42. Rectangular Radial Coupler

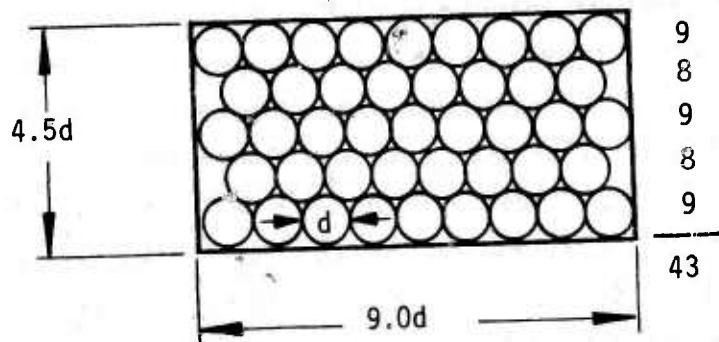


Figure 43. Rectangular Ferrule

Equations (116) and (117) can be used to calculate the geometrical area coverage of the fibers, G_{\square} , given by

$$G_{\square} = \frac{33d^2}{40.5d^2} = .815 \quad (118)$$

For $N = 43$, Figure 2 gives

$$D = 7.61d \quad (119)$$

and Eq (3) gives

$$\varnothing = \sqrt{43} d = 6.56d \quad (120)$$

From Eq (14) the area coverage of the fibers in a circular ferrule, G , is given by

$$G = \left(\frac{D}{d}\right)^2 = \left(\frac{6.56d}{7.61d}\right)^2 \quad (121)$$

$$G = .743$$

Comparison of Eqs (118) and (121) shows that in this case the area coverage of the rectangular ferrule is better than for the circular ferrule. Other specific numerical examples for larger numbers of fibers have shown that the rectangular area coverage is always equal to or better than the circular area coverage. When real fiber optic bundles are used which have some variation in fiber diameter the fibers do not stack uniformly and the two configurations are about equivalent, see Figure 34. Based on this reasoning, Figure 2 can be used to obtain worst case values of G for either rectangular or circular geometry.

When rectangular terminations are used, the optical connector must be keyed to increase proper alignment between the two rectangular shapes at the optical interface.

The transmission of the rectangular radial coupler can be calculated by referring to Figure 44. The relatively large dimensions of the rectangular rods used in the side arms makes it impractical to bend these rods to separate their ends. The glass could be heated and bent; however, the bend radius would have to be at least

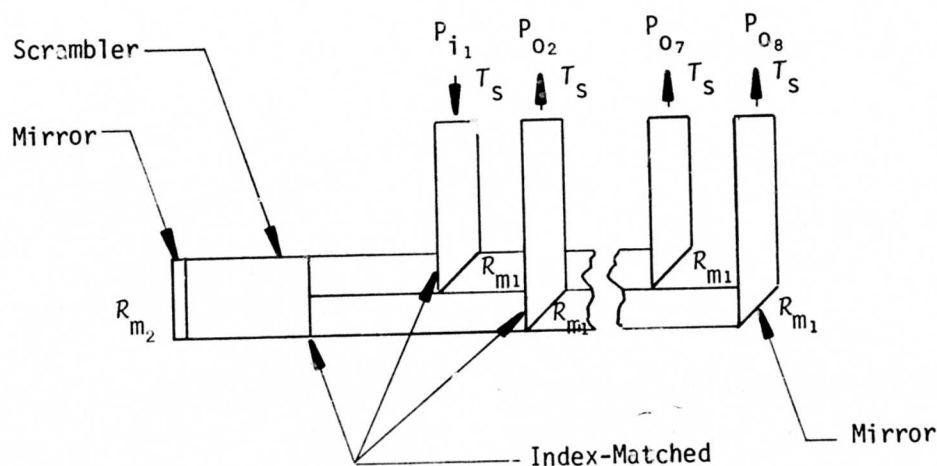


Figure 44. Calculation of T_{C*}

20 times the large dimension of the rectangle to preserve the NA_ϕ of the light traversing the side arm, see Appendix I. Figures 42 and 44 show the side arms folded through 90° by use of a 45° diagonal mirror. This construction technique keeps the coupler compact, separates the input/output ports and preserves NA_ϕ . The mirror can be either a dielectric mirror or a metal reflecting surface. The dielectric mirror will provide the highest reflectivity. For purposes of analysis, Figure 44 uses the symbol R_{m_1} for the diagonal mirrors and R_{m_2} for the mirror on the scrambler. The side arm/scrambler interfaces and side arm/side arm interfaces are all coupled with an index matching material.

Referring to Figure 44, input power incident on port No. 1, P_{i_1} , first encounters the transmissivity of the side arm rod

$$T_s = (1 - R_s) \quad (122)$$

where R_s is given by Eq (83). As the light transits side arm No. 1 it is reflected by the diagonal mirror reflectivity, R_{m_1} . The index matching material at the side arm/scrambler interface eliminates the reflection and the light moves from the side arm into the scrambler. The light is reflected by the dielectric mirror reflectivity, R_{m_2} , and spread uniformly over the exit surface of the scrambler rod. The 8 side arms cover the exit face of the scrambler with a packing fraction of 1.0; therefore, there is no termination loss at this interface. The light in any one of the exit side arms is determined by $C_{\square*}$ is defined in Eq (51). As the light transits any exit side arm it will again be reflected by the diagonal mirror with a reflectivity of R_{m_1} . At the exit end of any exit side arm, the light is attenuated by the transmissivity, T_s , given by Eq (122). When all of these factors are combined the resulting expression for $T_{\square*}$ is

$$T_{\square*} = T_s^2 R_{m_1}^2 R_{m_2} C_{\square*} \quad (123)$$

If Galileo fiber optic bundles are used the index of refraction of the scrambler and side arms will be $n = 1.62$. Then T_S can be determined from Eqs (122) and (83)

$$T_S = (1 - .056) = 0.944 \quad (124)$$

Using aluminum for the diagonal mirrors gives

$$R_{m_1} = 0.98 \quad (125)$$

and the reflectivity of the dielectric mirror on the scrambler will be

$$R_{m_2} = 0.996 \quad (126)$$

For an 8 station data bus, Eq (51) gives the value of $C_{\square\star}$

$$C_{\square\star} = .125 \quad (-9.03\text{dB}) \quad (127)$$

Substituting Eqs (124)-(127) into Eq (123) gives the ideal value of $T_{\square\star}$

$$T_{\square\star} = (.944)^2 (.98)^2 (.996) (.125) \quad (128)$$

$$T_{\square\star} = .106 \quad (-9.7\text{dB})$$

The corresponding ideal value of quality factor can be calculated using Eqs (127) and (128) with Eq (53); this gives

$$m_{\square\star} = (8)(.106)$$

$$m_{\square\star} = 0.848 \quad (-.72\text{dB}) \quad (129)$$

Comparing Eqs (128) and (129) to the ideal values for the cylindrical radial coupler in Table XII shows that the rectangular construction offers about a 4dB improvement in transmission over the fiber bundle construction. The system performance will improve more than 4dB with the rectangular construction because of lower losses at the plugable interfaces.

Equation (123) was developed using an ideal model so that the calculated value of T_{0*} would represent the maximum achievable performance. If additional losses not included in the model occur in the physical coupler then the transmission and quality factor will be lower than the calculated values. The most likely sources of excess loss are:

- scattering and absorption losses in the solid side arms and square scrambler rod,
- front surface reflections due to imperfect index matching, and
- losses due to misalignment of the glass parts.

The model for the rectangular radial coupler is not sufficiently accurate to predict the variation in coupling between the various arms. However, it is felt that the rectangular configuration will reduce the spread in T_x to 2/1 or less; thus, the dynamic range for this coupler is expected to be less than 3dB. The rectangular radial coupler has not been constructed; however, piece parts have been ordered and at least one of these couplers will be built on this contract.

The third radial coupler constructed and evaluated used unclad fiber bundles in the radial arms. The unclad 46mil bundle was purchased from Galileo Electro-Optics; the fibers were made entirely from the high-index core glass. In agreement with the discussion in Section II.E., these fibers are very fragile. This loss in strength

is felt to be the result of the absence of the surface compression present at the normal core/cladding interface. These unclad fibers exhibit mechanical properties that are similar to the etched fibers discussed in Section II.D. In addition to poor strength, the unclad fibers also show a much higher attenuation than was expected. The observation of optical coupling in the cladding glass discussed in Section II.B offered hope that the unclad fibers could be used successfully in short lengths such as side arms on couplers. In a conventional termination, the epoxy should serve as a cladding layer; air should serve as a cladding layer in the region between the terminations. Measured values of T_* on the unclad radial coupler were about 10dB lower than for coupler No. 2.

The original plan for the unclad bundle also included the construction of a compressed termination. However, as a result of the poor mechanical strength and high attenuation encountered in the radial coupler, no further work was done with the unclad fiber optic bundle.

3. T/Radial Comparison

The performance comparison for the in-line and radial data buses based on the measured performance of the couplers reaches the same general conclusions as the calculated comparison in Section III.A.3. The use of measured coupler performance makes it possible to predict the results expected from a practical system.

Recent component development has resulted in improved LEDs and detectors for data bus applications. The SPX 1775 LED is a hermetically sealed edge emitter designed for direct coupling to a 46mil diameter fiber optic bundle. This GaAs LED is capable of operating at 100mA bias and delivering a total output power of 2.0mW; of this total power, 1.5mW is effective in coupling to the NA and aperture of a 46mil diameter Galileo fiber optic bundle. From Eq (41) the value of m_L for the SPX 1775 LED is

$$m_L = \frac{1.5}{2.0} = 0.75 \quad (130)$$

The SPX 1777 is a hermetically sealed silicon planar photodiode that is also designed to interface directly with a 46mil diameter Galileo fiber optic bundle. This silicon detector provides a nominal responsivity of 0.5A/W including all interface losses; the 10-90% rise time is about 1ns. Work on the receiver and sync detection circuitry has resulted in a preliminary receiver design which requires a peak-to-peak signal power at the SPX 1777 detector of 0.15μW to achieve a bit error rate of 10^{-8} at a data rate of 10Mbit/s. The LED output power and required detector power give a maximum allowable attenuation of 41.25dB in the data bus.

For a data bus length of 100ft with 8 stations and fiber optic bundle with attenuation of 0.5dB/m, the value of a_0 from Eq (164) is

$$a_0 = 0.605 \quad (-2.18\text{dB}) \quad (131)$$

The worst case power ratio, R_{PT} , for an in-line data bus is given by Eq (45). For an 8 station in-line bus using 180mil diameter Galileo fiber optic bundles, Eq (45) becomes

$$R_{PT} = 0.5a_0 T_C T_{180} m_L m_C^2 T \left[a_0 T_C T_{180} T_T \right]^6 \quad (132)$$

where	$T_C = (1 - R_C) = .9433$	from Eq (4)
	$T_{180} = .6562$	from Table IV
	$m_L = .75$	from Eq (130)
	$a_0 = .605$	from Eq (131)

The measured performance of the split rod T coupler shown in Eq (95) gives

$$\begin{aligned} m_C^2 C_T &= .01258 \\ T_T &= .685 \end{aligned} \quad (133)$$

Using Eq (133) in Eq (132) with the other parameters shown gives the expected value of R_{pT} using 8 of the split rod T couplers.

$$R_{pT} = 5.03 \times 10^{-7} \quad (-62.98\text{dB}) \quad (134)$$

Using the quality factors indicated by Eq (95) but adjusting the coupling factor for an 8 station data bus gives

$$\begin{aligned} m_C^2 C_T &= .0247 \\ T_T &= .640 \end{aligned} \quad (135)$$

Using the values in Eq (135) in Eq (132) gives

$$R_{pT} = 6.58 \times 10^{-7} \quad (-61.82\text{dB}) \quad (136)$$

The expected dynamic range of this 8 station in-line data bus may be calculated from Eq (175) in Appendix II using the values shown above

$$D_{RT} = 5.28 \times 10^3 \quad (37.22\text{dB}) \quad (137)$$

The parameters of the ideal slotted rod T coupler with index matching are presented in Eq (93). Using the quality factors from Eq (93) but adjusting the coupling factor for an 8 station data bus gives

$$\begin{aligned} m_C^2 C_T &= .0218 \\ T_T &= .875 \end{aligned} \quad (138)$$

Using these values in Eqs (132) and (175) with $T_C = 1.0$ and $T_{180} = .6956$ for index matching at the plugable interfaces gives

$$\begin{aligned} R_{PT} &= 8.58 \times 10^{-6} \quad (-50.67\text{dB}) \\ D_{RT} &= 4.01 \times 10^2 \quad (26.00\text{dB}) \end{aligned} \quad (139)$$

The worst case fractional power ratio for a radial data bus can be calculated from Eq (58). For a 100ft long 8 station bus using 46mil diameter Galileo fiber optic bundles at the LED and detector interface, Eq (58) becomes

$$R_{p*} = \frac{m_L m_* T_{46} T_{fk} T_{fN} a_0^7}{16} \quad (140)$$

$$\begin{aligned} \text{where } m_L &= .75 && \text{from Eq (130)} \\ T_{46} &= .6119 && \text{from Table IV} \\ a_0^7 &= (.605)^7 = .0297 && \text{from Eq (131)} \end{aligned}$$

From Table XII the measured quality factor for radial coupler No. 2 is

$$m_* = .272 \quad (141)$$

The terms T_{fk} and T_{fN} in Eq (140) represent the plugable interface loss not included in m_* . The measured value of m_* given in Eq (141) includes input/output losses given by

$$T_{66} T_C = (.613)(.9433) = .578 \quad (142)$$

where T_{66} is given by Eq (99), and

$$T_C = (1 - R_C) = .9433 \text{ from Eq (4)}$$

The discussion in Section II.C. gives a measured transmission of 55% for a 65mil diameter fiber/fiber interface. Thus, it follows that for radial coupler No. 2

$$T_{fk} T_{fN} = \frac{(.55)^2}{T_{66} T_C} \quad (143)$$

$$T_{fk} T_{fN} = \frac{(.55)^2}{.578} = .523$$

Using Eqs (141) and (143) in Eq (140) with the other values shown gives the expected value of R_{p*} for a radial data bus using radial coupler No. 2.

$$R_{p*} = 1.21 \times 10^{-4} \quad (-39.17\text{dB}) \quad (144)$$

The measured dynamic range for radial coupler No. 2 is given in Eq (91)

$$D_{R*} = 2.9 \quad (4.62\text{dB}) \quad (145)$$

For the proposed rectangular radial coupler the value of $m_{\square*}$ is given by Eq (129). Since this coupler uses solid rod side arms it follows that when no matching fluid is used in the plugable interfaces

$$T_{fk} = T_C = .9433 \quad (146)$$

where $T_C = (1 - R_C) = .9433$ from Eq (4), (147)

and $T_{fN} = T_{66} = .613$

where T_{66} is given by Eq (99).

Using Eqs (129), (146) and (147) in Eq (140) gives the expected value of R_{p*} for an 8 station radial data bus using the proposed rectangular radial coupler.

$$R_{p*} = 4.18 \times 10^{-4} \quad (-33.79\text{dB}) \quad (148)$$

The expected dynamic range of this system is

$$D_{R*} \leq 2.0 \quad (<3.0\text{dB}) \quad (149)$$

The in-line and radial systems are compared in Table XIII. The measured radial system gives a detector signal that is 22.65dB greater than the measured in-line system. In a similar manner, the proposed rectangular radial system with index matching only at the scrambler gives 16.88dB more detector signal than the in-line system with complete index matching. The worst case power ratio for both of the in-line systems is higher than the 41.25dB maximum allowable attenuation while both of the radial systems have less than 41.25dB attenuation. The dynamic range of either of the radial systems is clearly superior to either of the in-line systems.

Based on the system comparison presented in Table XIII, the rectangular radial system with conventional fiber optic terminations is proposed for the 8-station EMI-EMP resistant data bus. The radial system with a fiber bundle coupler will be used as a back up approach. A radial coupler of the quality of coupler No. 2 will meet the system requirements for an 8-station, 100ft data bus at 10Mbit/s.

Table XIII. Data Bus System Comparison

<u>System</u>	<u>Coupler</u>	<u>R_P</u>	<u>D_R</u>
In-Line (a) 8-Station	Split Rod T No Index Match	-61.82dB	37.22dB
In-Line (b) 8-Station	Split Rod T Index Matched	-50.67dB	26.00dB
Radial (a) 8-Station	Fiber Optic No Index Match	-39.17dB	4.62dB
Radial (b) 8-Station	Rectangular Partial Match	-33.79dB	≤3.0dB

Maximum Allowable Attenuation = 41.25dB

(a) - measured coupler

(b) - calculated coupler

SECTION IV

CONCLUSIONS AND RECOMMENDATIONS

The purpose of this program is the development of a 10Mbit/s EMI/EMP Resistant Data Bus. The bus is to have 6 to 8 stations and a total length of 80 to 100ft. Optoelectronic technology has been selected to provide maximum EMI and EMP immunity. This approach uses noncoherent GaAs LEDs and silicon p-i-n photodiodes to transmit and receive optical signals; the transmission medium is flexible fiber optic bundles

The research and development effort described in this interim report has been devoted to the technology of fiber optic terminations. The program was directed toward analysis and experimental evaluation of conventional terminations and the development of techniques to reduce the termination losses. Good agreement has been achieved between analysis and experiment for conventional terminations; transmission values of 65.18% (34.82% loss) have been achieved for 188mil diameter Galileo fiber optic bundles. The various loss mechanisms are defined and evaluated. Techniques investigated for reducing the termination losses are

- etching of the optical fibers to remove the cladding glass in the region of the termination, and
- compressing the fiber bundle to remove the dead space between fibers in the region of the termination.

Both of these areas of investigation show promise; more effort will be required to perfect a workable manufacturing process in either area. The etching technique is limited by fiber breakage when the cladding is removed. Also, a reliable means of measuring the etch rate on individual fibers is needed. The developmental compression techniques were successful in reducing the dead space to 2.1% of the bundle area; this resulted in a termination transmission of 75.6% (24.4% loss).

Good progress has been made in reducing broken fibers in compressed terminations; however, more effort will be required to eliminate broken fibers. Unclad fiber optic bundles were investigated for use in short lengths such as side arms in passive couplers. These investigations were not successful due to the poor mechanical strength and high attenuation of the unclad fibers.

The passive coupler development effort investigated both in-line and radial data bus systems. Slotted rod and split rod T couplers were built and evaluated. The measured performance of these T couplers is in good agreement with calculated values. The split rod construction gave the best measured performance. Presently available LEDs, photodiodes and preamps set a maximum allowable attenuation of about 41.25dB for a 10Mbit/s data bus with a bit error rate of 10^{-8} . When used with conventional terminations, T coupler technology gives more than 41.25dB attenuation in a 100ft 8 station bus using 0.5dB/m conventional fiber optic bundles. A radial coupler was constructed that comes within 1.0dB of calculated performance. A 100ft 8 station radial data bus based on this coupler will have a total attenuation of about 39.2dB. This predicted system performance assumes the use of 0.5dB/m conventional fiber optic bundles and no index matching. The experimental radial coupler has a dynamic range of 4.62dB. This small dynamic range is very desirable in an optoelectronic data bus because of the unipolar nature of the optical signal. A rectangular radial coupler design is presented that should reduce the maximum attenuation of the data bus to 33.8dB and the dynamic range to 3.0dB or less. This radial coupler design uses a rectangular scrambler and solid glass side arms with rectangular cross section; index matching is used only at the scrambler interface and conventional terminations are used on all fiber optic bundles. The rectangular radial coupler is proposed for the EMI/EMP Resistant Data Bus to be constructed on this contract.

The realization of the performance advantage offered by radial couplers over T couplers places a different emphasis on the development of fiber optic bundle termination techniques. This new emphasis is further influenced by the use of a rectangular scrambler and solid glass side arms in the radial coupler. In this case, the critical technology is associated with the fabrication of the radial coupler; the system performance is improved to the point that conventional terminations can be used on all fiber optic bundles employed in the system. This approach uses a more sophisticated coupler to achieve greater ease of installation with the possibility of field terminations of the fiber optic bundles. This is a desirable trade off because the passive coupler is a manufactured item in any case and is not suited for construction or repair in the field. Based on these observations, it is recommended that the passive coupler effort on this program be devoted to the construction of an 8-station rectangular radial coupler. It is also recommended that no further effort be devoted to etched or compressed terminations unless such terminations are required for a specific application.

APPENDIX I
GEOMETRICAL MODEL
OF CLAD FIBER

The analysis of light transmission in clad glass fibers can often be carried out by applying the ray tracing techniques of geometrical optics. This analysis approach is useful for multimode fibers in which the core diameter is many times the wavelength of the light being transmitted. Clad fibers used for coupling to light emitting diodes (LEDs) must be of the multimode type to achieve useful coupling efficiencies. Thus, the geometrical model is appropriate for the fiber optic bundles used on this program.

A. GENERAL THEORY

Figure 45 shows a typical piece of a single clad glass fiber consisting of a high index core region, n_2 , and a lower index cladding region, n_3 . The clad fiber is surrounded by air, $n_1 = 1.0$; thus, $n_2 > n_3 > n_1$. The ends of the fiber are flat and perpendicular to the axis of the fiber.

If a ray of light crosses a boundary between two transparent media having different indices of refraction (air- n_1 /core- n_2), the ray is partially reflected and partially transmitted. For the reflected ray, the angle of reflection is equal to the angle of incidence, θ_1 . For normal incidence the reflectivity at the air/core boundary is

$$R = \left(\frac{n_1 - n_2}{n_1 + n_2} \right)^2 \quad (150)$$

This expression is the same as Eq (23) used in the report to calculate the effect of index matching fluids. For nonpolarized light Eq (150) is accurate to better than 10% for all angles of incidence between zero and 37° for $n_2/n_1 \geq 1.5^4$. There is a similar reflection loss at every interface boundary.

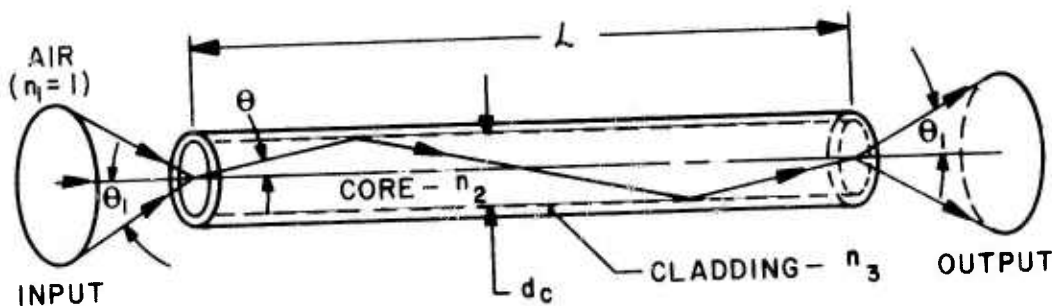


Figure 45. Clad Glass Fiber

The transmitted ray is refracted according to Snell's law³

$$n_2 \sin \theta_2 = n_1 \sin \theta_1 \quad (151)$$

Since $n_1 < n_2$, the internal angle θ_2 is always less than the external angle, θ_1 . Snell's law also applies to the core/cladding boundary as shown in Figure 46; in this case, the form of Snell's law is

$$n_2 \sin \theta_4 = n_3 \sin \theta_3 \quad (152)$$

From this equation it can be seen that if the incidence angle, θ_4 , has a certain critical value, θ_c , such that $\theta_3 = 90^\circ$, then the refracted ray becomes a surface wave along the interface boundary between the two media. If $\theta_4 > \theta_c$, total internal reflection occurs at the core/cladding interface and no light is transmitted into the cladding. From Eq (151) the expression for the critical angle is

$$\theta_c = \sin^{-1} \left(\frac{n_3}{n_2} \right) \quad (153)$$

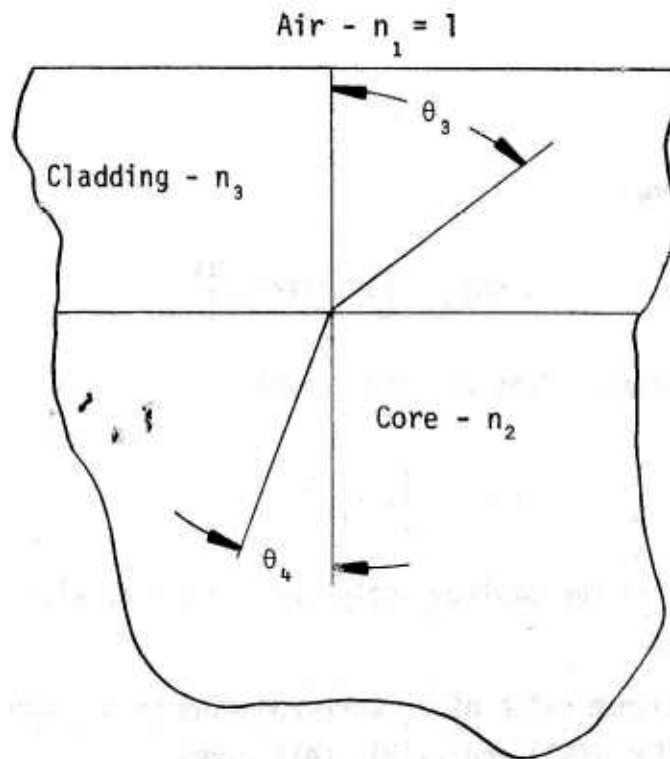


Figure 46. Core/Cladding Boundary

If a ray intersects the axis of a circular cylindrical fiber (meridional ray) at an angle θ_2 to the axis, Figure 45, the ray will be trapped in the core and conducted along the interior of the fiber by multiple total internal reflections provided

$$\theta_2 > \theta_{2m} = 90^\circ - \theta_c \quad (154)$$

From Eq (154)

$$\sin \theta_{2m} = \sin(90^\circ - \theta_c) = \cos \theta_c \quad (155)$$

Using the trig identity

$$\cos \theta_c = [1 - \sin^2 \theta_c]^{1/2} \quad (156)$$

Eq (155) becomes

$$\sin\theta_{2m} = \left[1 - \sin^2\theta_c\right]^{\frac{1}{2}} \quad (157)$$

Substituting for θ_c from Eq (153) gives

$$\sin\theta_2 = \left[1 - \left(\frac{n_3}{n_2}\right)^2\right]^{\frac{1}{2}} \quad (158)$$

The angle θ_{2m} is the maximum angle for a ray that will be trapped in the core glass.

The maximum value of θ_1 corresponding to θ_{2m} can be determined by combining Eqs (151) and (158); this gives

$$n_1 \sin\theta_{1m} = \left[n_2^2 - n_3^2\right]^{\frac{1}{2}} \quad (159)$$

All rays which strike the core with $\theta_1 < \theta_{1m}$ will be trapped in the core and conducted along the fiber with low loss.

The angles, θ_2 , of the trapped rays are preserved at each internal reflection and Snell's law, Eq (151), applies to both the entrance end and exit end of the fiber. Thus, any ray which is conducted along the fiber, $\theta_1 < \theta_{1m}$, will exit the fiber with the same angle, θ_1 , at which it entered.

From the definition of numeric aperture, the NA of any ray is

$$NA = n_2 \sin\theta_2 = n_1 \sin\theta_1 \quad (160)$$

and the limiting NA of the fiber optic bundle from Eq (159) is

$$NA = n_1 \sin\theta_{1m} = \left[n_2^2 - n_3^2\right]^{\frac{1}{2}} \quad (161)$$

Since $n_1 = 1.0$, the angle θ_{1m} is the half angle of the acceptance cone for the fiber. It is customary to refer to the NA shown in Eq (161) as the numeric aperture of the clad fiber.

From Figure 45 the optical path length of a ray, L_p , is independent of the core diameter and is given by

$$L_p = \frac{L}{\cos\theta_2} = \frac{n_2 L}{\left[n_2^2 - \sin^2\theta_1\right]^{\frac{1}{2}}} \quad (162)$$

The number of core/cladding reflections, NR, per unit length of fiber is dependent on the core diameter, d_c , and is given by

$$NR = \frac{1}{d_c} \frac{\sin\theta_1}{\left[n_2^2 - \sin^2\theta_1\right]^{\frac{1}{2}}} \quad (163)$$

This analysis has been performed for meridional rays in a straight fiber, Figure 45. If the fiber is bent, the reflection angles are not conserved. This means that a ray can exit at an angle different than the entrance angle. When bending of the fiber causes θ_2 to exceed θ_{2m} then part of the ray will escape from the fiber and thus represent a loss of light. Rays which enter the fiber such that they do not intersect the fiber axis (skew rays) describe helical paths as they are conducted along the fiber. A skew ray is illustrated in Figure 47. For a straight fiber the skew rays with $\theta_1 < \theta_{1m}$ are also trapped in the core and contribute to the exit light. For any given launch angle, skew rays experience more core/cladding reflections per unit length of fiber than meridional rays, see Eq (163). Angles are also conserved for skew rays so the exit angle is equal to the entrance angle. Skew rays will escape the fiber wall before meridional rays when the fiber is bent⁷.

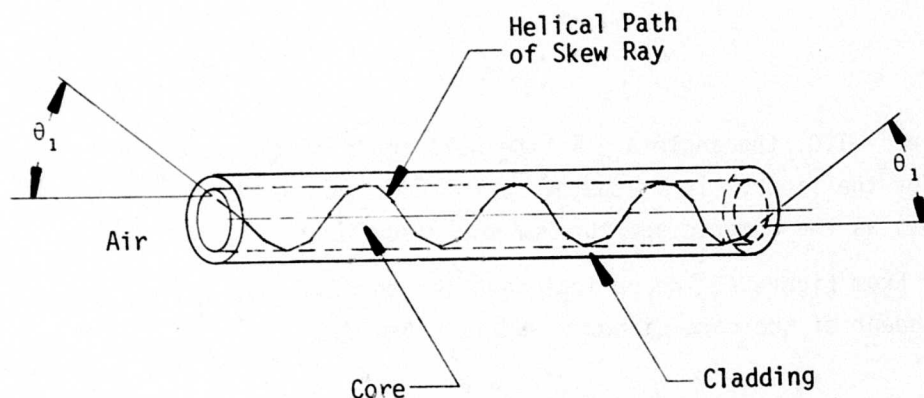


Figure 47. Skew Ray in a Clad Glass Fiber

While it is true that bending optical fibers can cause changes in exit angle and loss of light from the fiber wall, the bend must have a small radius to cause a noticeable effect. In fact, if the bending radius is greater than 20 times the core diameter⁷, d_c , the deviation from straight fiber characteristics is negligible. For 2.5mil diameter fibers, the bending radius must be less than 50mils for significant bending losses to be observed. A bend radius that small will normally not be encountered with the 45mil diameter bundles used on this program. In fact, the ability to make sharp bends with a radius equal to the bundle diameter is one of the desirable characteristics of a fiber optic bundle made up of a large number of small fibers. Not only is a bend radius of 20 times the core diameter allowed from optical considerations but also the mechanical properties of the fibers allow these bends without permanent mechanical damage or breakage.

B. OPTICAL LOSSES

One basic source of optical loss in clad glass fibers is the absorption of light by chemical impurities in the core glass. The most serious offenders in terms of absorption are transition metals and neighboring elements (Cr, Mn, Fe, Co, Ni) and water in

the form of OH^8 . Absorption loss in high NA fibers is typically less than 100dB/km at 900nm wavelength; absorption loss as low as 4dB/km⁹ at 900nm has been reported for low NA fibers. Absorption in the cladding layer can also increase the loss in the fiber. However, the absorption in the cladding is not as significant as absorption in the core glass.

Another important loss mechanism in fibers is scattering from imperfections in the core glass and at the core/cladding interface. Rayleigh scattering from the core glass remains after all other loss mechanisms have been removed from the fiber; therefore, Rayleigh scattering determines the minimum attenuation that can be achieved in an optical fiber. Some of the low-loss fiber made by Corning and BTL is within a few dB/km of the Rayleigh limit⁹. In Galileo fibers most of the attenuation seems to be the result of scattering at the core/cladding interface; this scattering loss may account for as much as 500dB/km of the observed total loss of 600dB/km.

Cladding thickness can also play an important role in determining fiber attenuation. The ray trace technique used in the preceding analysis predicted total internal reflection at the core/cladding interface. From this point of view, total reflection at the boundary requires that no energy be transferred to the cladding. Although there is no energy transfer to a lossless cladding layer, electromagnetic theory requires that finite values of field exist in the cladding layer in order to satisfy the continuity conditions at the core/cladding boundary. These fields in the cladding layer die off exponentially with x/λ where x is the distance from the core/cladding boundary and λ is the wavelength of light. The magnitude of the field is also dependent on the angle of incidence at the point of total reflection¹⁰.

If the cladding layer is too thin for a given wavelength, the exponentially decaying field will have an appreciable value at the outer surface of the cladding. This makes it possible, under the proper conditions, to couple light out of the fiber through the thin cladding layer -- see the discussion of frustrated total reflection in Ref 10. One way to enhance this loss mechanism is to surround the fiber with a fluid having index of refraction equal to the core glass. As a general rule the fiber is not required to operate under these conditions. The more typical situation is for the fiber to be surrounded by air over most of its length. In this case the air has a lower index of refraction than the cladding layer and no energy is transferred into the air. However, loss through the cladding can occur where the fibers touch the lossy jacket material or where dust or other foreign particles are present on the surface of the fiber. The best value of cladding thickness for a given type of fiber is usually a compromise between packing fraction and attenuation. It is also affected by other characteristics of the fiber. For example, a $3.0\mu\text{m}$ cladding thickness ($x/\lambda = 3.3$) is appropriate for the 600dB/km Galileo fiber. However, this would not be sufficient cladding thickness for Corning low-loss fiber which has an attenuation of 30dB/km.

In any event, the phenomenon of total internal reflection is mandatory in low-loss optical fibers because it provides reflection with significantly lower loss than could ever be achieved with a metal mirror coating on the fiber. The use of an adequately thick cladding layer on the fiber insures that the reflecting boundary is not contaminated or degraded by the fiber environment.

APPENDIX II

IN-LINE DATA BUS ANALYSIS

In an in-line data bus, the T couplers are connected with flexible fiber optic bundles as shown in Figure 48. As optical signal moves down the bus it must pass through the terminations at each end of the fiber optic bundles. Thus, the transmission of the terminations is an important parameter in determining system performance. Section II in the report describes various termination techniques and gives equations for calculating the transmission of a termination. Section III describes T couplers and defines various coupling, transmission and quality factors that describe coupler performance. In this analysis of an in-line data bus, the transmissions of the fiber optic terminations are included explicitly as separate factors apart from the losses and quality factors associated with the T couplers. This approach was used so that the resulting expressions would be more generally applicable and not limited to a specific construction technique. It allows system performance to be predicted from the separate characteristics of the independent parts.

For purposes of analysis, an in-line data bus of N stations uniformly distributed along a total length L will be considered. This configuration gives the correct result for a worst case condition of transmission between opposite ends of the data bus, and typical results for all intermediate path lengths. The average fiber optic attenuation between adjacent stations, a_0 , is given by

$$a_0 = \exp \left[\frac{-\alpha L}{N-1} \right] \quad (164)$$

where L is the total length of the bus, and

α is the loss coefficient of the fiber optic bundle.

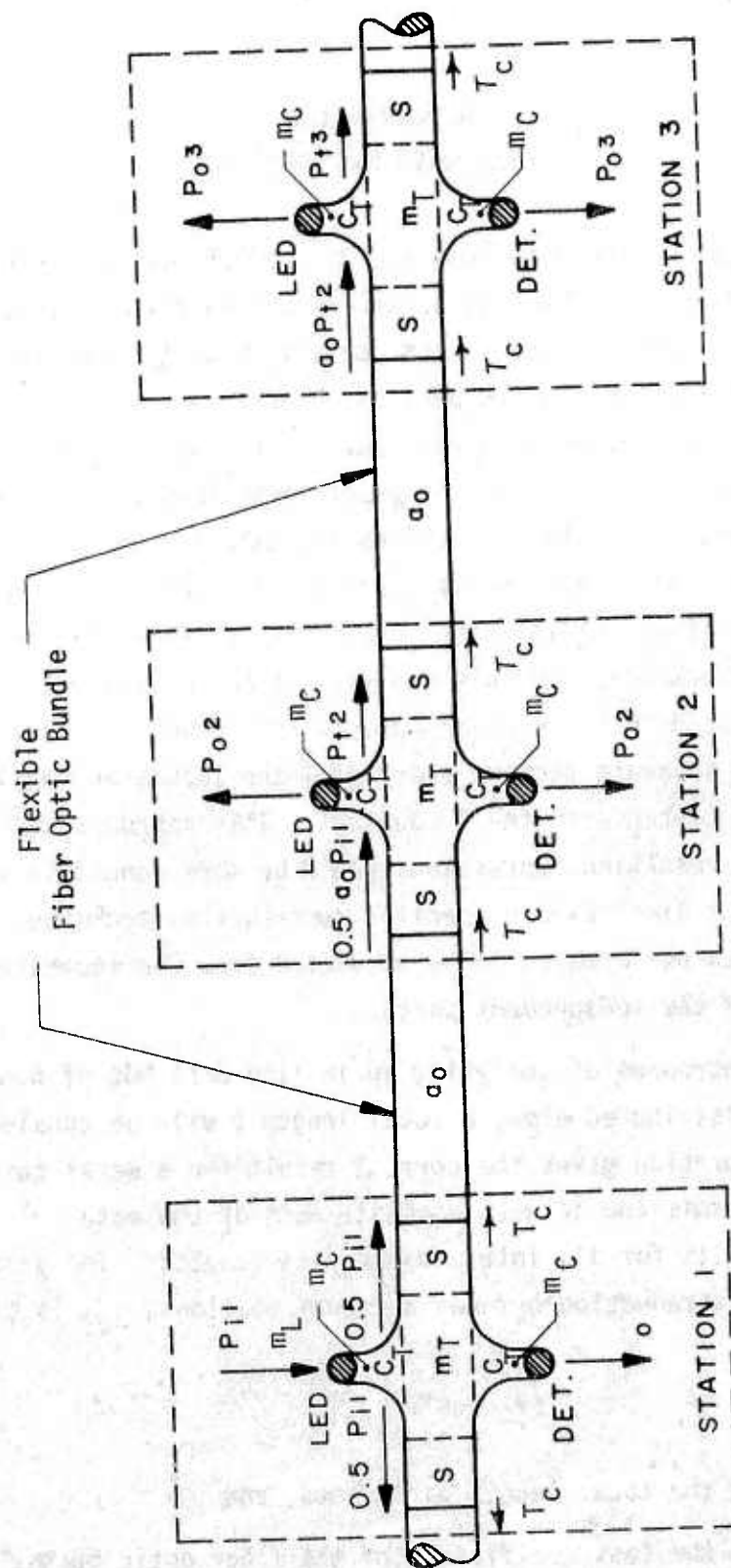


Figure 40. Signal Power Relationships in an In-Line Data Bus

When optical power is coupled into a fiber optic bundle, it is attenuated by the transmission of the input termination T_c given by Eq (18). As the light transits the fiber between stations it is attenuated by a_o given in Eq (164). As the light leaves the exit end of the fiber optic bundle a portion is reflected at the core/air interface; the fraction of light transmitted is given by $T_c = (1 - R_c)$ where R_c is given by Eq (4). Thus, the transmission of an average fiber optic bundle that interconnects two stations is

$$a_o T_c T_c = a_o (1 - R_c)^2 GR_a \quad (165)$$

The symbols a_o , T_c , and T_c are shown on Figure 48.

The signal power relationships in the in-line duplex data bus when station 1 is transmitting are shown in Figure 48. When an optical power, P_{i1} , is emitted by the LED of station 1, the power on the LED port is $m_L P_{i1}$, where m_L is the LED quality factor defined by Eq (41). The power coupled out at the detector port of station 2, P_{o2} , is given by

$$P_{o2} = [m_L m_C^2 C_T] [a_o T_c T_c] \frac{P_{i1}}{2} \quad (166)$$

The coupling quality factor, m_C is defined by Eq (39)

$$m_C = \frac{(\text{power at detector port})}{(\text{power into scrambler area attributed to detector port})} \quad (39)$$

the coupling factor, C_T , is defined by Eq (36)

$$C_T = \frac{(\text{scrambler area attributed to detector port})}{(\text{area of the scrambler})} \quad (36)$$

and $a_o T_c T_c$ is the total attenuation of the fiber optic bundle between station 1 and station 2 given by Eq (165). Referring to Eq (166), the term m_c enters once in the LED side arm of station 1 and again in the detector side arm of station 2. Front surface reflection losses at the scrambler input of station 2 are by definition included in m_c . The factor of $\frac{1}{2}$ in Eq (166) describes the split of the LED power between the two directions of transmission on the data bus.

The power transmitted to the output port of station 2, P_{t2} , is

$$P_{t2} = [m_L m_c^2] [a_o T_c T_c m_T (1-2C_T)] \frac{P_{i1}}{2} \quad (167)$$

where m_T is the transmission quality factor of the T coupler given by Eq (37)

$$m_T = \frac{T_T}{1 - 2C_T} \quad (37)$$

The signal at the detector port of station 3 is

$$P_{o3} = [m_L m_c C_T] [a_o^2 T_c^2 T_c^2 m_T (1-2C_T)] \frac{P_{i1}}{2} \quad (168)$$

and the power transmitted to the output port of station 3 is

$$P_{t3} = [m_L m_c^2] [a_o T_c T_c m_T (1-2C_T)]^2 \frac{P_{i1}}{2} \quad (169)$$

For station N, the power at the detector port as a fraction of the input power is

$$\frac{P_{oN}}{P_{i1}} = \left[\frac{a_o T_c T_c m_L m_c^2 C_T}{2} \right] [a_o T_c T_c m_T (1-2C_T)]^{N-2} \quad (170)$$

Equation (170) is the worst case power ratio, R_{PT} , given in Eq (45) in Section III. This worst case power ratio can be maximized by setting the derivative of R_{PT} with respect to C_T equal to zero, and solving for the optimum value of C_T . Inspection of Eq (170) shows that R_{PT} is of the form

$$R_{PT} = KC_T(1-2C_T)^{N-2} \quad (171)$$

where K is a constant given by

$$K = \left[\frac{a_o T_c T_{cm} m^2}{2} \right] \left[a_o T_c T_{cm} \right]^{N-2} \quad (172)$$

From Eq (171)

$$\frac{dR_{PT}}{dC_T} = K \left[(1-2C_T)^{N-2} - (2C_T)(N-2)(1-2C_T)^{N-3} \right] \quad (173)$$

Setting Eq (173) equal to zero gives

$$(1-2C_T) - (2C_T)(N-2) = 0 \quad (174)$$

which defines the optimum value of C_T given in Eq (46)

$$C_{opt} = \frac{1}{2(N-1)} \quad (46)$$

From Eq (46), C_{opt} is dependent only on the number of stations on the bus. Specifically, this means that the optimum value of C_T is independent of all of the factors included in the constant K , Eq (172). Equation (46) is a very general result with no limiting assumptions or approximations.

The use of the optimum coupling factor in an in-line data bus gives the maximum value of the worst case power ratio. This maximum value of R_{PT} is determined by substituting Eq (46) into Eq (45). The result is shown in Eq (48)

$$R_{PT}|_{\max} = \left[\frac{a_o T_c T_c m_L m_C^2}{4(N-1)} \right] \left[\frac{a_o T_c T_c m_T(N-2)}{(N-1)} \right]^{N-2} \quad (48)$$

The worst case dynamic range encountered at the various detectors in the in-line data bus occurs when station (N-1) transmits to station N followed by a transmission from station 1 to station N. This worst case dynamic range, D_{RT} , is equal to the ratio of the output power at station 2 to the output power at station N when station 1 is transmitting.

$$D_{RT} = \left[\frac{1}{a_o T_c T_c m_T(1-2C_T)} \right]^{N-2} \quad (175)$$

The value of D_{RT} when the coupling factor is C_{opt} is obtained by substituting Eq (46) into Eq (175). The result is presented in Eq (49)

$$D_{RT}|_{\text{opt}} = \left[\frac{1}{a_o T_c T_c m_T} \left(\frac{N-1}{N-2} \right) \right]^{N-2} \quad (49)$$

APPENDIX III

RADIAL DATA BUS ANALYSIS

In a radial data bus flexible fiber optic bundles are used for the connections between the stations and the radial coupler as shown in Figure 49. The length of a radial data bus (for signal attenuation) is not the total length of the fiber optic bundles used in the system. For the radial geometry, the length of the bus, L , will be taken as the greatest length of fiber optic bundle between any two stations on the bus. For the analysis, the radial coupler is assumed to be centrally located so that all other transmission paths between stations have lengths equal to or less than L . In this case the maximum fiber optic attenuation, a_m , is given by Eq (56) repeated here for convenience.

$$a_m = \exp[-\alpha L] \quad (56)$$

Comparison to Eq (164) in the T coupler analysis given in Appendix II shows that

$$a_m = a_o^{N-1} \quad (57)$$

where a_o is the average fiber optic attenuation between adjacent stations, and

N is the number of stations.

In order to facilitate the comparison between the radial and in-line data bus systems, the concept of average fiber optic attenuation per station will be retained in the radial data bus analysis with a_o defined by Eq (164).

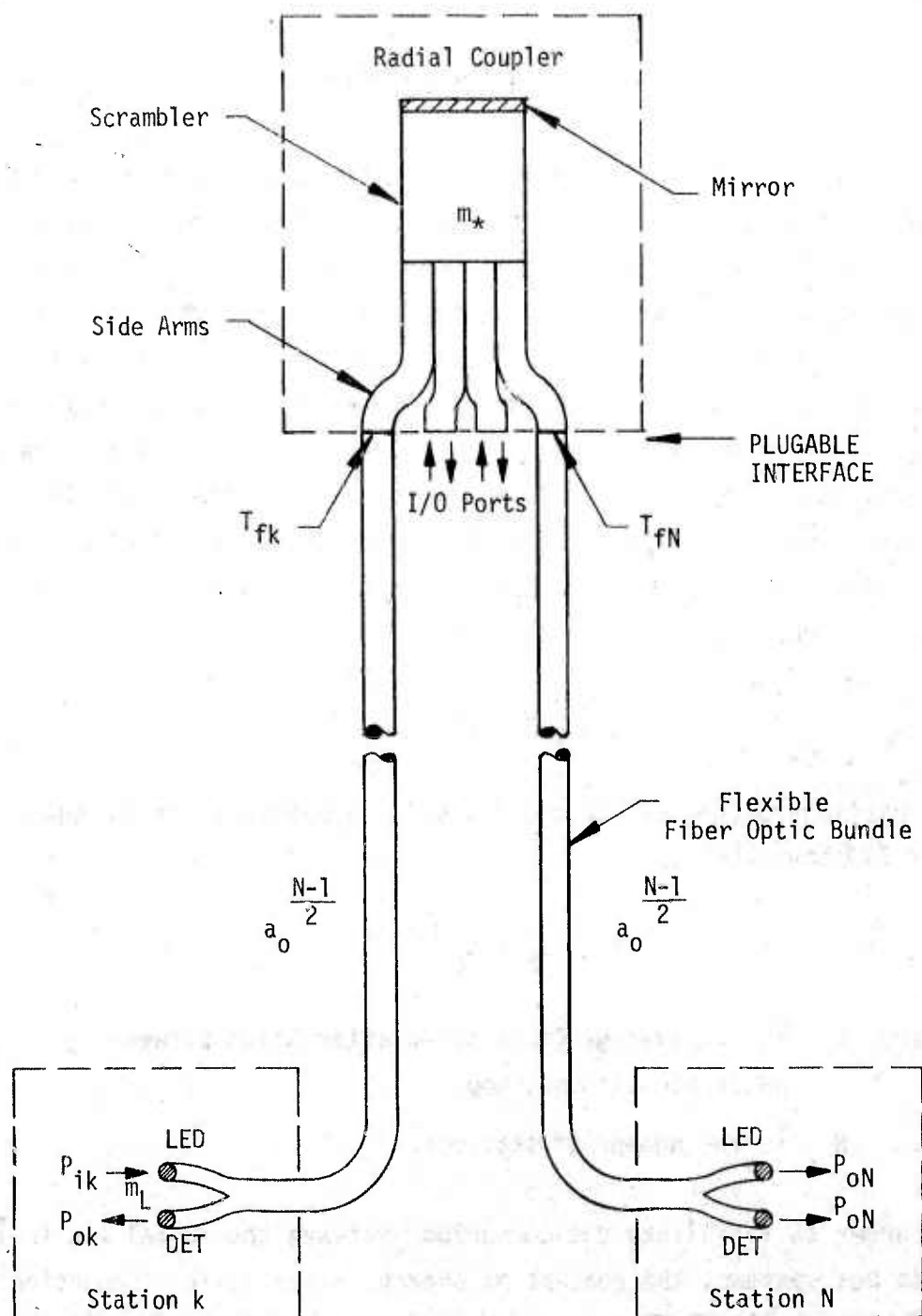


Figure 49. Signal Power Relationships in a Radial Data Bus

For the radial coupler, the coupling factor, C_* , is uniquely determined by the geometry. The value of C_* is given by Eq (51)

$$C_* = \frac{1}{N} \quad (51)$$

and the transmission factor, T_* , is given by Eq (53)

$$T_* = m_* C_* \quad (53)$$

where m_* is the radial coupler quality factor defined by Eq (50).

$$m_* = \frac{(\text{sum of output power at all ports})}{(\text{power in at input port})} \quad (50)$$

Combining Eqs (51) and (53) gives

$$T_* = \frac{m_*}{N} \quad (54)$$

For purposes of analysis the longest transmission path is assumed to be between stations k and N . When station k is transmitting, the signal power relationships can be determined from Figure 49. When an optical power, P_{ik} , is emitted by the LED of station k , the power at the LED port is $m_L P_{ik}$, where m_L is the LED quality factor defined by Eq (41). The power at the input port of the radial coupler, P_{if} , is given by

$$P_{if} = m_L T_c T_{fk} a_o^{\frac{N-1}{2}} P_{i1} \quad (176)$$

where T_c is the transmission of the fiber optic termination at the LED interface given by Eq (18)

$$T_c = (1-R_c)GR_a \quad (18)$$

The symbol T_{fk} represents the portion of the interface transmission at the radial coupler input port that can be attributed to the exit end of the fiber optic bundle between station k and the radial coupler.

When power is coupled into any port of a radial coupler, all N ports receive output power. In the ideal case of uniform power distribution in the radial coupler, the output power at the detector port of station N as a function of the station k LED power is

$$\frac{P_{oN}}{P_{ik}} = \frac{m_L m_* T_c T_{fk} T_{fN}^a o^{N-1}}{2N} \quad (177)$$

The symbol T_{fN} represents the portion of the interface transmission at the radial coupler output port that can be attributed to the entrance end of the fiber optic bundle between the radial coupler and station N. If the side arms of the radial coupler are made from fiber optic bundles, then these two interfaces are fiber bundle/fiber bundle interfaces and $T_{fk} = T_{fN}$. When solid side arms are used in the radial coupler the plugable interfaces are similar to fiber/scrambler interfaces used in the T coupler. In this case, $T_{fk} = T_c = 1-R_c$ where R_c is given by Eq (4) and $T_{fN} = T_c$ given by Eq (18). The values of T_{fk} and T_{fN} must be determined for each different radial coupler design; no part of T_{fk} or T_{fN} is included in m_* . The factor 2 in the denominator of Eq (177) results from the power split between the LED and detector ports at station N. Equation (177) is the worst case power ratio, R_{p*} , given in Eq (58) in Section III.A.2.

All of the signals on a radial data bus pass through the same centrally located radial coupler. If the radial coupler gives a uniform power distribution to all input/output ports, then the dynamic range of the radial data bus is due entirely to the difference in attenuation of the various fiber optic bundles.

If the stations of a radial data bus are uniformly spaced, the greatest distance between a station and the radial coupler is $0.5L$ and the shortest distance between a station and the coupler is $\frac{0.5L}{(N-1)}$. In this case, the fiber optic attenuation for the most distant station is $a_0^{\frac{N-1}{2}}$ and for the closest station is $a_0^{\frac{1}{2}}$. Assuming the radial coupler gives the uniform power division shown in Eq (51), the worst case dynamic range results at a station close to the radial coupler. The largest detector signal occurs when another close station transmits and the attenuation is a_0 . The smallest detector signal occurs when a distant station transmits and the attenuation is $a_0^{\frac{N}{2}}$. In this case the worst case dynamic range, D_{R*} , is given by Eq (178),

$$D_{R*} = \left[\frac{1}{a_0} \right]^{\frac{N-2}{2}} \quad (178)$$

For any given station the dynamic range can be significantly reduced by lowering the LED drive current in the stations that have short fiber optic bundles. If the drive currents are adjusted such that the optical power reaching the coupler is the same for all LEDs, then the dynamic range at any particular detector is 1.0. Each detector, on an individual basis receives the same power from all LEDs. However, this constant signal level is different for different detectors because of the variation in the fiber optic attenuation between the radial coupler and the various detectors. In this case, the ratio of power levels over all detectors is the ratio of the attenuation of the shortest ($a_0^{\frac{1}{2}}$) and longest ($a_0^{\frac{N-1}{2}}$) fiber optic bundles which is $a_0^{\frac{2-N}{2}}$.

The dynamic range of the radial data bus can in theory be reduced to the ideal value of 1.0 (zero dB) by including equal attenuation in all of the fiber optic bundles. In this case, each

detector receives the same signal regardless of which LED is transmitting and all detectors receive the same signal when any LED transmits. One way to make a uniform attenuation radial system is to make all of the fiber optic bundles the same length. A more practical way to achieve uniform attenuation is to include a neutral density filter element in the shorter fiber optic bundles to bring all fiber optic bundles to the same attenuation regardless of their length.

For the radial couplers built on this program, measured data presented in Section III.D.2. show that the coupling between the various ports is neither uniform nor reciprocal. This characteristic results from the mixing properties of the cylindrical scrambler rods used in the construction of the couplers which is described in Section III.B.. A rectangular scrambler rod is proposed to provide more uniform power distribution. In a practical radial data bus, the dynamic range will be determined by the uniformity of the power division provided by the radial coupler. The rectangular scrambler approach is expected to give a dynamic range of less than 2/1 ($\leq 3.0\text{dB}$).

REFERENCES

1. A.F. Milton and L.W. Brown, "Nonreciprocal Access to Multi-terminal Optical Data Highways" Proceedings, 1973 IEEE/OSA Conference on Laser Engineering and Applications, Washington, D.C.; May 30-June 1, 1973, pp 24-25.
2. W. Bart Bielawski, "A User's View of Optical Communications", IGC Conference; October 28-30, 1973.
3. J.R. Biard, "Optoelectronic Aspects of Avionic Systems", Final Technical Report AFAL-TR-73-164, Air Force Contract No. F33615-72-C-1565; June 1973, AD.
4. J.R. Biard and L.L. Stewart "Optoelectronic Data Bus", Final Technical Report AFAL-TR-73-271, Air Force Contract No. F33615-62-C-1911; October 1973, AD.
5. J.R. Biard, "Optoelectronic Aspects of Avionic Systems II", Final Technical Report AFAL-TR-75-45, Air Force Contract No. F33615-73-C-1272; May 1975.
6. H.F. Taylor, W.M. Caton and A.L. Lewis "Fiber Optics Data Bus System", DoD/Industry-Wide Integrated Optic and Fiber Optic Communications Conference, Naval Electronics Laboratory Center, San Diego, California; 15-17 May 1974.
7. O.M. Salati, "Handling Light With Fiber Optics", Electronic Industries, pp 102-108; December 1961.
8. W. Bart Bielawski, "Low-Loss Optical Waveguides: Current Status", Electro-Optical Systems Design, pp 22-28; April 1973
9. Mauro Di Domenico Jr. "Wires of Glass", Industrial Research, pp 50-54; August 1974.
10. John Strong, *Concepts of Classical Optics*, W. H. Freeman and Company, San Francisco and London; 1958.